Experimental and Theoretical Investigation of HDH Desalination Systems by Thermodynamic Balancing

BY

Mohamed Sobhy Aly Elzayed

A Thesis Presented to the

DEANSHIP OF GRADUATE STUDIES

KING FAHD UNIVERSITY OF PETROLEUM & MINERALS

DHAHRAN, SAUDI ARABIA

In Partial Fulfillment of the
Requirements for the Degree of

MASTER OF SCIENCE

In

MECHANICAL ENGINEERING

April 2019

KING FAHD UNIVERSITY OF PETROLEUM & MINERALS

DHAHRAN- 31261, SAUDI ARABIA

DEANSHIP OF GRADUATE STUDIES

This thesis, written by **MOHAMED SOBHY ALY ELZAYED** under the direction of his thesis advisor and approved by his thesis committee, has been presented and accepted by the Dean of Graduate Studies, in partial fulfillment of the requirements for the degree of **MASTER OF SCIENCE IN MECHANICAL ENGINEERING.**

Dr. Syed M. Zubair
(Advisor)

Dr. Zuhair M. Gasem
Department Chairman

Dr. Salam A. Zummo
Dean of Graduate Studies

Dr. Mohammed A. Antar
(Member)

24/12/19
Date

Dr. Atia Khalifa
(Member)

Dedicated

To

My Beloved Parents and Sisters

ACKNOWLEDGMENTS

All praise be to Allah, the Lord of all creation, the most gracious, the most merciful for his beneficence that he granted me the strength, health, and knowledge to complete this Thesis. And all prayers and blessings of Allah be upon our master, the noblest Prophet Muhammad (P.B.U.H.).

The work presented in this thesis could not have been completed without the help and support of many individuals; I am extremely thankful and grateful for all their contributions.

My deepest thanks go to my adviser, Dr. Syed M. Zubair, for all his encouragement, support, and help over the past two years. He has patiently guided me in the correct direction and has served to further my interests and abilities in the thermal sciences.

I would also like to thank my committee member, Dr. Mohammed A. Antar, who has been working with me day and night, for his extraordinary support in the experimental work that without him I could never finish this work. I especially thank him for teaching ME 460 (Desalination Course) in the unique and awesome way he does that was a motivation for me to do research in the desalination field. Also, special thanks to my committee member, Dr. Atia Khalifa, for his assistance and valuable comments.

I extend my appreciation to Dr. Mostafa Sharqawy for his great efforts in designing the experimental setup and to Dr. Fadi Al-Badour for helping me to deal with the data acquisition system in the experimental work.

Many thanks to my research groupmate, Mohamed Ali Ahmed, for helping me in the theoretical study.

Thank you to Mr. Peter (Electrical technician) for his help during experiments.

My heartfelt thanks are due to my parents and sisters for their prayers, guidance, and moral support throughout my academic life. My parents' advice, to strive for excellence, has made all this work possible.

To my friend, Ahmed Gamil El-gamasy, thanks for your advice to apply to KFUPM.

Finally, I am so thankful for the authority of King Fahd University of Petroleum and Minerals for giving me the opportunity to pursue my master's degree in mechanical engineering.

TABLE OF CONTENTS

ACKNOWLEDGMENTS ..... **V**

TABLE OF CONTENTS ..... **VII**

LIST OF TABLES ..... **IX**

LIST OF FIGURES ..... **X**

LIST OF ABBREVIATIONS ..... **XII**

ABSTRACT ..... **XV**

ملخص الرسالة ..... **XVII**

CHAPTER 1 INTRODUCTION **1**

1.1 Classification of HDH cycles. **4**

CHAPTER 2 LITERATURE REVIEW **7**

2.1 Closed-air open-water (CAOW) water-heated system. **11**

2.2 Multi-effect CAOW water-heated system **19**

2.3 Goals of the current study. **21**

2.4 Objectives of the current study. **22**

CHAPTER 3 THERMODYNAMIC BALANCING OF HDH DESALINATION **23**

3.1 Modeling. **23**

3.1.1 Balancing Definition 23

3.1.2 Enthalpy pinch definition. 27

3.1.3 Conservation equations and solution method. 30

3.1.4 Second law analysis 36

3.1.5 Assumptions and approximations. 44

3.1.6 Property packages. 45

3.2 Results and Discussion. **46**

3.2.1 Model validation. 46
3.2.2 Variation of total exergy destroyed rate with enthalpy pinch. 50
3.2.3 Variation of GOR with enthalpy pinch and number of extractions. 50
3.2.4 Variation of GOR with minimum and maximum temperature. 54
3.2.5 Limitation of thermodynamic balancing. 62
3.2.6 Design example 67

3.3 Chapter conclusions. 93

CHAPTER 4 EXPERIMENTAL WORK 94

4.1 Experimental setup description. 94
4.1.1 Humidifier. 97
4.1.2 Dehumidifier 97
4.1.3 Other components 97
4.1.4 Instrumentation 98

4.2 Test Procedure. 99

4.3 Results and Discussion. 103
4.3.1 Optimum performance at the thermodynamic balancing condition. 107
4.3.2 Minimum dehumidifier energy effectiveness at the on-design condition. 107
4.3.3 Input heat rate effect on the performance parameters. 108
4.3.4 Experimental validation against the theoretical model. 111
4.3.5 The single and double extraction effect on the performance 113

4.4 Chapter conclusions. 117

CHAPTER 5 CONCLUSIONS AND RECOMMENDATIONS 118

REFERENCES 121

APPENDIX A: SOLUTION ALGORITHM FOR THE FIXED-EFFECTIVENESS MODELING 126

APPENDIX B: EXPERIMENTAL DATA ANALYSIS 127

VITAE 129

LIST OF TABLES

Table 2-1: Summary of previous studies for water heated CAOW systems 15
Table 3-1: The percentage error between the current model and Chehayeb et al. [34] model for the zero extraction 47
Table 3-2: The percentage error between the current model and Chehayeb et al. [34] model for the single extraction cycle 48
Table 3-3: The percentage error between the current model and Chehayeb et al. [34] model for the double extraction cycle. 49
Table 3-4: The optimal mass flow rate ratio of a zero extraction cycle. 72
Table 3-5: The optimal conditions of a single extractions cycle at T_{min} = 20 (°C) 73
Table 3-6: The optimal conditions of a single extractions cycle at T_{min} = 25 (°C) 74
Table 3-7: The optimal conditions of a single extractions cycle at T_{min} = 30 (°C). 75
Table 3-8: The optimal conditions of a single extractions cycle at T_{min} = 35 (°C). 76
Table 3-9: The optimal conditions of a double extraction cycle at T_{min} = 20 (°C). 77
Table 3-10: The optimal conditions of a double extraction cycle at T_{min} = 25 (°C). 78
Table 3-11: The optimal conditions of a double extraction cycle at T_{min} = 30 (° C). 79
Table 3-12: The optimal conditions of a double extraction cycle at T_{min} = 35 (° C). 80
Table 3-13: Performance parameters of a zero extraction cycle at T_{min} = 20 (°C). 81
Table 3-14: Performance parameters of a zero extraction cycle at T_{min} = 25 (°C). 82
Table 3-15: Performance parameters of a zero extraction cycle at T_{min} = 30 (°C). 83
Table 3-16: Performance parameters of a zero extraction cycle at T_{min} = 35 (°C). 84
Table 3-17: Performance parameters of a single extraction cycle at T_{min} = 20 (°C). 85
Table 3-18: Performance parameters of a single extraction cycle at T_{min} = 25 (°C). 86
Table 3-19: Performance parameters of a single extraction cycle at T_{min} = 30 (°C). 87
Table 3-20: Performance parameters of a single extraction cycle at T_{min}= 35 (°C). 88
Table 3-21: Performance parameters of a double extraction cycle at T_{min} = 20 (°C) 89
Table 3-22: Performance parameters of a double extraction cycle at T_{min} = 25 (°C). 90
Table 3-23: Performance parameters of a double extraction cycle at T_{min} = 30 (°C) 91
Table 3-24: Performance parameters of a double extraction cycle at T_{min} = 35 (°C). 92
Table 4-1: A summary of test parameters. 102
Table 4-2: Table of test parameters for Q = 3.3 kW 104
Table 4-3: Table of test parameters for Q = 5.5 kW. 105
Table 4-4: Table of test parameters for Q = 8.2 kW. 106
Table 4-5: The effect of MR and input heat rate on the performance parameters. 111
Table 4-6: Balanced cases for different added heat rates. 112
Table 4-7: Validation between experimental balanced cases and zero extraction model 113
Table 4-8: Comparison between the system enthalpy pinch and the critical enthalpy pinch (Ψ_1 and Ψ_2) 116

LIST OF FIGURES

Figure 1-1: The rain cycle [1] 2
Figure 1-2: The solar still [5] 2
Figure 1-3: The processes of a simple HDH cycle. 4
Figure 1-4: HDH systems classification based on cycle configuration. 5
Figure 2-1: CAOW -Water heated HDH cycle. 12
Figure 2-2: The CAOW water heated HDH cycle on the psychometric chart [1]. 12
Figure 2-3: Psychometric chart of multi-effect CAOW water-heated HDH cycle [1]. 19
Figure 2-4: Multi-effect CAOW water-heated HDH cycle. 20
Figure 3-1: Temperature distribution of an unbalanced dehumidifier [35]. 25
Figure 3-2: Temperature distribution of a dehumidifier with a single extraction [35]. 25
Figure 3-3: Temperature distribution of a dehumidifier with multi extractions [35]. 26
Figure 3-4: Temperature distribution of a humidifier with multi extractions [35]. 26
Figure 3-5: Temperature enthalpy diagram of a thermodynamic balanced HDH cycle without extraction [13]. 29
Figure 3-6: A control volume including a section of the humidifier and another section of the dehumidifier separated by the water heater [30]. 33
Figure 3-7: An infinitesimally small control volume of the humidifier [30]. 33
Figure 3-8: An infinitesimally small control volume of the dehumidifier [30]. 34
Figure 3-9: Temperature enthalpy diagram of a thermodynamically balanced HDH cycle with multi extractions [30]. 36
Figure 3-10: A multi extraction HDH cycle with the inlet/outlet condition of each component. 39
Figure 3-11: Dehumidifier control volume with the inlet/outlet condition. 40
Figure 3-12: Humidifier control volume with the inlet /outlet condition. 41
Figure 3-13: Water heater control volume with the inlet/outlet condition. 42
Figure 3-14: The total exergy destroyed rate of zero, single and double extraction cycle versus the enthalpy pinch at T_{max} = 80 ^{o}C and T_{min} = 20 ^{o}C. 51
Figure 3-15: The GOR of a zero extraction cycle versus enthalpy pinch of the humidifier and dehumidifier at T_{max} = 80 ^{o}C and T_{min} = 20 ^{o}C. 52
Figure 3-16: The GOR of a single extraction cycle versus enthalpy pinch of the humidifier and dehumidifier at T_{max} = 80 ^{o}C and T_{min} = 20 ^{o}C. 53
Figure 3-17: The GOR of a double extraction cycle versus enthalpy pinch of the humidifier and dehumidifier at T_{max} = 80 ^{o}C and T_{min} = 20 ^{o}C. 54
Figure 3-18: The effect of maximum and minimum temperature on GOR of the zero extraction cycle at Ψ = 0 kJ/kg. 56
Figure 3-19: The effect of maximum and minimum temperature on the GOR of zero extraction cycle at Ψ = 40 kJ/kg. 57
Figure 3-20: The effect of maximum and minimum temperature on the GOR of single extraction cycle at Ψ = 0 kJ/kg. 58

Figure 3-21: The effect of maximum and minimum temperature on GOR of the single extraction cycle at Ψ = 16 kJ/kg. 59
Figure 3-22: The effect of maximum and minimum temperature on GOR of the double extraction cycle at Ψ = 0 kJ/kg. 60
Figure 3-23: The effect of maximum and minimum temperature on GOR of the double extraction cycle at Ψ = 10 kJ/kg. 61
Figure 3-24: The gain output ratio of zero, single and double extraction cycle versus enthalpy pinch at T_{max} = 80 ^{o}C and T_{min} = 20 ^{o}C. 62
Figure 3-25: The effect of maximum temperature on Ψ_1 and Ψ_2 at T_{min} = 20 ^{o}C..... 63
Figure 3-26: The effect of minimum temperature on Ψ_1 and Ψ_2 at T_{max} = 80 ^{o}C..... 64
Figure 3-27: A Schematic diagram of a double extraction cycle..... 66
Figure 4-1: Schematic diagram of the HDH experimental setup for studying water-heated, air-heated, and balanced HDH cycles [50]: (1) float valve, (2) seawater tank, (3) pump, (4) distilled water tank, (5) level indicator, (6) valve, (7) flow meter, (8) air fan, (9) water coil (heat exchanger), (10) water heater, (11) air heater, (12) sprinklers, (13) packing material. 95
Figure 4-2: Photograph of the HDH experimental setup for studying water-heated and air-heated HDH cycles. 96
Figure 4-3: The experimental test procedure. 101
Figure 4-4: The effect of MR and input heat rate on productivity..... 109
Figure 4-5: The effect of MR and input heat rate on the recovery ratio. 110
Figure 4-6: The effect of MR and input heat rate on the gain output ratio. 110
Figure 4-7: The Single and double extraction effect on the GOR at Q = 5.5 kW. 114
Figure 4-8: The Single and double extraction effect on the RR at Q = 5.5 kW. 115
Figure 4-9: The single and double extraction effect on productivity at Q = 5.5 kW..... 115
Figure 4-10: Enthalpy pinch effect on GOR for zero, single and double extraction cycle at T_{max} = 56.3 ^{o}C and T_{min} = 26.9 ^{o}C using the theoretical model. 116

LIST OF ABBREVIATIONS

ACRONYMS

HDH	Humidification Dehumidification
GOR	Gained Output Ratio
RR	Recovery Ratio
TBT	Top Brine Temperature
TTD	Terminal Temperature Difference
MSF	Multi-Stage Flash
MED	Multi-Effect Distillation
RO	Reverse Osmosis

SYMBOLS

C_p	Specific heat capacity at constant pressure (J/kg.)
$\dot{H}$	Total enthalpy rate (W)
h	Specific enthalpy (J/kg)
h^*	Water and moist air enthalpy rate normalized by dry air mass flow rate (J/kg dry air)
h_{fg}	The heat of vaporization (J/kg)

HCR	Heat Capacity Ratio (-)
$\dot{m}$	Mass flow rate (kg/s)
m_r	Water - to air mass flow rate ratio (-)
MR	Feedwater to air mass flow rate ratio (-)
Q	Heat rate (W)
s	Specific entropy (J/kg. K)
$\dot{S}$	Total entropy rate (W/K)
T	Temperature

GREEK

Δ	Difference /Change
ϵ	System effectiveness (-)
η	Efficiency (-)
ϕ	Relative humidity (-)
ψ	Enthalpy pinch (J/kg dry air)
ω	Absolute humidity (kg /kg dry air)
ξ	Specific flow exergy (J/kg)

$\dot{\Xi}$	Total exergy Rate (W)

SUBCRIPTS

a	Air
c	Cold
D or deh	Dehumidifier
da	Dry air
h	Hot
H or hum	Humidifier
loc	Local
in	Entering
max	Maximum
min	Minimum
out	Leaving
pw	Product water
w	Water

ABSTRACT

Full Name : MOHAMED SOBHY ALY ELZAYED

Thesis Title : Experimental and Theoretical Investigation of HDH Desalination Systems by Thermodynamic Balancing.

Major Field : Mechanical Engineering

Date of Degree : Shaaban 1440 (H) [April 2019 (G)]

The Humidification dehumidification (HDH) desalination is one of the thermal desalination techniques that is suitable for the small scale and off-grid applications. The HDH has the advantage to deal with high salinity feedwater making it one of the best options to treat the produced water from the natural gas wells. The main disadvantage of the HDH technique is the low thermal efficiency leading to high water production cost. Thermodynamic balancing of the heat and mass exchangers improves energy efficiency by minimizing the total rate of exergy destroyed.

The current study is mainly focused on how to improve the performance of the HDH cycle using the thermodynamic balancing approach both theoretically and experimentally. The balancing of the HDH cycle thermodynamically may be achieved by changing the mass flow rate ratio to reach the modified heat capacity ratio that is equal to unity or by using multiple extractions and injections between the humidifier and dehumidifier. The first part of this study is focused on using the temperature-enthalpy diagram model to investigate the enthalpy pinch, the bottom temperature, and top temperature effect on the performance of zero, single, and double extraction cycles. The second part is an

experimental study to investigate the effect of operating conditions like the mass flow rate ratio and the input heat rate on the performance of the HDH cycle. The performance parameters are represented by the gain output ratio, recovery ratio, productivity, energy effectiveness, and enthalpy pinch. The experimental results in a laboratory environment showed that the optimum operating condition is the thermodynamically balanced dehumidifier case at which the modified heat capacity ratio is equal to unity.

ملخص الرسالة

الاسم : محمد صبحى على الزايد

عنوان الرسالة : دراسة عملية ونظرية لأداء التحلية بطريقة الترطيب والتجفيف من خلال الاتزان الثرموديناميكى.

التخصص : الهندسة الميكانيكية

تاريخ الدرجة العلمية : شعبان ١٤٤٠ هجريا الموافق ابرايل ٢٠١٩ ميلاديا

تعتبر تقنية التحلية باستخدام الترطيب والتجفيف واحدة من الطرق التى تستخدم الفصل الحرارى فى التحلية والتى تمتاز بانها مناسبة اقتصاديا للتطبيقات ذات الاستهلاك المنخفض للمياه والاماكن النائية المعزولة عن شبكة الكهرباء والمرافق .تمتازعملية التحلية بالترطيب والتجفيف ايضا بانها لها القدرة على التعامل مع مياه تغذية ذات درجة ملوحة عالية لذا فهى خيار امثل لتحلية المياه المفصولة هيدروليكيا من ابار الغاز الطبيعى ولكن يعيب هذه التقنية انها ذات كفاءة حرارية منخفضة .من المعلوم ان الاتزان الثرموديناميكى للمبادلات الحرارة والكتلة يعظم الكفاءة الحراية لانه يؤدى الى تقليل الفقد فى الطاقة المتاحة .

تنصب هذه الدراسة على تعظيم الكفاءة الحراية لتقنية الترطيب والتخفيف عن طريق تحقيق الاتزان الثرموديناميكى للمجفف نظريا وعمليا .يمكن تحقيق الاتزان الثرموديناميكى للمجفف اما بتغير نسبة مياه التغذية الى الهواء المار بالدورة او باستنزاف الهواء من المرطب الى المجفف فى اكثر من نقطة بطول المجفف والمرطب.تنقسم هذه الدراسة الى جزئين اساسين ، الجزء الاول يتعلق بنمذجة الأداء النظرى لتقنية الترطيب والتجفيف فى حالة تحقيق الاتزان الثرموديناميكى سواء باستنزاف هواء من المرطب الى المجفف او بدون استنزاف ، بينما الجزء الاخر يمثل دراسة تحقيق الاتزان الثرموديناميكى للمجفف عمليا مع تغير ظروف تشغيل .العوامل االتى يتم من خلالها الحكم على اداء تلك التقنية تتمثل فى الانتاجية لكل ساعة ونسبة المياه المحلاة الى مياة التغذية ونسبة المياه االملاحة فى صورة طاقة الى الطاقة المستهلكة.

فى نهاية تلك الدراسة تم الوصول الى حالة الاتزان الثرومودينامیکى للمجفف والتى اثبتت النتائج انها تعتبر نقطة التشغيل الامثل لتلك التقنية .

CHAPTER 1

INTRODUCTION

The HDH desalination is one of the thermal desalination techniques that imitate the rain cycle. As shown in Figure 1-1, the rain cycle consists of two consecutive processes (humidification and dehumidification). Due to the heating of Ocean's water by the solar irradiation, the produced water vapor under the action of heat and mass transfer humidifies the atmospheric air forming clouds (humidification process). When the clouds are cooled off, the water vapor will condensate forming rains (dehumidification process). HDH cycle also uses a gas carrier like air to remove some water vapor from the saline water to obtain pure water by cooling off the gas carrier to condensate the water vapor [1, 2].

The HDH technique may be considered an advanced model of the solar still. The solar still is mainly based on the greenhouse effect for increasing the saline water temperature. As shown in Figure 1-2, the transmitted solar irradiation from the transparent cover made from glass will be absorbed by the black surface at the bottom of the solar still. The radiation emitted from the absorber cannot transmit through the cover as the emitted radiation has short wavelengths. The absorbed heat from the sun causes an increase in the temperature of the saline water forming water vapor. water vapor condensates by the upper cover, as it has a lower temperature, producing pure water. The solar still has an advantage of its simple construction and easy maintenance. It also may be used for producing small quantities of pure water in remote areas where there is not any power supply [3–7].

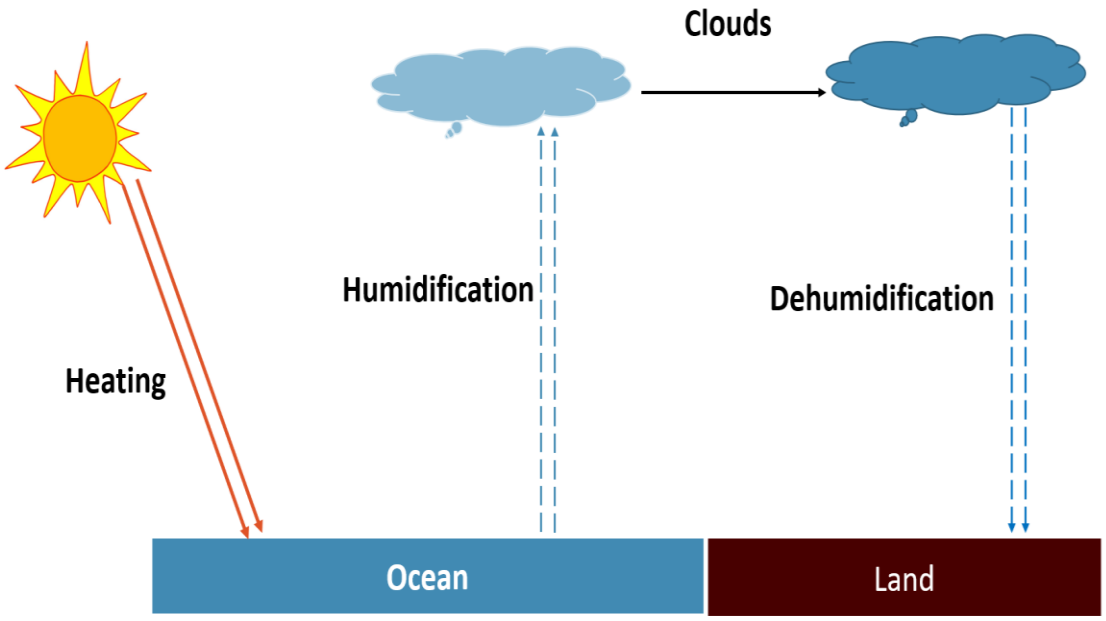

Figure 1-1: The rain cycle [1].

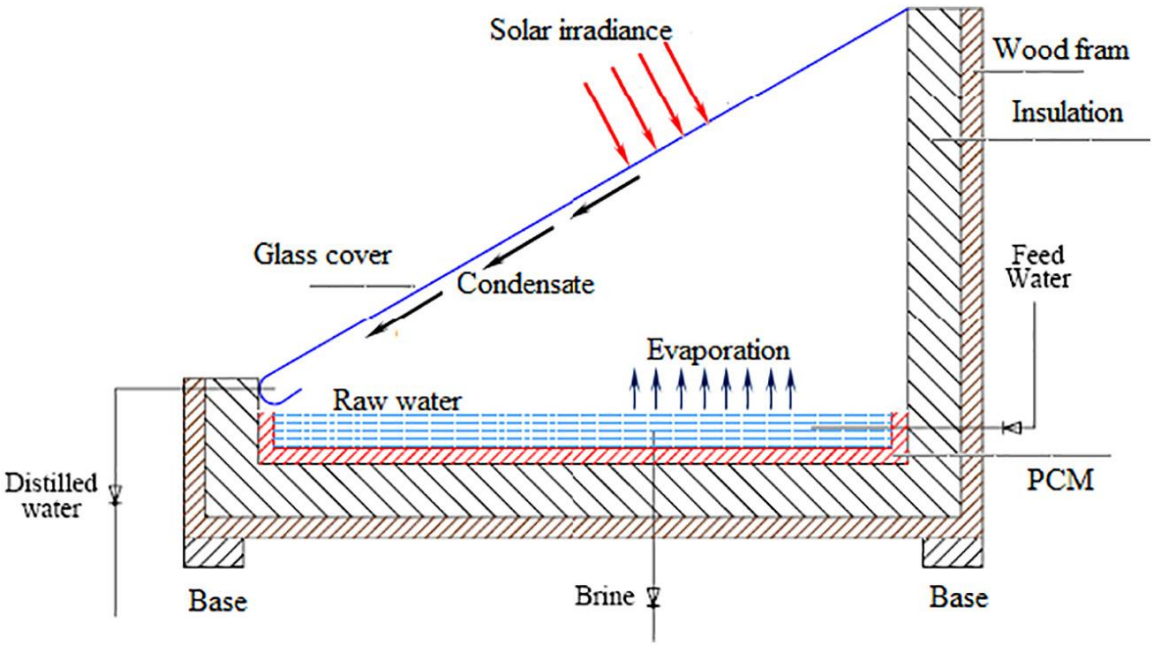

Figure 1-2: The solar still [5].

There are several drawbacks to solar stills. The low gain output ratio (less than 0.5) of the solar still is the most prohibitive disadvantage of this technique. The Low gain output ratio here means that it is required to use huge areas to produce small quantities of water. There are some reasons that are responsible for the low gain output ratio of the solar still. One of these reasons is that the latent heat of condensing the water vapor is lost through the glass cover to the ambient atmosphere. There are some researchers that make use of the latent heat of condensing the water vapor by using multi-effects solar still. Although the multi-effect solar still leads to an increase in the gain output ratio, the solar stills still have a low gain output ratio compared with the other techniques [5–7].

In the solar still, all the functional processes such as absorbing solar energy, evaporation, and condensation occur within the same component, so the improvement of the thermal efficiency of each process is limited and difficult. The thermal efficiency of each process may be improved by conducting each process in a separated component instead of using a single component for all the processes, so the overall efficiency of the system may be increased [1].

HDH cycle also may be considered separated component solar still. For example, as shown in Figure 1-3, the process of absorbing heat from the sun may be more efficient by using a separated solar water heater and the latent heat of condensation may be recovered in the dehumidifier to preheat the seawater before injecting it in the water heater. The evaporation process occurs in a separate unit (humidifier) while the condensation process occurs in another separated unit (dehumidifier). Thus, it is easy to improve the effectiveness of each unit separately and to optimize the system, so the HDH system has higher productivity than the solar still [1].

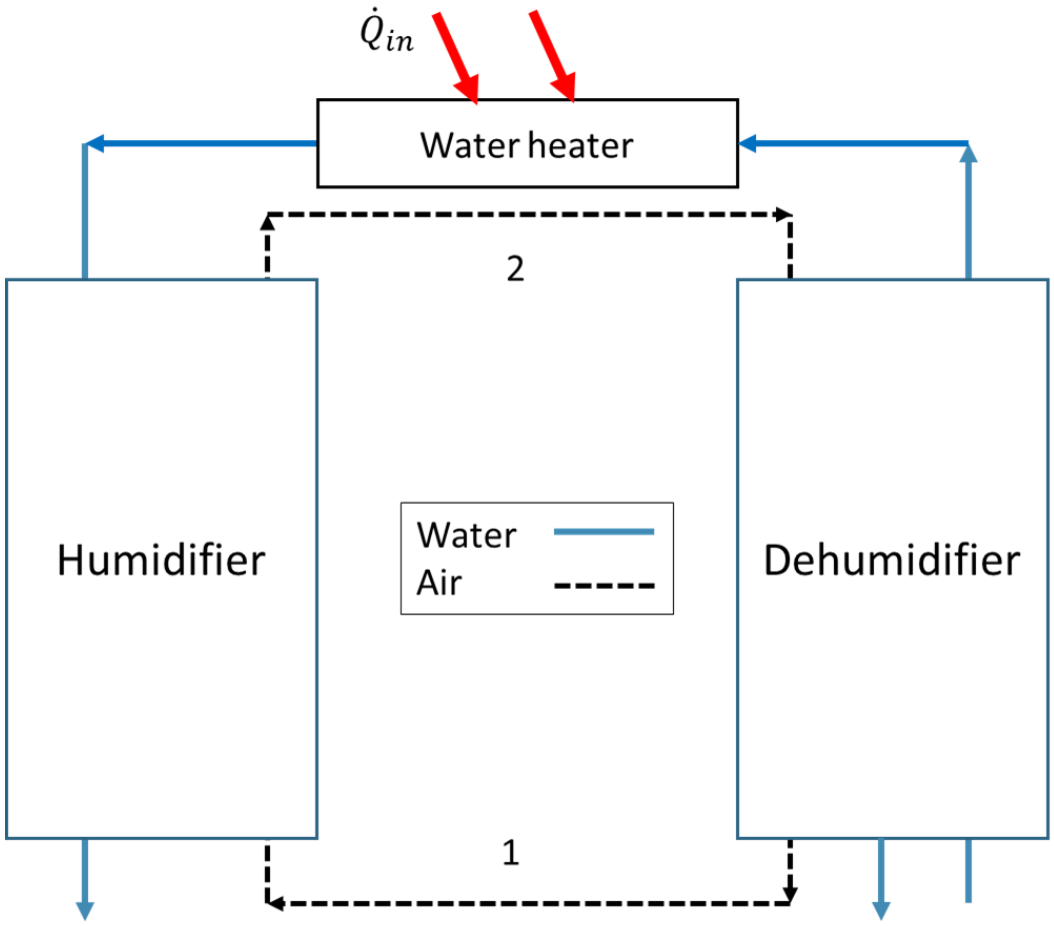

Figure 1-3: The processes of a simple HDH cycle.

1.1 Classification of HDH cycles.

There are several categories for HDH cycles based on different criteria. The first criteria are the type of energy input. The energy input may be solar energy gathered by an air solar collector or a water solar collector, electrical energy produced for example by a wind turbine, geothermal energy or waste energy from exhaust gases produced from a gas turbine cycle or an internal combustion engine. According to this type of classification, it is easy to understand the advantage of using the HDH technique. The HDH technique does not need high-grade energy to produce pure water.

The second criterion for classifying the HDH cycles as shown in Figure 1-4 is the cycle configuration. There are two different configurations for the HDH cycle which are a **CWOA** "closed water-open-air" cycle and a **CAOW** "closed air-open water" cycle. In the CAOW cycle, the air passes through a closed-loop while the water passes through an open loop. To illustrate, the exited air from the dehumidifier after condensation of the water vapor carried by air to obtain pure water is recirculated to be humidified again while the out water from humidifier does not recirculate. On the other hand, in the CWOA cycle, the water passes in a closed-loop while the air passes in an open loop. The driving force for recirculating the air may be natural due to the density gradient caused by the temperature gradient or mechanically by a fan or a blower. Although the cycle configuration of using open loops for both the air and the water at the same time is possible, the designers for the HDH systems avoid using this configuration because of its low thermal efficiency.

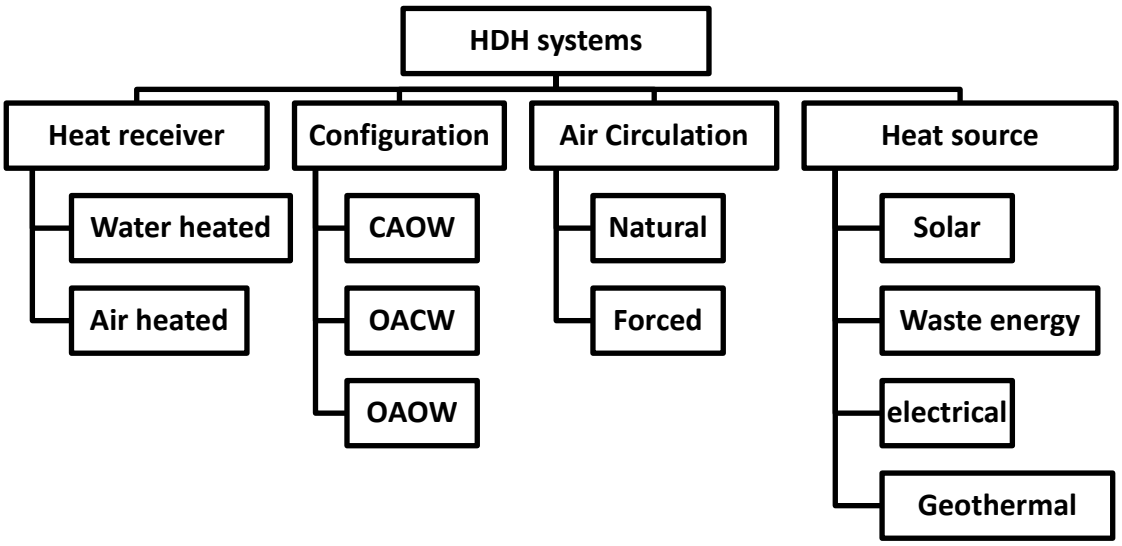

Figure 1-4: HDH systems classification based on cycle configuration.

An open-loop for the water or the air leads to waste thermal energy without recovering. Also, it is impossible to design a cycle configuration with closed loops for both the air and the water at the same time. The closed loops for the air or the water lead to recovering the waste energy carried by air or the water. However, closing the stream paths of the air and the water at the same time leads to a lower temperature difference between the air stream and the water stream. The temperature difference between the hot stream and the cold stream is the driving force for the heat transfer during the evaporation process in the humidifier and the condensation process in the dehumidifier.

Many researchers have conducted several comprehensive studies to improve the performance of each component of the HDH system separately (the humidifier, the dehumidifier, and the heater). The objective of all previous studies was to obtain the best overall efficiency of the HDH system to produce pure water by the cheapest possible cost. Also, some researchers have investigated economic analysis for the HDH system. These studies have stated that producing pure water by HDH systems is still expensive. Understanding the merit of each cycle configuration can lead to an increase in the overall thermal efficiency of the HDH system, so optimizing the cycle itself can lead to a decrease in the cost of the pure water produced by an HDH system.

The third criteria for classifying the HDH cycles is the type of the fluid stream that is heated by the input energy source. The HDH cycles may be air-heated cycles or water-heated cycles. The performance and the analysis of the air heated cycle are fully different compared with the water heated cycle. For the case of using solar energy as a heat source, a water solar collector may be used in the water-heated cycle and also an air solar collector may be used for the air heated cycle.

CHAPTER 2

LITERATURE REVIEW

First, to be able to understand the analysis of the several different HDH systems conducted in the previous studies, it is necessary to define some performance parameters.

1- Gained Output Ratio (GOR): it is a dimensionless parameter that estimates the ratio between the heat required to transform the amount of the produced pure water from saturated liquid to saturated vapor and the total heat added to the system.

$$GOR = \frac{\dot{m}_{pw}.h_{fg}}{\dot{Q}} \tag{2-1}$$

Where $\dot{m}_{pw}$ is the produced pure water, $\dot{Q}$ is the total heat input to the cycle and h_{fg} is the latent heat of evaporation. h_{fg} may be estimated at the inlet water temperature to the cycle or at the saturation temperature corresponding to the operating pressure. The GOR may be considered the efficiency of the desalination process. The high product water does not always mean high GOR. To illustrate, some systems require massive heat input to obtain high productivity [8–10].

2- Recovery ratio (RR): it is a dimensionless parameter that estimates the amount of the produced pure water divided by the amount of the feed seawater input to the system. For instance, the RR may be considered a measure of the extracted pure water from the seawater, so it also is called the extraction efficiency [11]. Unfortunately, HDH cycles have lower RR compared with other desalination techniques like MED and MSF [1].

On the other hand, in the desalination techniques that have higher RR like MED and MSF, it requires complex processes for dealing with the brine water causing fouling and scaling. HDH systems have an advantage that they may not need these complex processes.

$$RR = \frac{\dot{m}_{pw}}{\dot{m}_{w}} \tag{2-2}$$

where $\dot{m}_{pw}$ and $\dot{m}_{w}$ are the product and feed water, respectively.

3- Mass flow rate ratio (MR): it is a dimensionless parameter that equals the feed seawater mass flow rate entering the dehumidifier ($\dot{m}_{w}$) divided the mass flow rate of the dry air entering the humidifier ($\dot{m}_{da}$) [8].

$$MR = \frac{\dot{m}_{w}}{\dot{m}_{da}} \tag{2-3}$$

4- Energy effectiveness (ϵ): according to a comprehensive study which has been done by Narayan et al. [12], the effectiveness of heat and mass transfer systems may be defined based on the maximum allowable temperature difference, the maximum allowable change in the absolute humidity, or the maximum allowable change in the enthalpy rate. In our study, energy effectiveness is defined based on the maximum allowable enthalpy rate difference as follows:

$$\epsilon = \frac{\Delta\dot{\mathrm{H}}}{\Delta\dot{\mathrm{H}}_{\mathrm{max}}} \tag{2-4}$$

The energy effectiveness may be defined as the ratio between the actual enthalpy rate difference ($\Delta\dot{\mathrm{H}}$) and the maximum allowable change in the enthalpy rate($\Delta\dot{\mathrm{H}}_{\mathrm{max}}$). $\Delta\dot{\mathrm{H}}_{\mathrm{max}}$ may be estimated either by the hot fluid stream or by the cold fluid stream based

on their heat capacity rates. $\Delta\dot{H}_{max}$ is always estimated by the lower heat capacity rate fluid stream ($Note\ that\ \dot{H} = \dot{m}\,.\,h$). $\Delta\dot{H}_{max}$ may be estimated either by the hot fluid stream or by the cold fluid stream, based on their heat capacity rates ($\dot{m}\,.\,c_p$). $\Delta\dot{H}_{max}$ is always estimated by the lower heat capacity rate fluid stream.

5- The dehumidifier effectiveness (ϵ_D): it may be defined by this equation

$$\epsilon_D = \max\left(\epsilon_{D,air}, \epsilon_{D,water}\right) \tag{2-5}$$

$$\epsilon_{D,air} = \frac{h_{a,in} - h_{a,out}}{h_{a,in} - h_{a,out,ideal}} \tag{2-6}$$

$$\epsilon_{D,water} = \frac{h_{w,out} - h_{w,in}}{h_{w,out,ideal} - h_{w,in}} \tag{2-7}$$

Where h represents the enthalpy, the subscript (a) represents the humid air, (w) represents the water. The ideal condition for the exiting air from the dehumidifier is humid air at the minimum possible temperature (seawater inlet temperature) which has relative humidity equal to 1 (fully saturated humid air) [8–10].

6- The humidifier effectiveness (ϵ_H): In the same way, it may be defined by this equation.

$$\epsilon_H = \max\left(\epsilon_{H,air}, \epsilon_{H,water}\right) \tag{2-8}$$

$$\epsilon_{H,air} = \frac{h_{a,out} - h_{a,in}}{h_{a,out,ideal} - h_{a,in}} \tag{2-9}$$

$$\epsilon_{H,water} = \frac{h_{w,in} - h_{w,out}}{h_{w,in} - h_{w,out,ideal}} \tag{2-10}$$

The ideal condition for the air at the humidifier exit is saturated air (relative humidity equal 1) at the maximum possible temperature which equals the water inlet temperature to the humidifier. On the other hand, the ideal condition for the water at the humidifier exit is subcooled water at the temperature which equals the wet-bulb temperature for the humid air at the humidifier inlet [8–10].

7- Top temperature or maximum temperature**:** for all HDH cycles, the top temperature is the temperature of the heated fluid at the heater outlet. For instance, in the water heated HDH cycle, the top temperature is the water temperature at the water heater exit (the temperature of the injected heated water to the humidifier) [1].

8- The bottom temperature or minimum temperature**:** is the feedwater temperature at the dehumidifier inlet which is the minimum temperature in the cycle [1].

9- Modified heat capacity ratio (HCR): It is a dimensionless parameter that equals to the ratio between the maximum allowable heat transfer to the cold stream ($\Delta\dot{H}_{max,cold}$) and the maximum allowable heat transfer from the hot stream ($\Delta\dot{H}_{max,hot}$). It may be described as:

$$HCR = \frac{\Delta\dot{H}_{max,cold}}{\Delta\dot{H}_{max,hot}} \quad (2\text{-}11)$$

The cold stream in the humidifier is the air and the hot stream is the water. On the other hand, the cold stream in the dehumidifier is the water and the hot stream is the air [13].

2.1 Closed-air open-water (CAOW) water-heated system.

As shown in Figure 2-1, a simple CAOW-HDH cycle consists of three main parts which are the humidifier, the water heater, and the dehumidifier. In the humidifier, the hot water exiting from the water heater is injected through nozzles placed at the top of the humidifier to be in direct contact with the air coming from the bottom of the humidifier in a counter direction. The path describing the change in the temperature and the humidity ratio on the psychometric chart is represented in Figure 2-2 by line 1-2. Due to the heat and the mass transfer from the water to the air, the temperature and the humidity ratio of the air increase along with the humidifier height. In the dehumidifier, the hot humid air exiting from the humidifier is cooled using seawater pathing through the heat exchanger tubes to condensate some of the water vapor carried by the dry air to obtain pure water. The path describing the change in the air properties (the temperature and the humidity ratio) during the dehumidification process may be presented on the psychometric chart by line 2-1 as shown in Figure 2-2 [1, 2].

The humid air exiting from the dehumidifier is recirculated again mechanically by a fan or a blower or naturally to the humidifier, so the air stream is a closed path. The cooling feed seawater is heated by recovering the condensation latent heat of the water vapor during the dehumidification process. The preheated water exiting from the dehumidifier is heated again by any heat source (solar energy, waste energy, and geothermal energy) within any heat exchanger before injecting it in the humidifier [1, 2].

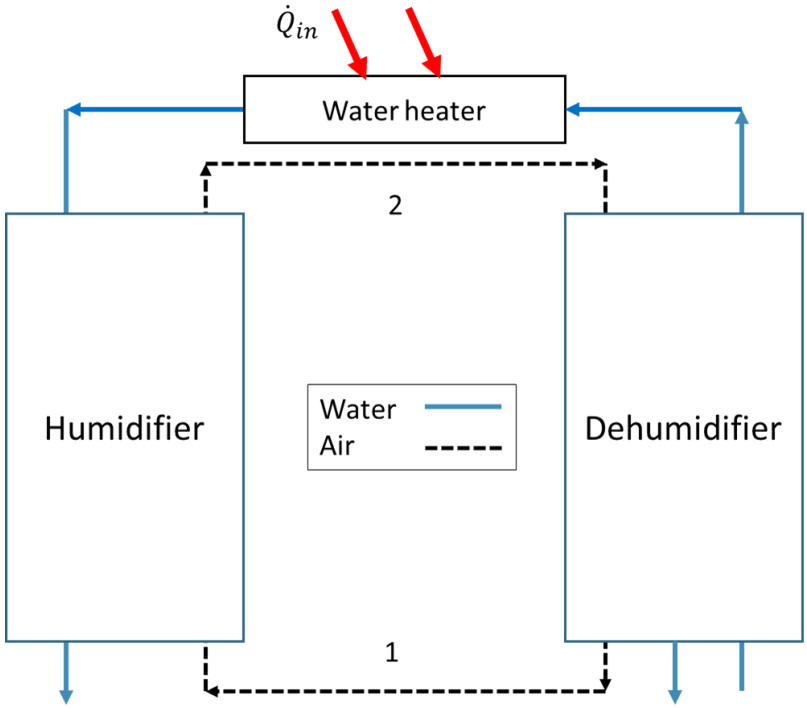

Figure 2-1: CAOW -Water heated HDH cycle.

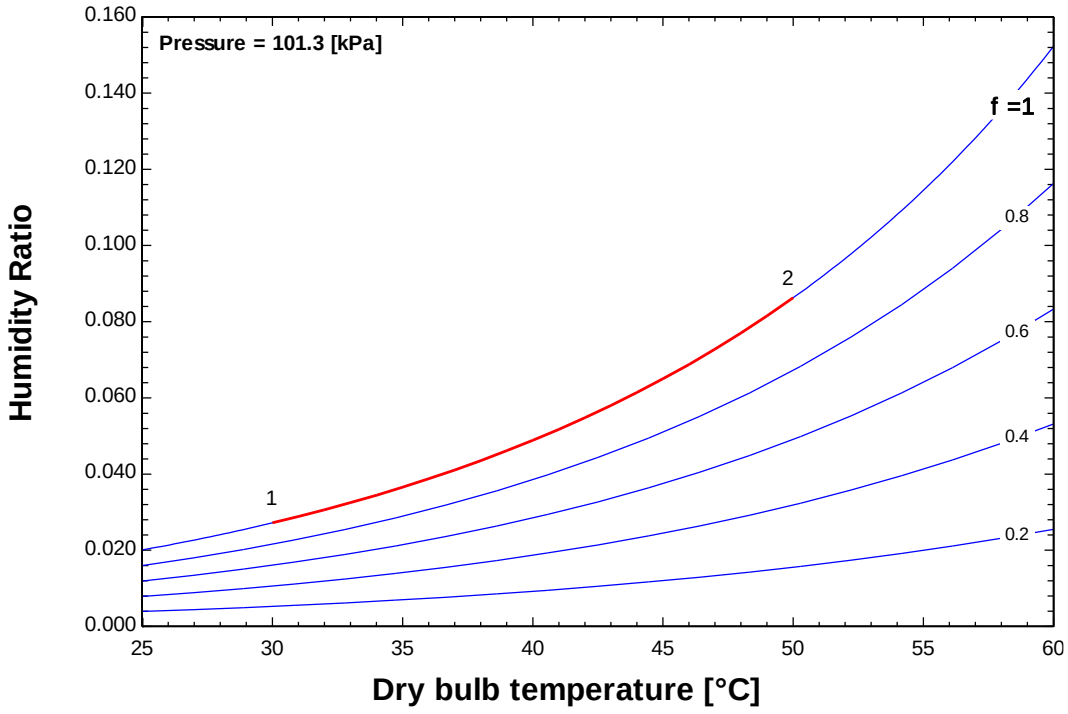

Figure 2-2: The CAOW water heated HDH cycle on the psychometric chart [1].

Many previous studies have been conducted on the performance of this type of HDH cycle. As shown in Table 2-1, there is a summarized description of the system used in each previous study and the main important observation related to the performance parameters of each system. From these previous studies, there are some common observations leading to optimizing the performance of this type of HDH cycle. The first observation is that the performance parameters of HDH systems (RR, GOR, and $\dot{m}_{PW}$) are functions in both of the dry airflow rate ($\dot{m}_{da}$) and the feed water mass flow rate ($\dot{m}_w$). For instance, for a fixed mass flow rate of dry air ($\dot{m}_{da}$), the performance parameter has an optimum value corresponding to a certain mass flow of the feed water ($\dot{m}_w$). The second common observation is that the natural air circulation cycle has higher performance than the forced air circulation cycle for the same size and the same operating conditions for the CAOW–water heated HDH cycle. The exact explanation for this observation (higher performance for natural air circulation) could not be illustrated in the previous studies [14–21].

Based on the previous studies mentioned in Table 2-1 [14–21], The GOR of this type of HDH cycle fluctuates between 1.2 and 4.5. Instead of using GOR to estimate the energy efficiency of the HDH cycle, the energy consumption rate may be used which has a value between 140 and 550 kW.h/m^3 [1]. The other desalination techniques like MED, RO and MSF are more energy-efficient than the HDH technique. For instance, the energy consumption rate for RO plants fluctuates between 4 and 10 kW.h/m^3 [1]. On the other hand, the energy consumed in HDH cycles may be free energy like solar energy or waste energy from exhaust gases, so the GOR is a thermal analysis parameter and not a direct economic analysis parameter for producing pure water.

According to the previous study conducted by Ben-Bacha et al. [16], the reason for the lower GOR value for the HDH system in this study was that the system did not make use of the latent heat of condensing water vapor transferred to the cooling water. For instance, the cooling water after passing through the dehumidifier was rejected and another stream of water was injected in the humidifier. To obtain a higher GOR value, Müller-Holst et al. [19] designed an intensive latent heat recovery HDH system. To sum up, recovering the latent heat has a significant effect on energy consumption and the cost of producing pure water in the HDH cycles.

Table 2-1: Summary of previous studies for water heated CAOW systems

Ref.	Main features of the unit	Outcomes
Al-Hallaj et al. [15]	• The heat input is by a flat plate water solar collector. • The top temperature range is 50 to 70 ^{o}C. • Air circulation is by natural convection or forced convection (for comparison) • Two different sizes and material units (Bench unit –pilot unit). • Humidifiers of wooden surfaces the surface area for the bench unit = 87 m^2/m^3, and for the pilot unit = 14 m^2/m^3 • The condenser surface area of the humidifier for the bench unit = 0.6 m^2 and for the pilot unit = 8 m^2.	• Productivity is a function of the feedwater flow rate ($\dot{m}_w$). • As $\dot{m}_w$ increases, the productivity increases to an optimum value and after that productivity decreases since the overall heat transfer coefficient is a function of $\dot{m}_w$. • At lower top temperatures, the performance of the force circulation cycle is better than the natural circulation cycle and at higher top temperatures, the natural circulation cycle has better performance than the forced circulation cycle.
Ben-Bacha et al. [16]	• Simulation and experimental study. • The heat source was by a solar collector (Area = 6 m^2) or by geothermal energy. • The control input parameters were the inlet water temperature and the humidity and the temperature of the inlet air. • The cooling fluid was salty water from a well. • Using Thorn trees as packing material in the humidifier. • Polypropylene was the material of the dehumidifier plates.	• The productivity of the system ($\dot{m}_{pw}$) is about 19 kg/day. • Using thermal storage saves 16 % of the required area of the solar collector to obtain the same productivity of the system ($\dot{m}_{pw}$). • The most important parameters that govern the performance of the system are the inlet water temperatures to the system, the inlet feed water mass flow rate ($\dot{m}_w$) and the inlet air mass rate.

Farid et al. [17]	• The heat input was by a solar collector (Area = 1.9 m^2). • Forced air circulation cycle. • The packed bed was made of wooden shaving. • Using a shell and tube heat exchanger for the dehumidification process.	• The productivity of the system = 12 L/m^2 • The effect of the air mass flow rate on productivity cannot be described. • $\dot{m}_w$ influenced the productivity • There was an optimum $\dot{m}_w$ corresponding to the maximum productivity.
Garg et al. [18]	• The heat input was by a flat plate solar collector (Area = 2 m^2). • Natural air circulation only • Using a 500 L thermal storage tank to be able to run the system longer hours. • Humidifier: 1.5 × 0.5 ×1.00 m. • Dehumidifier: 1.5 × 0.5×0.5 m. • The cooling fluid in the dehumidifier was water (There was heat recovery).	• The water inlet temperature to the humidifier influenced the performance of the cycle. • The heat losses in the humidifier and the dehumidifier influenced the performance judging of the system.
Nafey et al. [14]	• The heat input was by two heaters (a solar concentrator water heater and a solar air heater). • The packed bed material in the humidifier was the canvas. • There was not any heat recovery in the dehumidifier.	• The maximum productivity ($\dot{m}_{pw}$) was 1.2 Kg /h. and about 10.25 kg daily. • For the same inlet air temperature, as the air mass flow rate increases, the productivity decreases. • For the same feedwater mass flow rate to the humidifier, as the air mass flow rate increases, the productivity decreases.

Nawayseh et al. [20]	• An experimental comprehensive study on three systems having different designs for the humidifier and the dehumidifier (In Jordon and Malaysia). • A comprehensive study on the mass and the heat transfer mechanism in the humidifier and the dehumidifier. • Solar collectors used as heat sources. • The maximum water temperature was from 70 to 80 ^{o}C. • Natural and forced air circulation. • The packing material in the humidifier was wooden plates (inclined and vertical). • There was heat recovery in the dehumidifier.	• The maximum $\dot{m}_{pw}$ was about 2.5 L/h. • The water mass flow rate had greater effects on the mass and heat transfer coefficients and productivity than the air mass flow rate. • The natural circulation cycle had better performance than the forced circulation cycle.
Müller-Holst et al. [19]	• Natural air circulation cycle. • 38 m^2 solar collector as a heat source. • The maximum water temperature in the cycle was from 80 to 90 ^{o}C. • For operating the system 24 hours continuously, a 2 m^2 thermal storage tank has been used. • The exit water temperature from the dehumidifier reaches 75 ^{o}C due to the heat recovery.	• The productivity was about 0.5 m^3 daily. • The GOR of the system fluctuated between 3 and 4.5. • The economic benefit of using a thermal storage tank to be able to operate the system 24 hours continuously is to reduce the cost of producing pure water by 50%

Klausner et al. [19]	• Untraditional HDH system. • The heat input was by waste heat from a power plant. • The topwater temperature was 60 ^{o} C. • Using polyethylene as packing material in the dehumidifier (direct contact type). • Using some of the product pure water as a cooling fluid to recover the heat from the brine hot water exiting from the humidifier and the humid air in the condenser.	• As $\dot{m}_w$ increases, RR decreases and the energy required for producing 1 kg of the pure water increases (neglected solar energy consumption). • The RR in this study called the production efficiency. • The RR for this system reaches 8%. • As $\dot{m}_w$ increases, the productivity increases • The productivity, RR and the energy required for producing 1kg of pure water are a function in $\dot{m}_{da}$ and $\dot{m}_w$
Younis et al. [21]	• Theoretical and experimental study • The solar irradiation heats the saline water exiting in a solar pond (thermal open storage tank with a bottom area equals 1700 m^2) to be injected after that in the humidifier. • Using fans for circulating the air (forced convection cycle). • Using brackish seawater as a cooling fluid in the dehumidifier and to recover the condensation latent heat of water vapor in the humid air.	• Productivity is a function in the $\dot{m}_w$ and $\dot{m}_{da}$ • Changing $\dot{m}_{da}$ has a greater effect on productivity than changing $\dot{m}_w$. • The maximum productivity was about 14 kg /hr.

2.2 Multi-effect CAOW water-heated system

As mentioned in the previous section, recovering the latent heat in the dehumidifier improves the thermal efficiency of the HDH cycle. One of the ways that used to enhance recovering the heat in the CAOW water heated HDH cycle is to extract some of the humid air from the humidifier at several different points to the dehumidifier as shown in Figure 2-4 [22–26]. This improvement has been conducted by Müller-Holst et al. [19] called the multi-effect HDH cycle. After that many studies have discussed in detail the reason for improving the thermal efficiency of the HDH cycle using multi extractions by applying thermal analysis on the cycle (entropy generation analysis). Using multi-effects in the CAOW water heated HDH cycle causes a decrease in the total entropy generation in the cycle [27].

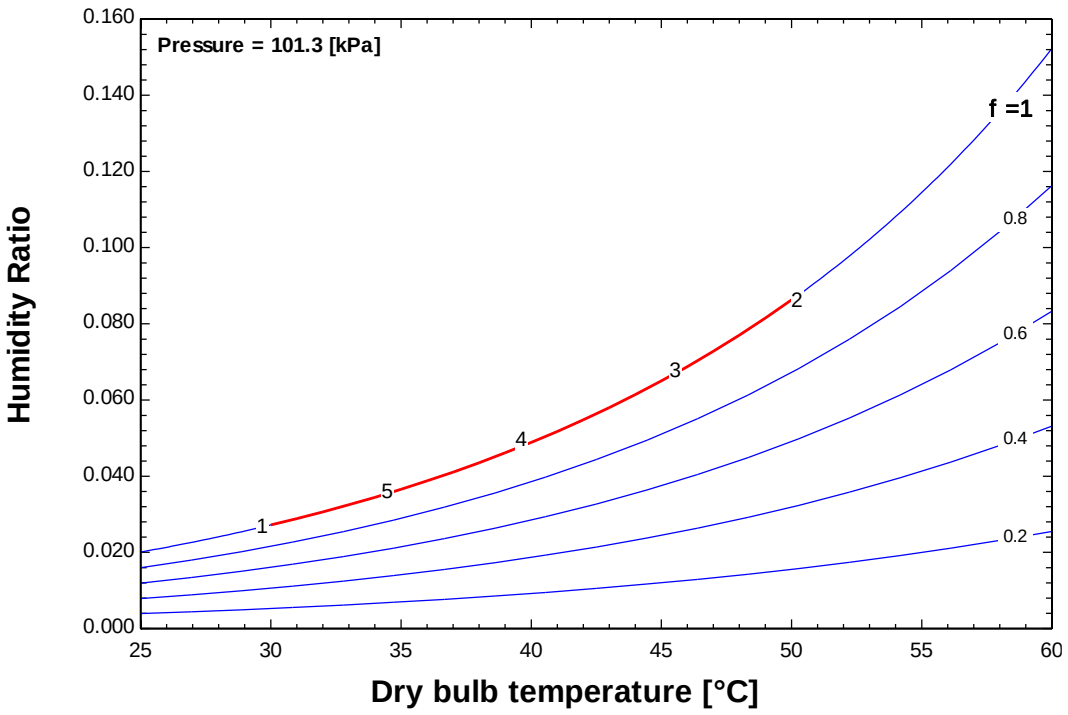

Figure 2-3: Psychometric chart of multi-effect CAOW water-heated HDH cycle [1].

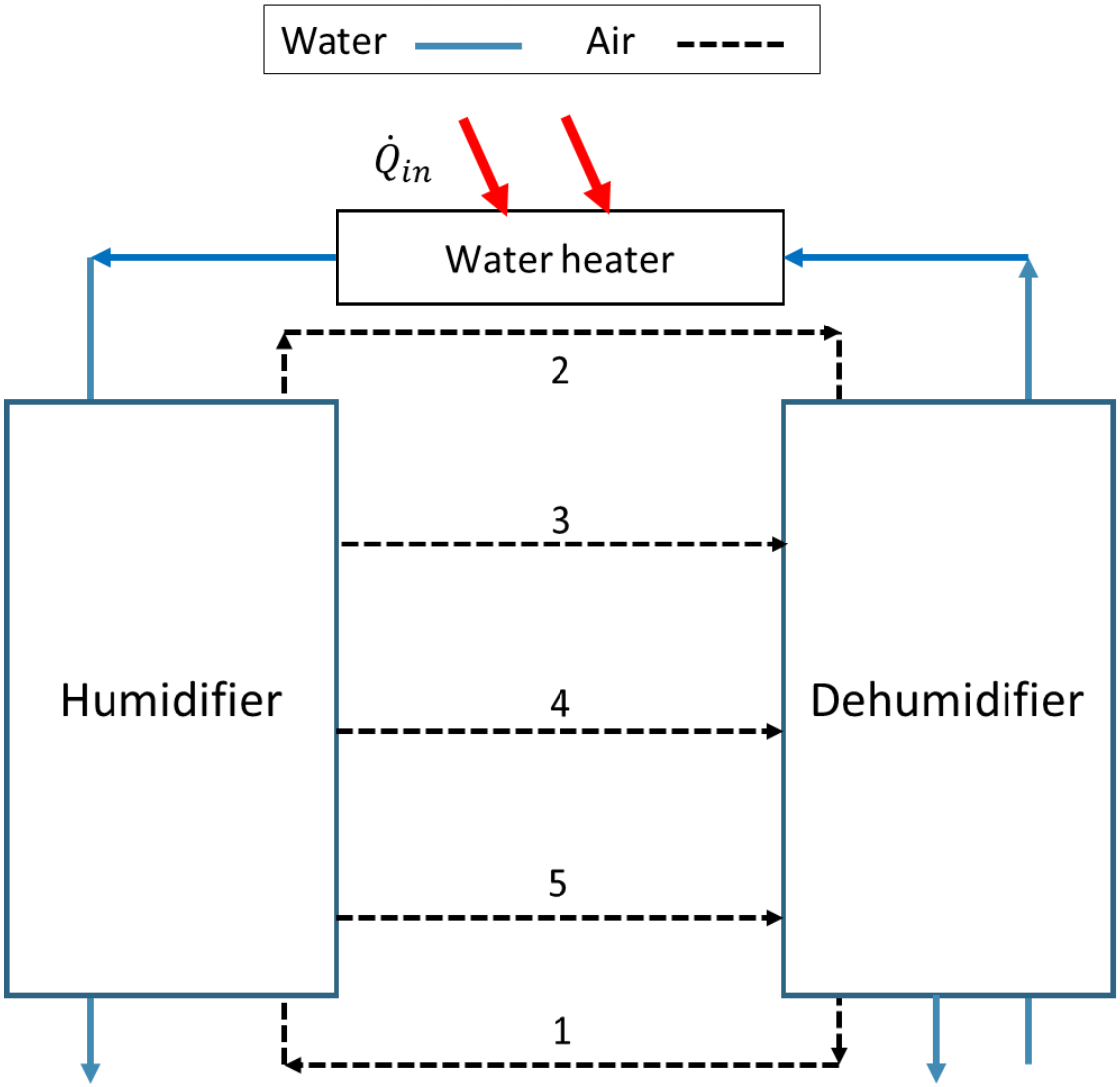

Figure 2-4: Multi-effect CAOW water-heated HDH cycle.

2.3 Goals of the current study.

This work focuses on the thermodynamic balancing of the humidification dehumidification desalination cycle through air extractions and injections. The first part of this study (Chapter 3) models a complete HDH system with multiple air extractions and injections from a fixed-effectiveness perspective by using the enthalpy pinch, as defined by Narayan et al [13], as a measure of the size of the components used. This approach is useful since it allows the modeling of the heat and mass exchangers used without the need for a specific transport model and allows the understanding of the thermodynamics of the cycle.

In Chapter 3, we present the model and its solution algorithm, and we study the effect of the enthalpy pinch and the number of extractions/injections, single and double, on the performance of the system. In addition, we present results that can be used as guidelines in the design of HDH systems, such as optimal positions of the extractions/injections, as well as optimal operating mass flow rate ratios in each stage. Also, it is important to specify the limitation of using single and double extractions considering the effect of maximum and minimum temperatures.

In Chapter 4, We present an experimental investigation to achieve thermodynamic balancing, consequently the optimum performance of the system. The first part is related to the zero extraction cycle, and we study the effect of operating conditions like the mass flow rate ratio and the input heat rate on the performance parameters (GOR, RR, and Productivity). The second part is related to the effect of using single and double extractions on the performance parameters.

2.4 Objectives of the current study.

The overall objective of this research is to study the closed-air open-water humidification-dehumidification desalination system. In this research, the HDH system was investigated by making both theoretical and experimental studies and optimized with the main objective of providing a positive contribution to the environment protection. Also, in this research, extraction technique (thermodynamic balancing) was applied between the dehumidifier and the humidifier to decrease energy consumption which increases the system performance. The specific objectives of the current study are ordered in sequence and can be summarized as follows:

1. An updated literature review is conducted to examine the state of HDH systems in general and the effect of thermodynamic balancing on enhancing the system performance.

2. Steady-state mathematical formulation and investigation of simultaneous heat and mass transfer for both dehumidifier and humidifier with/without considering extraction between the dehumidifier and humidifier. In this regard, a computer program using Matlab® and EES® software was used to simulate the system.

3. The performance of the system as a function of system design parameters was studied. The impact of operating parameters was studied and the critical operating variables were evaluated.

4. Different experiments (considering thermodynamic balancing) were conducted under different operating conditions and compared with the simulated results.

CHAPTER 3

Thermodynamic Balancing of HDH Desalination.

3.1 Modeling

3.1.1 Balancing Definition

According to the principle of diffusion, the difference in temperature between the hot stream and the cold stream is the driving force in the heat exchanger devices while the difference in mass concentration is the driving force in the mass exchanger devices. In the HDH cycle, for example, the humidifier is a heat and mass exchanger, so the driving force is the difference in the mass concentration and the difference in temperature. The HDH cycle may be called a balanced HDH cycle when the driving force between the saline water and humid air is kept the same along both streams in the humidifier and the dehumidifier [28].

The balanced HDH cycle may be considered the ideal operating condition cycle. For instance, balancing the humidifier causes the mass transfer from the saline water to the humid air to be optimized while balancing the dehumidifier causes the rate of condensation of water vapor to be optimized and the heat recovered from the humid air to be maximized. As the temperature difference (gap) between the hot and the cold stream in the thermal balanced HDH cycle is fixed, the temperature profile (variation) of the saline water is parallel to the temperature profile (variation) of the humid air in both humidifier and dehumidifier. On the other hand, in the thermal unbalanced HDH cycle, the dissimilarity

in the heat capacity rate ($\dot{m}\ c_p$)between the hot and the cold streams causes the temperature profile of the humid air to be not parallel to the temperature profile of the saline water in both humidifier and the dehumidifier. When the hot stream becomes unable to transfer more heat to the cold stream (as both streams have different heat capacity rates), the temperature gap between both profiles increases as shown in Figure 3-1. Therefore, the performance of the thermal unbalanced cycle is less efficient than the thermal balanced HDH cycle [28].

According to numerous previous studies [27, 29–34], extracting the humid air from the humidifier to be injected in the dehumidifier has been suggested to balance the HDH cycle. Adjusting the heat capacity ratio of the humid air and the saline water by extraction and injection between the humidifier and the dehumidifier may make the temperature gap between the humid air and the saline water nearly fixed. As shown in Figure 3-2, using a single extraction of saline water stream from the dehumidifier to the humidifier can adjust the temperature profile shape of the saline water in the dehumidifier to be more parallel to the humid air temperature profile as compared with unbalance case in Figure 3-1. As shown in Figure 3-3 and Figure 3-4, using multiple extraction and injection between the humidifier and dehumidifier can make the temperature gap between the saline water and the humid air fixed along the length of the humidifier and the dehumidifier (fully balanced).

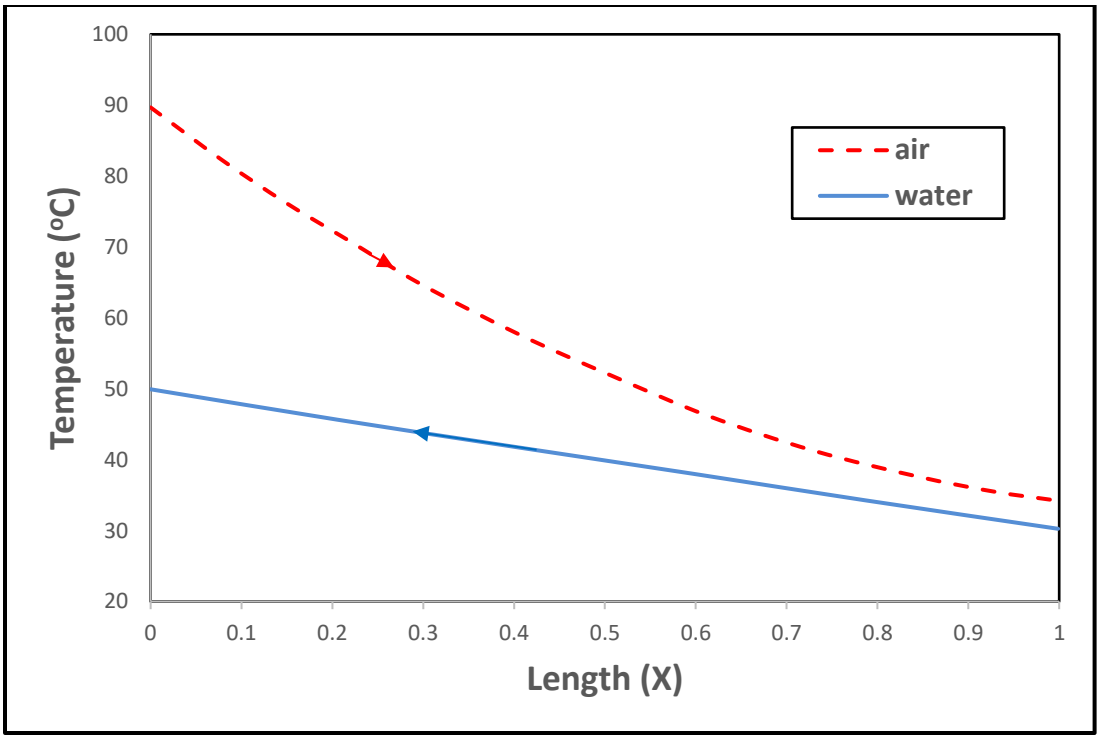

Figure 3-1: Temperature distribution of an unbalanced dehumidifier [35].

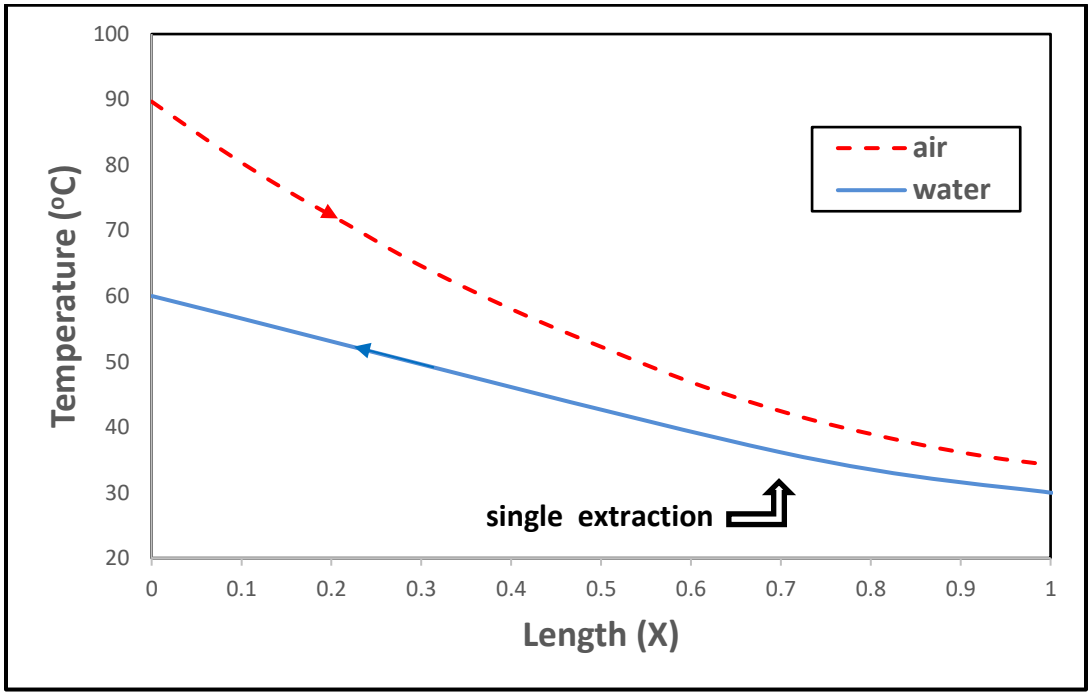

Figure 3-2: Temperature distribution of a dehumidifier with a single extraction [35].

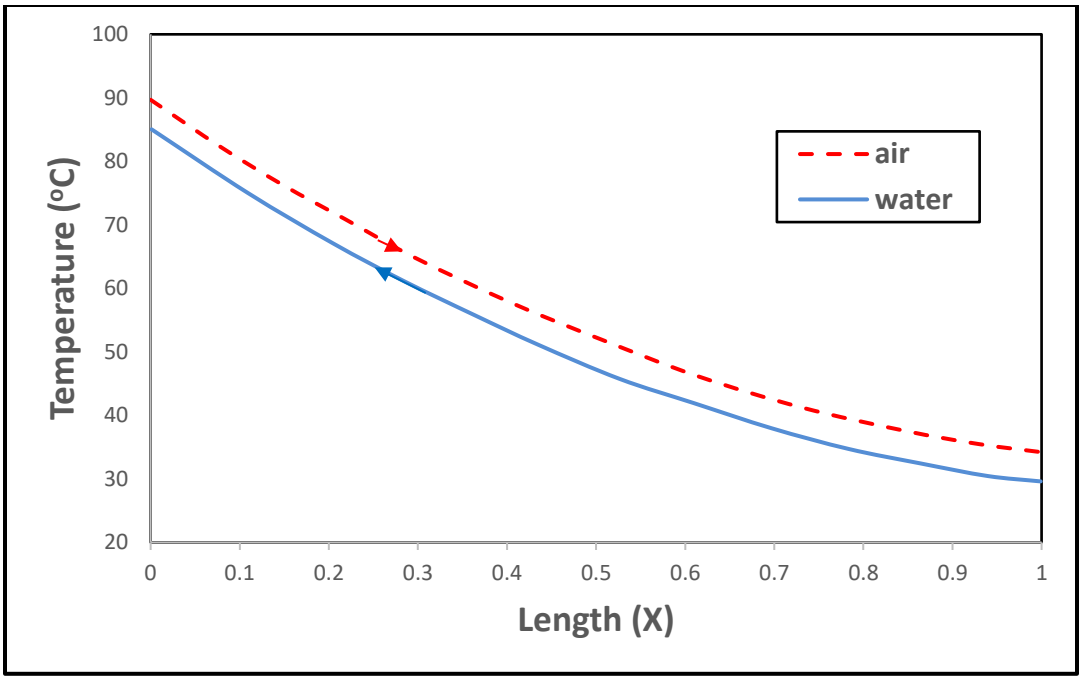

Figure 3-3: Temperature distribution of a dehumidifier with multi extractions [35].

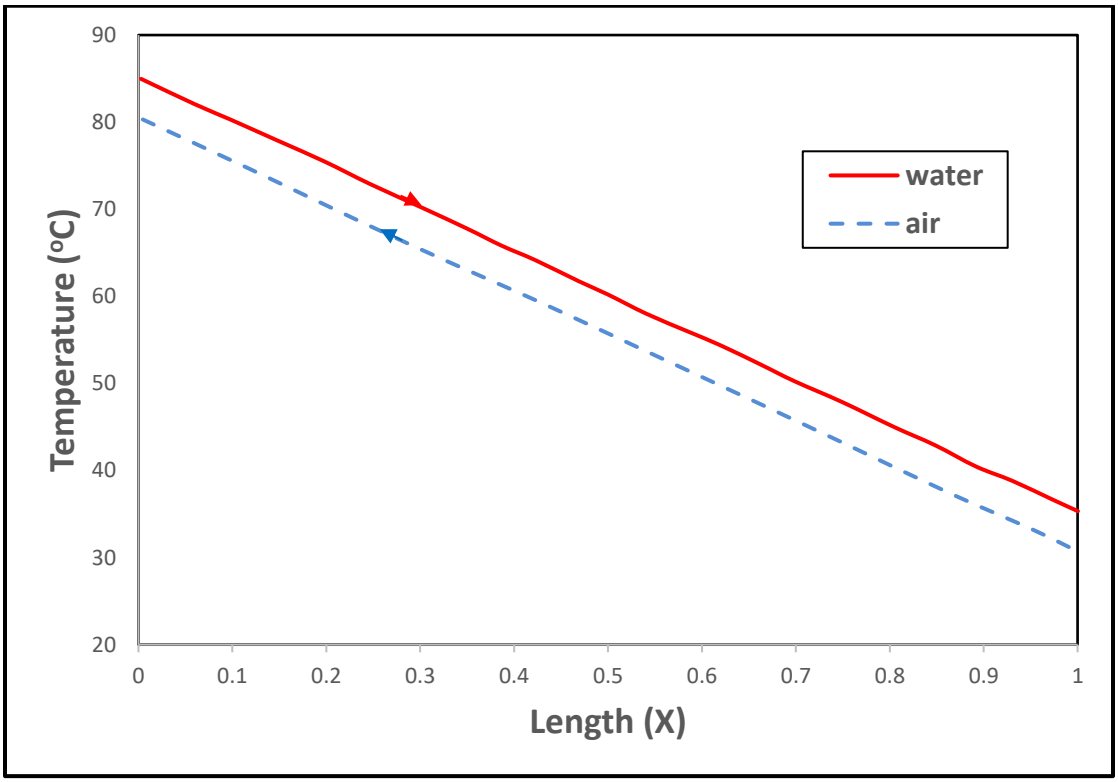

Figure 3-4: Temperature distribution of a humidifier with multi extractions [35].

According to previous studies [29, 30, 36] on the thermodynamic analysis of the heat and mass exchangers devices like humidifiers and dehumidifiers, the total entropy generation is minimized when the modified heat capacity ratio (HCR) equals to unity. Therefore, the performance of the HDH cycle is optimized when the HCR of the dehumidifier equals unity. This condition may also be considered the thermodynamic balancing condition for any control volume with fixed energy effectiveness. The HCR is a dimensionless parameter that equals to the ratio between the maximum allowable heat transfer to the cold stream ($\Delta\dot{H}_{max,cold}$) and the maximum allowable heat transfer from the hot stream ($\Delta\dot{H}_{max,hot}$) as mentioned before in equation (2-11).

3.1.2 Enthalpy pinch definition.

According to previous studies [27, 29, 30, 34], The performance of the balanced HDH cycle may be estimated by a graphical method that mainly depends on the temperature-enthalpy diagram (THD). As shown in Figure 3-5, the THD describes the temperature change related to the specific enthalpy change for the humid air, saline water, and the pure water along the length of the humidifier and the dehumidifier. h^* is the enthalpy of the air or the water divided by the mass of the dry air. One of the merits of this diagram is to determine the enthalpy pinch at any position along with the humidifier and dehumidifier simply.

The local enthalpy pinch is the difference between the maximum allowable change in the specific enthalpy (Δh^*_{max}) and the actual change in the specific enthalpy (Δh^*) at any position as described below:

$$\psi_{local} = \Delta h^*_{max} - \Delta h^* \quad (3\text{-}1)$$

For example, as shown in Figure 3-5, the local enthalpy pinch at the dehumidifier outlet may be estimated as:

$$\psi_{deh,c} = \Delta h^*_{max,cold} - \Delta h^* \quad (3\text{-}2)$$

The local enthalpy pinch at the dehumidifier inlet may be estimated as:

$$\psi_{deh,h} = \Delta h^*_{max,hot} - \Delta h^* \quad (3\text{-}3)$$

The enthalpy pinch may be considered as an alternative to the definition of energy effectiveness. The enthalpy pinch and the energy effectiveness are a measure of the enthalpy lost as a result of the fixed size of the heat and mass exchanger. The energy effectiveness may be estimated as a function in the enthalpy pinch as follows:

$$\epsilon = \frac{\Delta h^*}{\Delta h^*_{max}} = \frac{\Delta h^*}{\Delta h^* + \psi_{pinch}} \quad (3\text{-}4)$$

ψ_{pinch} is the enthalpy pinch at the pinch point. The pinch point is the position at which the temperature difference between the hot- and cold-stream is minimum and consequently, the local enthalpy pinch is minimum. As shown in Figure 3-5, the pinch point of the dehumidifier is located either at the dehumidifier inlet or at the dehumidifier outlet. On the other hand, the pinch point of the humidifier is located at an intermediate position along the length of the humidifier (The position at which the slope of the humid air stream on THD is equal to the linear slope of water stream). Generally, the ψ_{pinch} of the humidifier and the humidifier may be defined as:

$$\psi_{pinch} = \min(\psi_{local}) = \min(\Delta h^*_{max} - \Delta h^*) \quad (3\text{-}5)$$

For the dehumidifier, it may be simplified as:

$$\psi_{pinch} = \min(\psi_{local}) = \min(\psi_{deh,c} - \psi_{deh,h}) \quad (3\text{-}6)$$

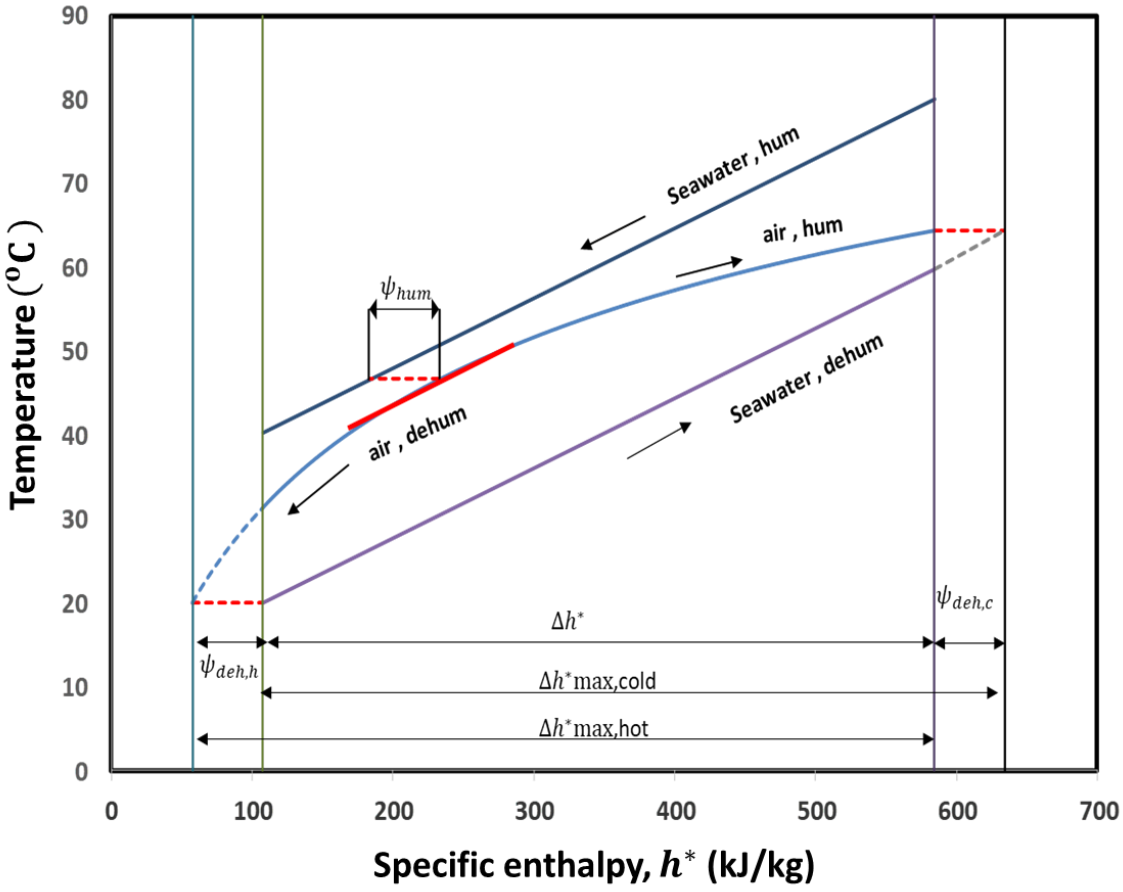

Figure 3-5: Temperature enthalpy diagram of a thermodynamic balanced HDH cycle without extraction [13].

The HCR of the dehumidifier may be described in another form (Figure 3-5) as:

$$\mathrm{HCR} = \frac{\Delta \dot{\mathrm{H}}_{\mathrm{max,cold}}}{\Delta \dot{\mathrm{H}}_{\mathrm{max,hot}}} * \frac{\dot{m}_{da}}{\dot{m}_{da}} = \frac{\Delta h^*{}_{\mathrm{max,cold}}}{\Delta h^*{}_{\mathrm{max,hot}}} = \frac{\Delta \mathrm{h}^* + \psi_{deh,c}}{\Delta \mathrm{h}^* + \psi_{deh,h}} \quad (3\text{-}7)$$

For a thermodynamically balanced HDH cycle, from the previous equation, $\psi_{deh,c} = \psi_{deh,h}$ as the HCR_{deh} = 1 and, for an unbalanced dehumidifier $\psi_{deh,cold} \neq \psi_{deh,hot}$. In the multi extraction and injection HDH cycle, the balancing condition may be applied for each stage of the humidifier and the dehumidifier.

3.1.3 Conservation equations and solution method.

As presented in Figure 3-6, the control volume consists of a part of the humidifier and a part of the dehumidifier separated by the water heater. The boundary of the control volume crosses the humidifier and dehumidifier in a certain position. At this position, the humid air temperatures in both the humidifier and dehumidifier are equal. Therefore, the specific humidity is the same in both the humidifier and dehumidifier since at this position the humid air is fully saturated during the cycle. This position represents a vertical line on the THD at which the specific enthalpy is constant. The mass balance of water stream passing through the control volume may be expressed as:

$$\dot{m}_{w,hum} = \dot{m}_{w,deh} - \dot{m}_{pw,loc} \quad (3\text{-}8)$$

where $\dot{m}_{pw,loc}$ represents the pure water mass flow rate produced during the part of the dehumidifier intersected by the control volume. As the saline cooling water in the dehumidifier is not in direct contact with the humid air, the $\dot{m}_{w,deh}$ remains constant along the length of the dehumidifier. Therefore, the local mass flow rate of the saline water at any section of the humidifier may be estimated as:

$$\dot{m}_{w,hum} = \dot{m}_w - \dot{m}_{pw,loc} \quad (3\text{-}9)$$

where $\dot{m}_w$ is the saline water mass flow rate exiting from the water heater.

Figure 3-7 and Figure 3-8 represent two control volumes for two small slides of both the humidifier and dehumidifier. These two slides are formed as a result of moving the boundary of control volume in Figure 3-6 intersected both of the humidifier and dehumidifier from a certain position to another position. The THD model is based on applying the mass and energy balance on these two infinitesimally small control volumes (see Figure 3-6, Figure 3-7, and Figure 3-8). For the control volume in Figure 3-8, the mass and energy balance may be expressed as:

$$\dot{m}_{pw,1} - \dot{m}_{pw,2} = \dot{m}_{da}(\omega_2 - \omega_1) \quad (3\text{-}10)$$

$$(\dot{\mathrm{H}}_2 - \dot{\mathrm{H}}_1)_w - (\dot{\mathrm{H}}_2 - \dot{\mathrm{H}}_1)_{pw} = (\dot{\mathrm{H}}_2 - \dot{\mathrm{H}}_1)_a \quad (3\text{-}11)$$

The energy balance may be expressed in another form as:

$$\dot{m}_w C_{p,w} (\mathrm{T}_2 - \mathrm{T}_1)_w - \left[(\dot{m}C_pT)_{pw,2} - (\dot{m}C_pT)_{pw,1}\right] = \dot{m}_{da}(h_2^* - h_1^*) \quad (3\text{-}12)$$

The change in the local pure water during this infinitesimally small control volume may be neglected as compared with the temperature change. In this regard, the cooling saline water temperature and the pure water temperature at each section through the dehumidifier length may be considered the same. Therefore, the energy balance equation may be expressed as:

$$(\dot{m}_w - \dot{m}_{pw,loc})C_{p,w}(\mathrm{T}_2 - \mathrm{T}_1)_w = \dot{m}_{da}(h_2^* - h_1^*) \quad (3\text{-}13)$$

Therefore, the stream path of the water in the dehumidifier may be represented by a linear path on the THD as shown in Figure 3-5. From the previous equation, the slope of the linear path may be expressed as:

$$\frac{dT_w}{dh^*} = \frac{1}{m_r\, C_{p,w}} \tag{3-14}$$

where the mass flow rate ratio (m_r) is equal to:

$$m_r = \frac{\dot{m}_w - \dot{m}_{pw,loc}}{\dot{m}_{da}} \tag{3-15}$$

By the same way, the energy balance for the control volume of the humidifier (see Figure 3-7) may be expressed as:

$$(\dot{\mathrm{H}}_2 - \dot{\mathrm{H}}_1)_w = (\dot{\mathrm{H}}_2 - \dot{\mathrm{H}}_1)_a \tag{3-16}$$

Using equation (3-9) to estimate the local saline water mass flow rate in the humidifier, the previous energy balance equation may be expressed as:

$$\left(\dot{m}_w - \dot{m}_{pw,loc}\right) C_{p,w} (\mathrm{T}_2 - \mathrm{T}_1)_w = \dot{m}_{da}(h_2^* - h_1^*) \tag{3-17}$$

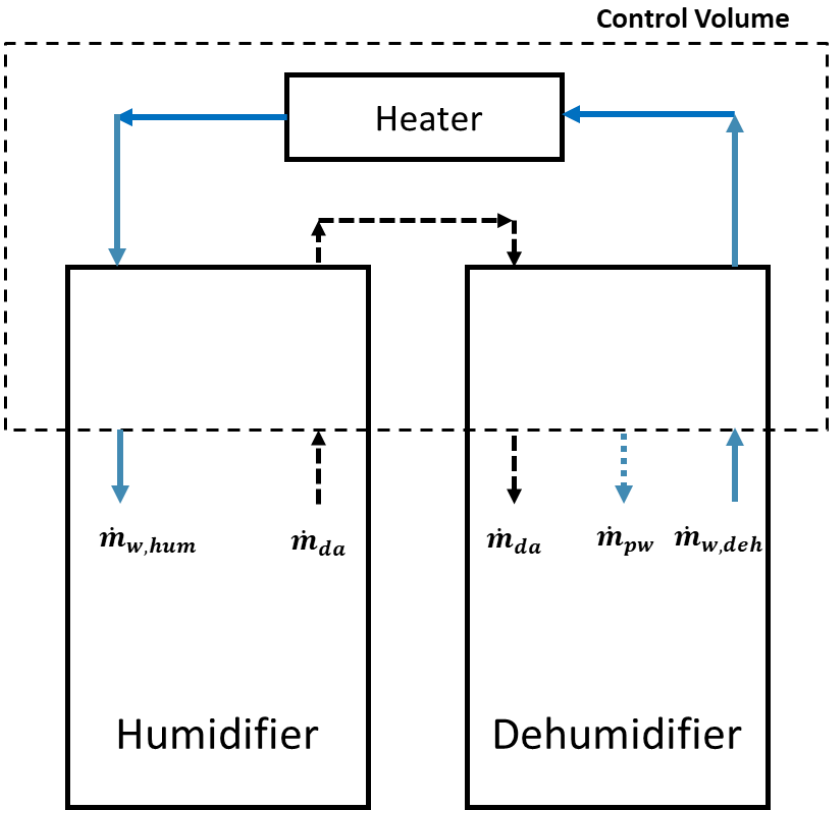

Figure 3-6: A control volume including a section of the humidifier and another section of the dehumidifier separated by the water heater [30].

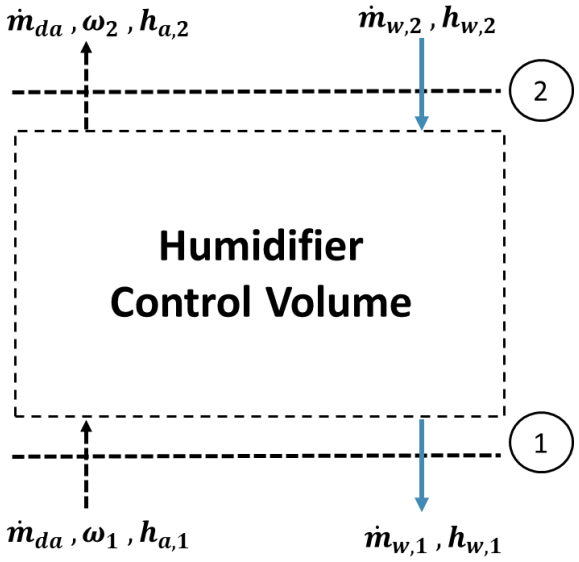

Figure 3-7: An infinitesimally small control volume of the humidifier [30].

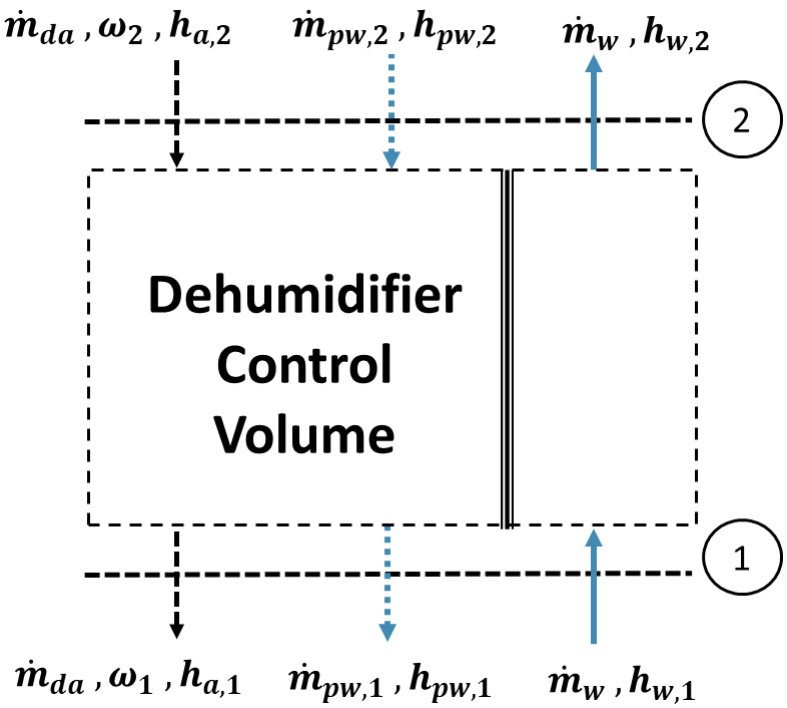

Figure 3-8: An infinitesimally small control volume of the dehumidifier [30].

Therefore, the stream path of saline water inside the humidifier on the THD is also a linear path with the same slope of the linear path representing the water stream in the dehumidifier that may also be estimated by the equation (3-14). According to equation (3-14), changing the mass flow rate ratio leads to a change in the slope of the linear paths representing the water stream inside both the humidifier and dehumidifier. Extracting the humid air from the humidifier at different positions to the dehumidifier leads to dividing the length of the humidifier and dehumidifier to multi-stages. As each stage has a different m_r, the slope of the water stream on the THD, as shown in Figure 3-9 is adjusted at each stage. Therefore, the temperature gap between the air stream and water stream becomes nearly fixed leading to balance the heat and mass transfer in both the humidifier and dehumidifier.

The procedure to solve the aforementioned system of equations (refer to Eqs. 3-8 - 3-17) of a thermodynamically balanced closed-air open-water, water-heated HDH system is described in the following paragraph.

The THD model is mainly based on the trial and error approach as shown in the flowchart of the model algorithm (see Appendix A). The input parameters of this model are the top temperature (water temperature exiting from the water heater), the bottom temperature (inlet feedwater temperature to the dehumidifier), the enthalpy pinch of the humidifier and dehumidifier and the number of extraction (N). Using this algorithm, all the performance parameters like GOR, RR, heat duty and the condition of the humid air and water through all the cycles can be estimated. The temperatures and mass flow rates of humid air extracted from the humidifier to dehumidifier leading to balancing condition can also be evaluated by this model.

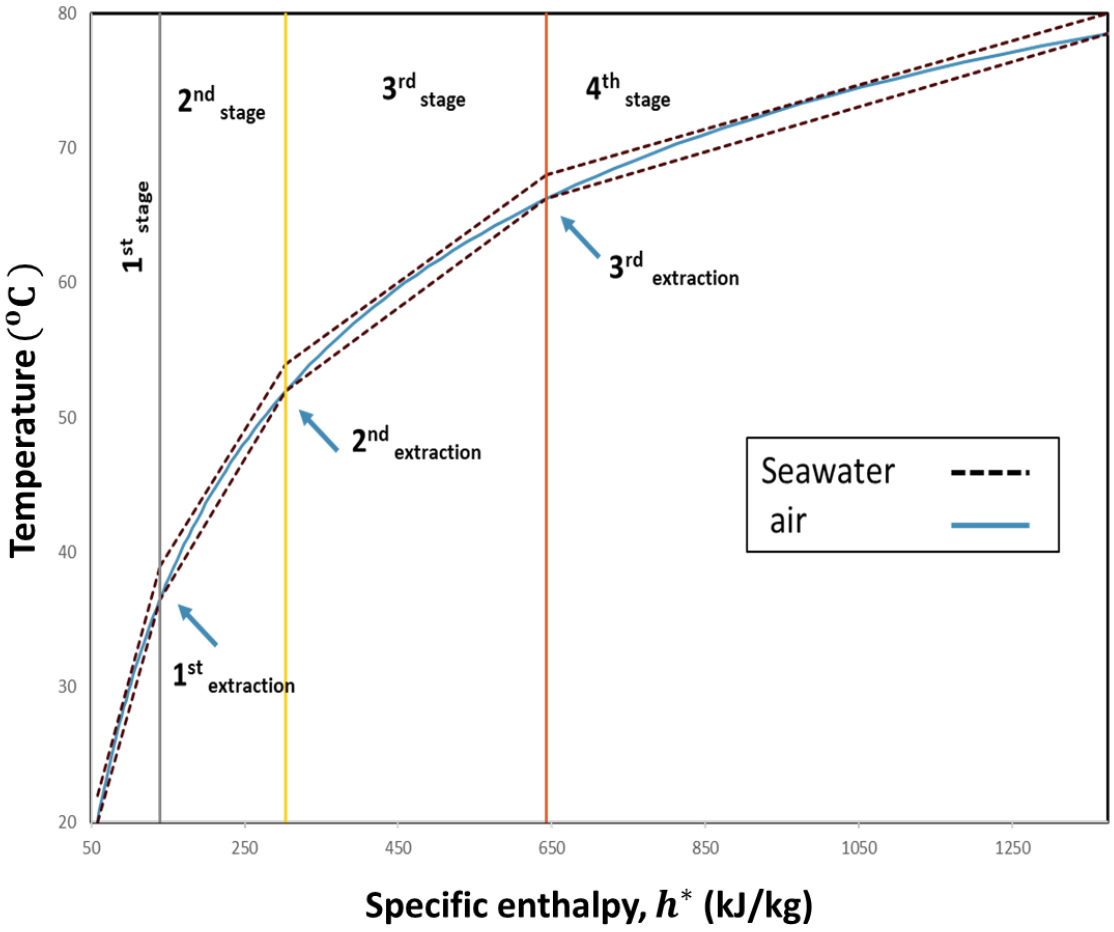

Figure 3-9: Temperature enthalpy diagram of a thermodynamically balanced HDH cycle with multi extractions [30].

3.1.4 Second law analysis

After estimating the inlet/outlet conditions of each component of the multi extractions HDH cycle by THD model, the second law analysis and consequently the exergy balance may be applied for each component of the cycle. Exergy is a measure of the maximum shaft work that may be produced from the system as a result of its non-equilibrium state with the environment. The physical exergy of the system is produced due to the difference in temperature (thermal exergy) and pressure (mechanical exergy) of the system compared

with the environment while the chemical exergy is due to the difference in chemical composition. Therefore, the exergy is not only a function in the system state but also is a function of the environment state. The origin of the exergy word is due to a Greek origin, in addition, the two words ex and ergon in the Greek language mean from work [37]. The exergy is also called essergy, availability and utilizable energy in many previous studies in the literature. The flow stream exergy of any substance ($\dot{\Xi}$) may be expressed as:

$$\dot{\Xi} = \dot{m} \,.\, \xi = \dot{\Xi}_{chemical} + \dot{\Xi}_{physical} \tag{3-18}$$

$$\dot{\Xi}_{physical} = \dot{m}[(h - h_o) - T_o(s - s_o)] \tag{3-19}$$

$$\dot{\Xi}_{chemical} = \sum_{i}^{n} w_s(\mu^* - \mu_i^o) \tag{3-20}$$

Where h, ξ, s, w_s, and μ are the specific enthalpy, specific exergy, specific entropy, mass fraction and the chemical potential. The subscript or the superscript (o) symbolizes the dead state conditions of the environment. The superscript (*) denotes that the only physical conditions are estimated at the dead state while the chemical conditions are at the same initial state.

The second law analysis is a measure of irreversible losses of the system by estimating the total entropy generation rate ($\dot{S}_{gen}$), the total exergy destroyed rate($\dot{\Xi}_d$) and the second law efficiency (η_{II}). For an open system at steady-state condition, the $\dot{S}_{gen}$and $\dot{\Xi}_d$ maybe expressed as:

$$\dot{S}_{gen} = \dot{S}_{out} - \dot{S}_{in} \geq 0 \tag{3-21}$$

$$\dot{\Xi}_d = \dot{\Xi}_{in} - \dot{\Xi}_{out} = T_o \dot{S}_{gen} \geq 0 \quad (3\text{-}22)$$

The inlet /outlet entropy may be due to the mass transfer or heat transfer between the system and environment while the exergy may be transferred between the system and environment due to mass, heat or work. According to Clausius inequality, the total entropy generation rate and consequently the total exergy destroyed rate is equal to zero for reversible processes. As the irreversibility in the system increases, the $\dot{S}_{gen}$ and $\dot{\Xi}_d$ increase. Therefore, the $\dot{S}_{gen}$ and $\dot{\Xi}_d$ are impossible to be negative for any process. The second law efficiency may be defined as the ratio between the useful exergy rate and the inlet exergy rate. The second law efficiency is equal to unity for reversible processes (the maximum value). The second law efficiency decreases as the irreversibility of the process increases. The minimum value of the second law efficiency is equal to zero [37– 42].

The second law efficiency may be expressed as:

$$\eta_{II} = \frac{\dot{\Xi}_{useful}}{\dot{\Xi}_{in}} = 1 - \frac{\dot{\Xi}_d}{\dot{\Xi}_{in}} \quad (3\text{-}23)$$

Figure 3-10 shows the inlet/exit conditions for each component of the multi extractions CAOW water heated HDH cycle. Therefore, the second law analysis may be conducted for each component separately, as presented in the next sections.

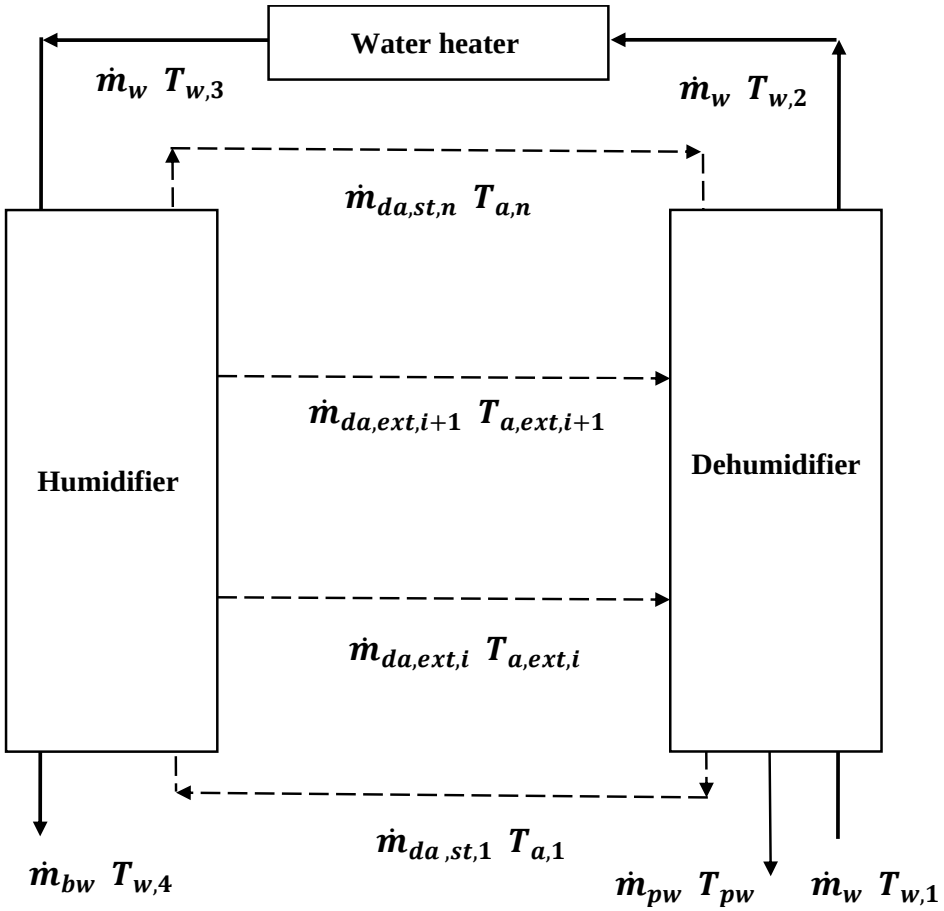

Figure 3-10: A multi extraction HDH cycle with the inlet/outlet condition of each component.

Dehumidifier

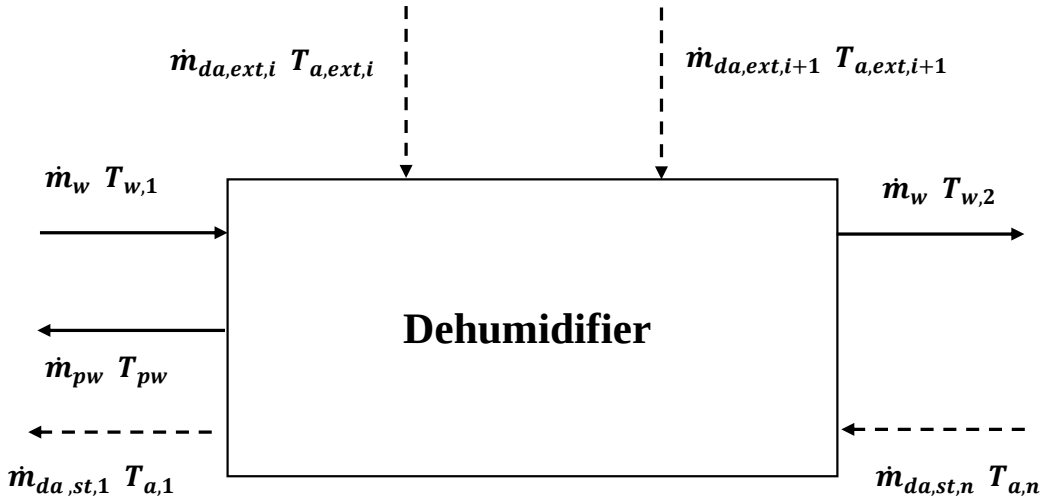

Figure 3-11: Dehumidifier control volume with the inlet/outlet condition.

$$\dot{m}_{da,st,n}\ s_{a,n} + \dot{m}_w\ s_{w,1} + \sum_{i=1}^{N}(\dot{m}_{da,ext,i}\ s_{a,ext,i}) - \left[\dot{m}_w\ s_{w,2} + \dot{m}_{da,st,1}\ s_{a,1} + \dot{m}_{pw}\ s_{pw}\right] + \dot{S}_{gen.D} = 0 \tag{3-24}$$

$$\dot{\Xi}_{d,D} = \dot{m}_{da,st,n}\ \xi_{a,n} + \dot{m}_w\ \xi_{w,1} + \sum_{i=1}^{N}(\dot{m}_{da,ext,i}\,\xi_{a,ext,i}) - \left[\dot{m}_w\ \xi_{w,2} + \dot{m}_{da,st,1}\ \xi_{a,1} + \dot{m}_{pw}\ \xi_{pw}\right] = T_o\dot{S}_{gen.D} \tag{3-25}$$

$$\eta_{II,D} = 1 - \frac{\dot{\Xi}_{d,D}}{\dot{m}_{da,st,n}\ \xi_{a,n} + \dot{m}_w\ \xi_{w,1} + + \sum_{i=1}^{N}(\dot{m}_{da,ext,i}\,\xi_{a,ext,i})} \tag{3-26}$$

Humidifier

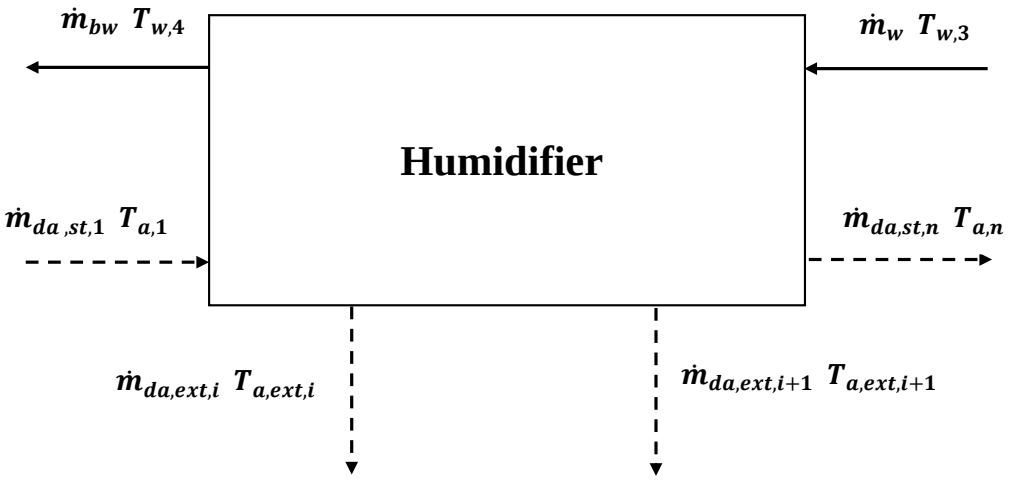

Figure 3-12: Humidifier control volume with the inlet /outlet condition.

$$\dot{m}_{da,st,1}\ s_{a,1} + \dot{m}_{w}\ s_{w,3} - \left[\dot{m}_{bw}\ s_{w,4} + \dot{m}_{da,st,n}\ s_{a,n} + \sum_{i=1}^{N}(\dot{m}_{da,ext,i}\ s_{a,ext,i})\right] + \dot{S}_{gen.H} = 0 \quad (3\text{-}27)$$

$$\dot{\Xi}_{d,H} = \dot{m}_{da,st,1}\ \xi_{a,1} + \dot{m}_{w}\ \xi_{w,3} - \left[\dot{m}_{bw}\ \xi_{w,4} + \dot{m}_{da,st,n}\ \xi_{a,n} + \sum_{i=1}^{N}(\dot{m}_{da,ext,i}\ \xi_{a,ext,i})\right] = T_o\ \dot{S}_{gen.H} \quad (3\text{-}28)$$

$$\eta_{II,H} = 1 - \frac{\dot{\Xi}_{d,H}}{\dot{m}_{da,st,1}\ \xi_{a,1} + \dot{m}_{w}\ \xi_{w,3}} \quad (3\text{-}29)$$

Water heater

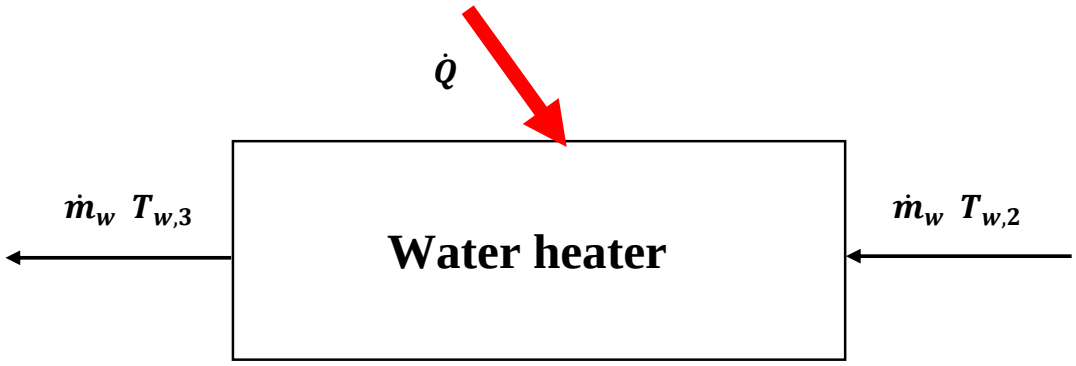

Figure 3-13: Water heater control volume with the inlet/outlet condition.

$$\dot{m}_w \ s_{w,2} + \dot{S}_{tran,HT} - \dot{m}_w \ s_{w,3} + \dot{S}_{gen.HT} = 0 \tag{3-30}$$

In the water heater, the entropy transferred to the system is not by mass flow only but also by heat flow. $\dot{S}_{tran,HT}$ is the rate of entropy transferred as a result of heat flow to the system. The difference between the wall tube temperature and water bulk temperature ($T_b(x)$) is fixed (ΔT) along the length of the tube (L) as the heat is transferred with constant heat flux ($\dot{Q}/L$).Therefore, the water bulk temperature along the tube length (x) may be defined as:

$$T_b(x) = T_{HT,in} + \frac{(\dot{Q}/L)}{\dot{m}_w C_{p,w}} \ x \tag{3-31}$$

The wall tube temperature may also be defined as:

$$T_{wall}(x) = T_b(x) + \Delta T = (T_{HT,in} + \ \Delta T) + \frac{(\dot{Q}/L)}{\dot{m}_w C_{p,w}} \ x \tag{3-32}$$

Therefore, the inlet entropy rate and exergy rate to the system due to heat transfer may be estimated as:

$$\dot{S}_{tran,HT} = \int_0^L \frac{\dot{Q}(x)}{T_{wall}(x)}\, dx = \dot{m}_w C_{p,w}\, \log\left[\frac{\dot{Q}}{\dot{m}_w C_{p,w}\,(T_{HT,in} + \Delta T)} + 1\right] \quad (3\text{-}33)$$

$$\dot{\Xi}_{trans,HT} = \int_0^L (1 - \frac{T_o}{T_{wall}(x)})\, \dot{Q}(x)\, dx = \dot{Q} - T_o \dot{S}_{tran,HT} \quad (3\text{-}34)$$

Therefore, the exergy destroyed in the water heater and second law efficiency may be defined as:

$$\dot{\Xi}_{d,HT} = \dot{m}_w\ \xi_{w,2} + \dot{\Xi}_{trans,HT} - \dot{m}_w\ \xi_{w,3} \quad (3\text{-}35)$$

$$\eta_{II,HT} = 1 - \frac{\dot{\Xi}_{d,HT}}{\dot{m}_w\ \xi_{w,2} + \dot{\Xi}_{trans,HT}} \quad (3\text{-}36)$$

3.1.5 Assumptions and approximations.

a) The effect of changing the salinity of the water through the cycle is neglected (the salinity of the water in the cycle = 35 ppt) [13, 43].

b) The specific heat of the water is fixed and estimated at an average temperature = 50 ^{o}C.

c) The relative humidity of humid air through the cycle equal to 1 (the uncertainty of this assumption is less than 10% as proved in previous studies [13, 43]).

d) The effect of changing the mass flow rate ratio at each stage as a result of changing the local pure water mass flow rate along the dehumidifier length is neglected (the error due to this assumption is less than 5% as proved in a previous study [43]). On the other hand, each stage has a different m_r compared with the other stages due to the humid air extraction and injection between the humidifier and dehumidifier .

e) The cooling saline water temperature and pure water temperature at each section through the dehumidifier length may be considered the same.

f) Neglecting the heat losses from each component of the cycle.

g) All the processes in the cycle under the steady-state condition.

h) Neglecting the change in the potential and kinetic energy through each component of the cycle.

i) Neglecting the consumed mechanical energy by a blower or a fan compared with the consumed thermal energy.

3.1.6 Property packages.

The Engineering Equation Solver (EES) software [44] can be used to calculate the properties of the humid air and seawater accurately. The ESS program uses the correlations developed by Lemmon [45] to estimate the ideal gas properties, the correlations developed by Hyland and Wexler [46] to estimate the humid air properties which are validated with the properties in ASHRAE Fundamentals [47] and the correlations developed by IAPWS [48] to estimate the pure water properties. Recently, the seawater library has been added to the EES program to estimate the seawater properties using the correlations presented by Sharqawy et al. [49].

3.2 Results and Discussion.

3.2.1 Model validation.

The current model has been validated against a model conducted in a previous study conducted by Chehayeb et al. [34] for a zero, single and double thermodynamically balanced water heated HDH cycle. The validation case was for the same minimum and maximum temperature in the cycle. The minimum temperature in the cycle is equal to inlet feedwater temperature to the dehumidifier that is equal to 20 ^{o}C in this case. The maximum temperature in the cycle is the inlet feed water temperature to the humidifier which is equal to 80 ^{o}C.

Table 3-1, Table 3-2 and Table 3-3 show the percentage error between the GOR by the current model and the GOR by Chehayeb et al. [34] model. The maximum error is about 3% for the double extraction model, about 1.9 % for the single extraction model and about 1 % for the zero-extraction model. The reason for this small error between the current model and Chehayeb et al. [34] is primarily due to using a different discretization and tolerance criteria.

Table 3-1: The percentage error between the current model and Chehayeb et al. [34] model for the zero extraction

Ψ (kJ/kg)	GOR (Chehayeb et al. model)	GOR (current model)	percentage error (%)
0	2.91	2.94	0.54
1	2.87	2.91	0.20
2	2.84	2.87	0.09
3	2.79	2.84	0.20
4	2.76	2.80	0.12
5	2.73	2.77	0.05
6	2.70	2.74	0.01
7	2.67	2.71	0.19
8	2.64	2.67	-0.36
9	2.61	2.64	-0.78
10	2.58	2.61	-0.29
11	2.54	2.58	0.21
12	2.52	2.55	-0.23
13	2.49	2.52	0.53
14	2.46	2.49	-0.37
15	2.44	2.47	-0.75
16	2.41	2.44	-0.68
17	2.39	2.41	-0.32
18	2.36	2.38	-0.16
19	2.33	2.35	0.46
20	2.32	2.33	-0.40
21	2.28	2.30	-0.19
22	2.25	2.2	0.01
23	2.23	2.25	-0.04
24	2.21	2.22	-0.37
25	2.18	2.20	-0.67
26	2.16	2.17	-0.73
27	2.13	2.15	0.47
28	2.11	2.12	0.13
29	2.09	2.10	-0.47

Table 3-2: The percentage error between the current model and Chehayeb et al. [34] model for the single extraction cycle

Ψ (kJ/kg)	GOR (Chehayeb et al. model)	GOR (current model)	percentage error (%)
0	8.52	8.65	1.46
1	8.19	8.3	1.31
2	7.87	7.97	1.20
3	7.60	7.65	0.69
4	7.33	7.36	0.37
5	7.09	7.08	-0.22
6	6.81	6.81	0.05
7	6.59	6.56	-0.42
8	6.37	6.32	-0.74
9	6.15	6.09	-0.90
10	5.94	5.87	-1.17
11	5.74	5.66	-1.29
12	5.56	5.46	-1.85
13	5.36	5.27	-1.69
14	5.17	5.08	-1.67
15	5.00	4.91	-1.82
16	4.81	4.74	-1.50
17	4.63	4.57	-1.40
18	4.48	4.41	-1.51
19	4.32	4.25	-1.51
20	4.16	4.10	-1.38
21	4.02	3.96	-1.52
22	3.88	3.82	-1.56
23	3.74	3.68	-1.53
24	3.59	3.55	-1.37
25	3.42	3.41	-0.22
26	3.30	3.29	-0.30
27	3.17	3.16	-0.32
28	3.06	3.04	-0.84
29	2.94	2.91	-0.79

Table 3-3: The percentage error between the current model and Chehayeb et al. [34] model for the double extraction cycle.

Ψ (kJ/kg)	GOR (Chehayeb et al. model)	GOR (current model)	percentage error (%)
0	17.60	18.13	2.92
1	16.16	16.56	2.36
2	14.92	15.19	1.76
3	14.01	13.97	-0.33
4	12.88	12.89	0.04
5	11.97	11.92	-0.49
6	11.18	11.04	-1.34
7	10.39	10.24	-1.54
8	9.49	9.50	0.07
9	8.70	8.81	1.31
10	8.13	8.18	0.50
11	7.57	7.57	0.04
12	7.01	7.00	-0.06
13	6.44	6.45	0.07
14	5.88	5.90	0.37

3.2.2 Variation of total exergy destroyed rate with enthalpy pinch.

Figure 3-14 shows the effect of the enthalpy pinch on the total exergy destroyed rate of the zero, single, and double thermodynamically balanced HDH cycle at $T_{max} = 80\ ^{o}C$ and $T_{min} = 20\ ^{o}C$. It is clear that increasing the enthalpy pinch leads to an increase in the total exergy destroyed. Increasing the enthalpy pinch means decreasing the energy effectiveness according to the equation (3-4). As the dehumidifier energy effectiveness decreases, the recovered latent heat of condensation decreases. Consequently, the systems need to add more heat to reach the same maximum temperature ($T_{max} = 80\ ^{o}C$). Therefore, the total exergy destroyed rate increases due to the increase in the heat input and by decreasing the thermal efficiency of the humidifier and dehumidifier. Using single and double extraction leads to a decrease in the total exergy destroyed. Changing the mass flow rate ratio by extraction leads to adjust the slope of the water stream on the THD (see Figure 3-9) to be parallel to the humid air stream. Therefore, the temperature gap between the water and humid air stream decreases compared to the zero extraction case (Figure 3-5), thus leading to minimizing the total exergy destroyed.

3.2.3 Variation of GOR with enthalpy pinch and number of extractions.

Figure 3-15, Figure 3-16, and Figure 3-17 show that the GOR of the HDH cycle is a function of enthalpy pinch of the humidifier and dehumidifier, in addition to the number of extractions. Decreasing the enthalpy pinch leads to an increase in the GOR of the HDH cycle by minimizing the total exergy destroyed rate. The total exergy destroyed is further decreased by using the single and double extractions, thus GOR further increases.

Decreasing the enthalpy pinch of humidifier leads to improve the evaporation process. On the other hand, decreasing the enthalpy pinch of the dehumidifier leads to improve the condensation process. It can be seen in Figure 3-15, Figure 3-16, and Figure 3-17, the enthalpy pinch of dehumidifier has more effect on the GOR than the humidifier enthalpy pinch. The reason for this observation is that if the humidifier energy effectiveness is higher than the dehumidifier energy effectiveness, the condensation process will be less efficient than the evaporation process.

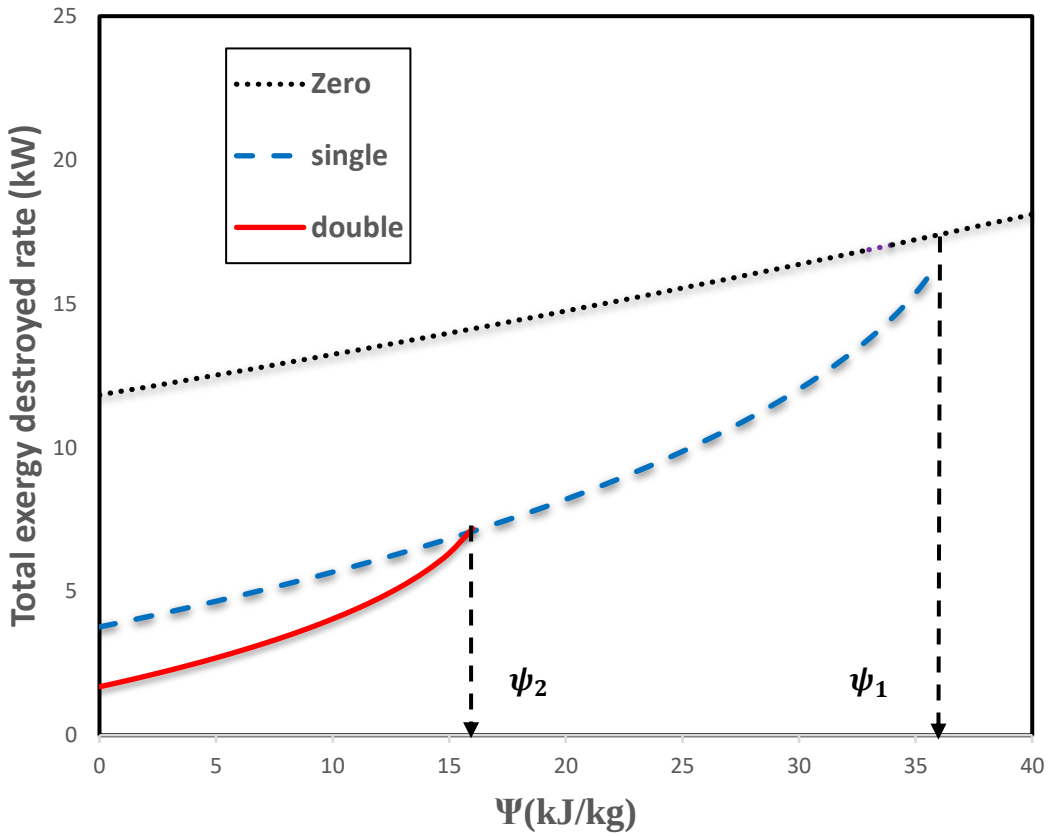

Figure 3-14: The total exergy destroyed rate of zero, single and double extraction cycle versus the enthalpy pinch at T_{max} = 80 ^{o}C and T_{min} = 20 ^{o}C.

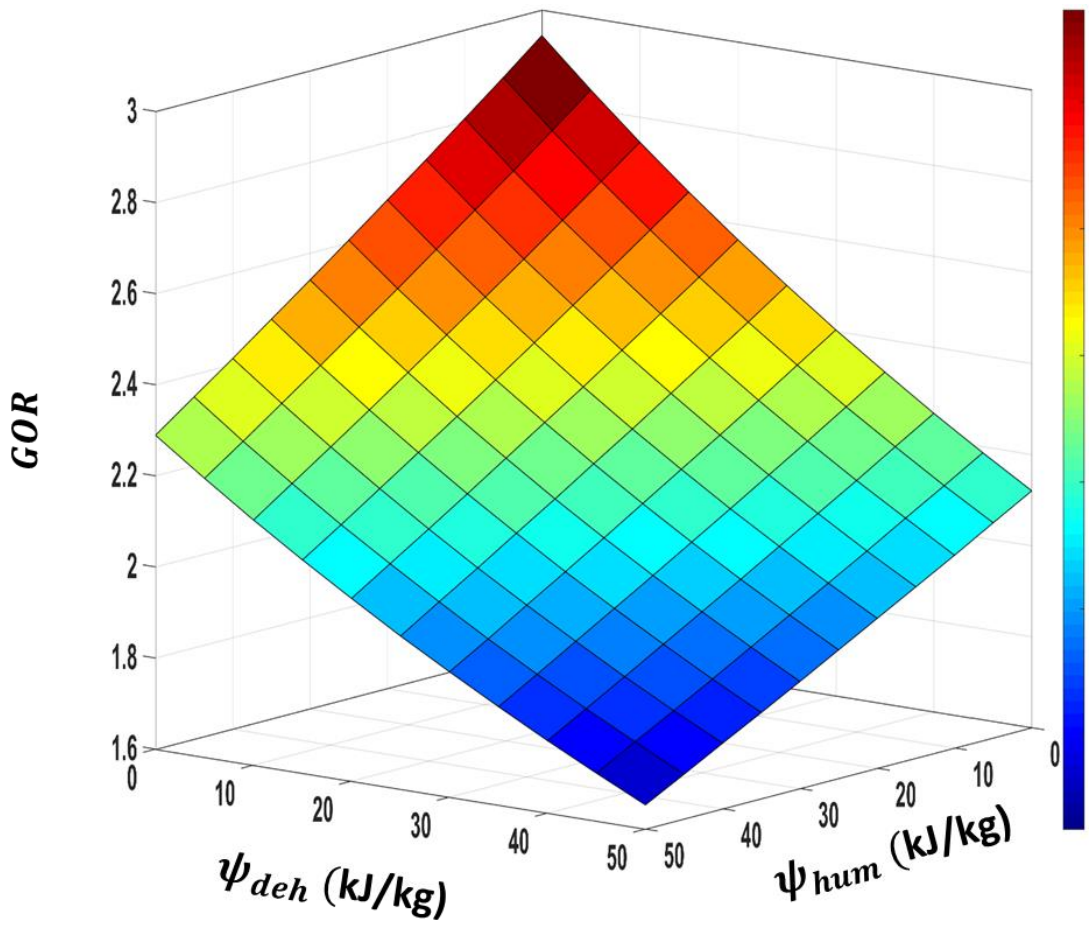

Figure 3-15: The GOR of a zero extraction cycle versus enthalpy pinch of the humidifier and dehumidifier at T_{max} = 80 ^{o}C and T_{min} = 20 ^{o}C.

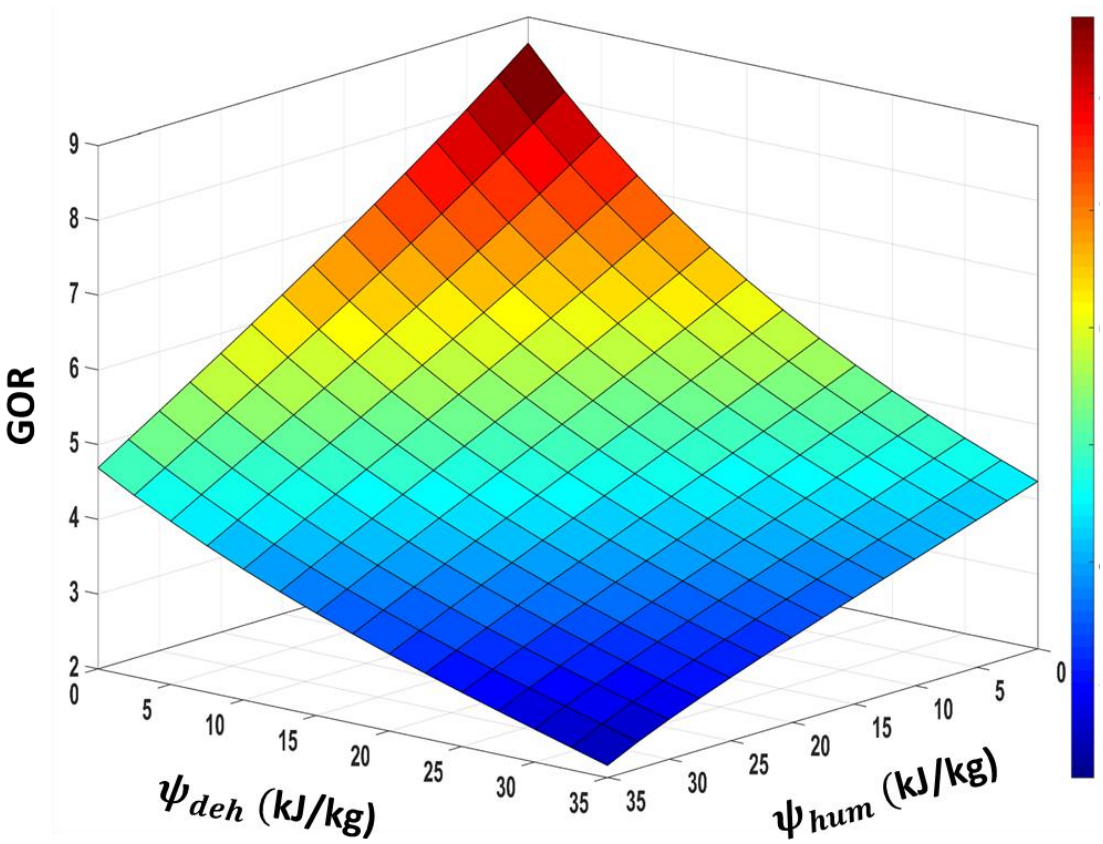

Figure 3-16: The GOR of a single extraction cycle versus enthalpy pinch of the humidifier and dehumidifier at T_{max} = 80 ^{o}C and T_{min} = 20 ^{o}C.

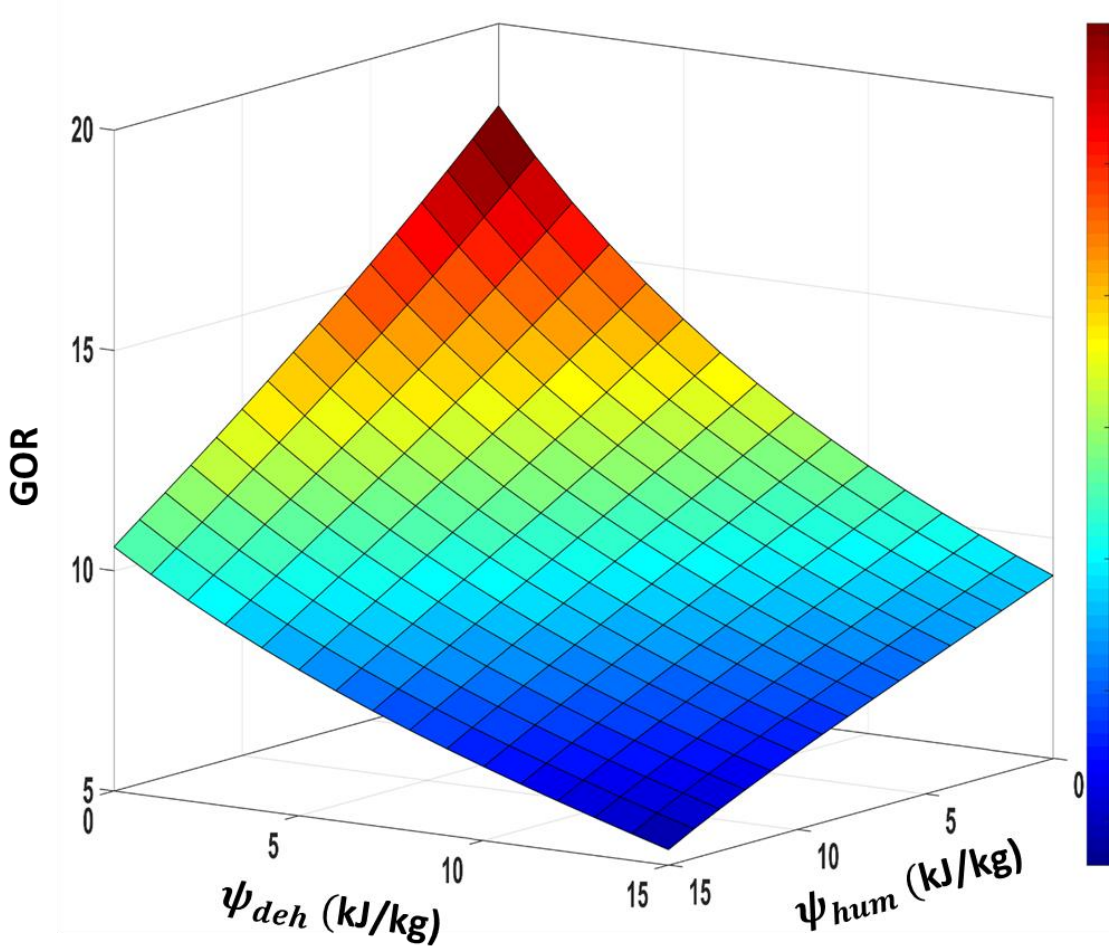

Figure 3-17: The GOR of a double extraction cycle versus enthalpy pinch of the humidifier and dehumidifier at T_{max} = 80 °C and T_{min} = 20 °C.

3.2.4 Variation of GOR with minimum and maximum temperature.

Figure 3-18 and Figure 3-19 show the effect of maximum and minimum temperature on the GOR of the zero-extraction cycle at low enthalpy pinch ($\psi = 0\ kJ/kg$) and high enthalpy pinch ($\psi = 40\ kJ/kg$). The effect of the minimum temperature on the GOR is the same at low and high enthalpy pinch. As the system has the same enthalpy pinch, increasing the minimum temperature (feed water to the dehumidifier) leads to increase exit water temperature from the dehumidifier and thus the system needs to add less heat to reach

the same maximum temperature. Therefore, the GOR increases by increasing the minimum temperature at the same enthalpy pinch and maximum temperature.

At high enthalpy pinch, increasing the maximum temperature leads to an increase in the GOR as shown in Figure 3-19. On the other hand, at low enthalpy pinch, increasing the maximum temperature leads to a decrease in the GOR as shown in Figure 3-18. According to equation (2-1), GOR is a function of the input heat and the product water. Increasing the product water (numerator) has a positive effect on the GOR and increasing the heat input (denominator) has a negative effect on the GOR. Increasing the maximum temperature leads to increase the heat input (denominator). On the other hand, increasing the maximum temperature leads to increases the product water (numerator). If the increase in the product water (numerator) is higher than the increase in heat input, the GOR increases. Otherwise, the GOR decreases. For instance, at $\psi = 0\ kJ/kg$, the heat input increases by 104 % to increase the maximum temperature from $60\ ^oC$ to $80\ ^oC$ and the product water increases by 46 %. Therefore, at low enthalpy pinch, the GOR decreases by increasing the maximum temperature. At $\psi = 50\ kJ/kg$, the heat input increases by 6 % to increase the maximum temperature from $60\ ^oC$ to $80\ ^oC$ and the product water increases by 100 %. Therefore, at high enthalpy pinch, the GOR increases by increasing the maximum temperature.

Figure 3-20 and Figure 3-21 show the effect of minimum and maximum temperature of the single extraction cycle on the GOR at a low and high enthalpy pinch. While Figure 3-22 and Figure 3-23 show the effect of minimum and maximum temperature of the double extraction cycle on the GOR. It is evident from these figures that the zero, single and double extraction cycles have the same trend.

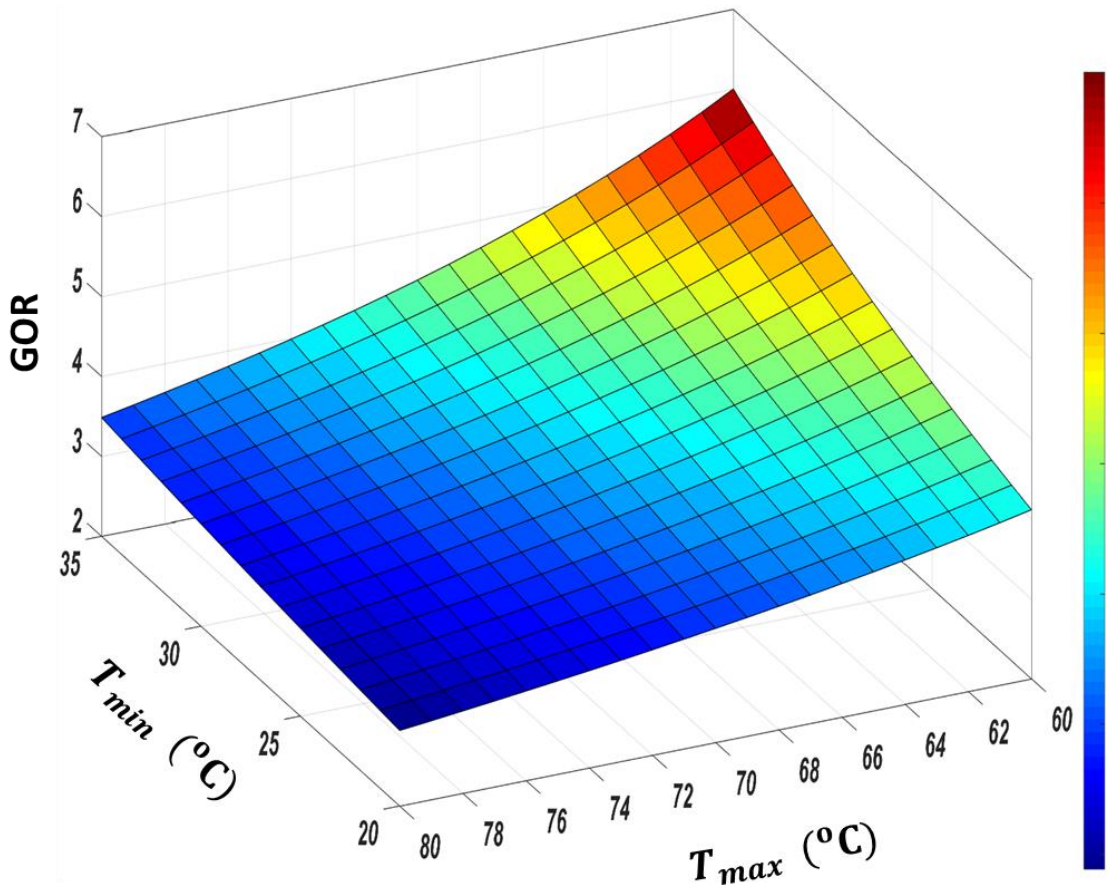

Figure 3-18: The effect of maximum and minimum temperature on GOR of the zero extraction cycle at $\Psi = 0$ kJ/kg.

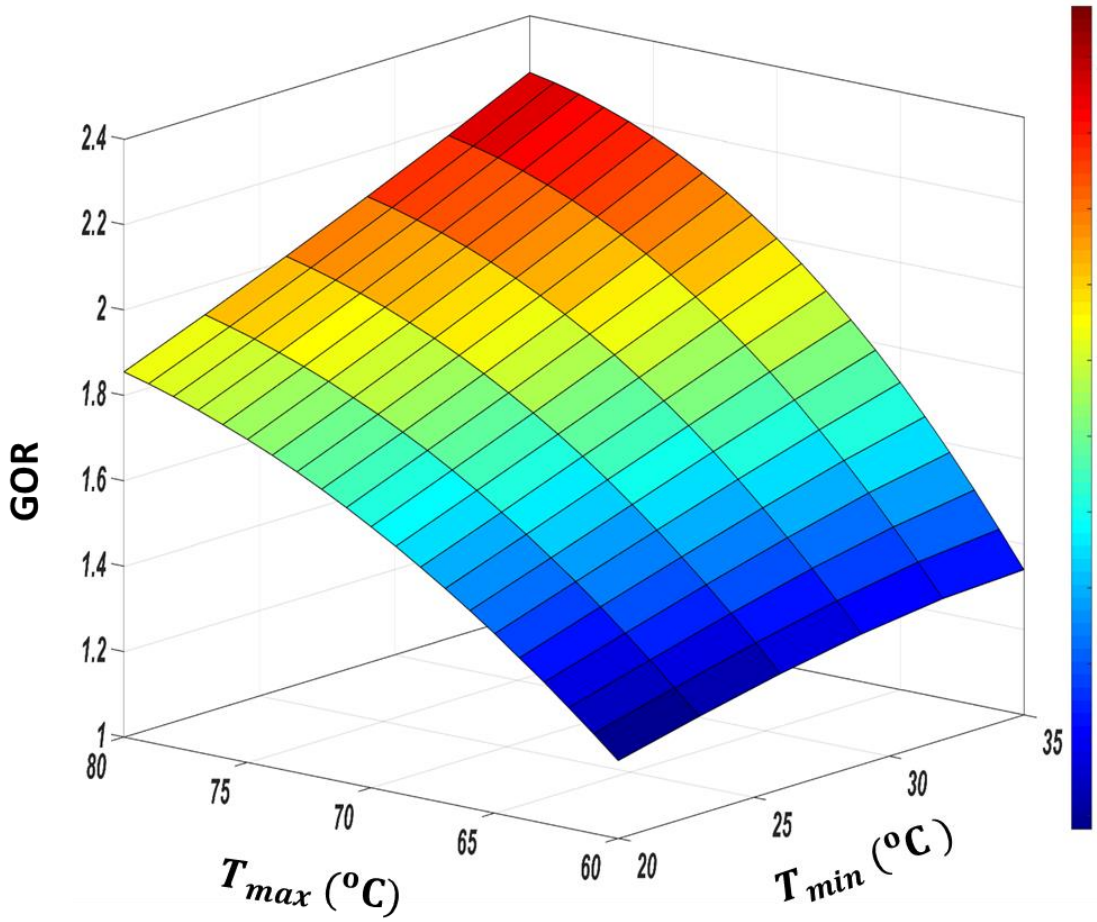

Figure 3-19: The effect of maximum and minimum temperature on the GOR of zero extraction cycle at Ψ = 40 kJ/kg.

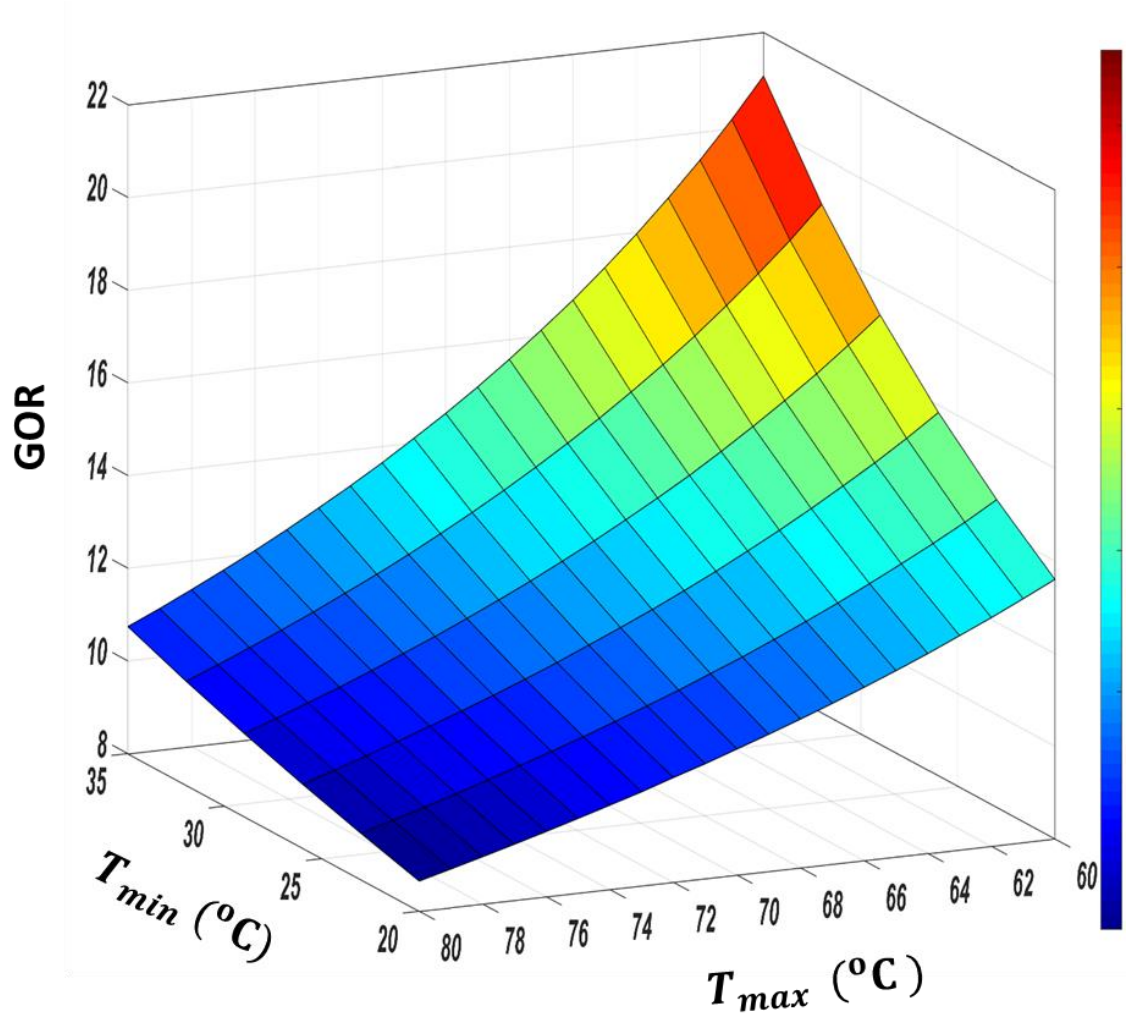

Figure 3-20: The effect of maximum and minimum temperature on the GOR of single extraction cycle at Ψ = 0 kJ/kg.

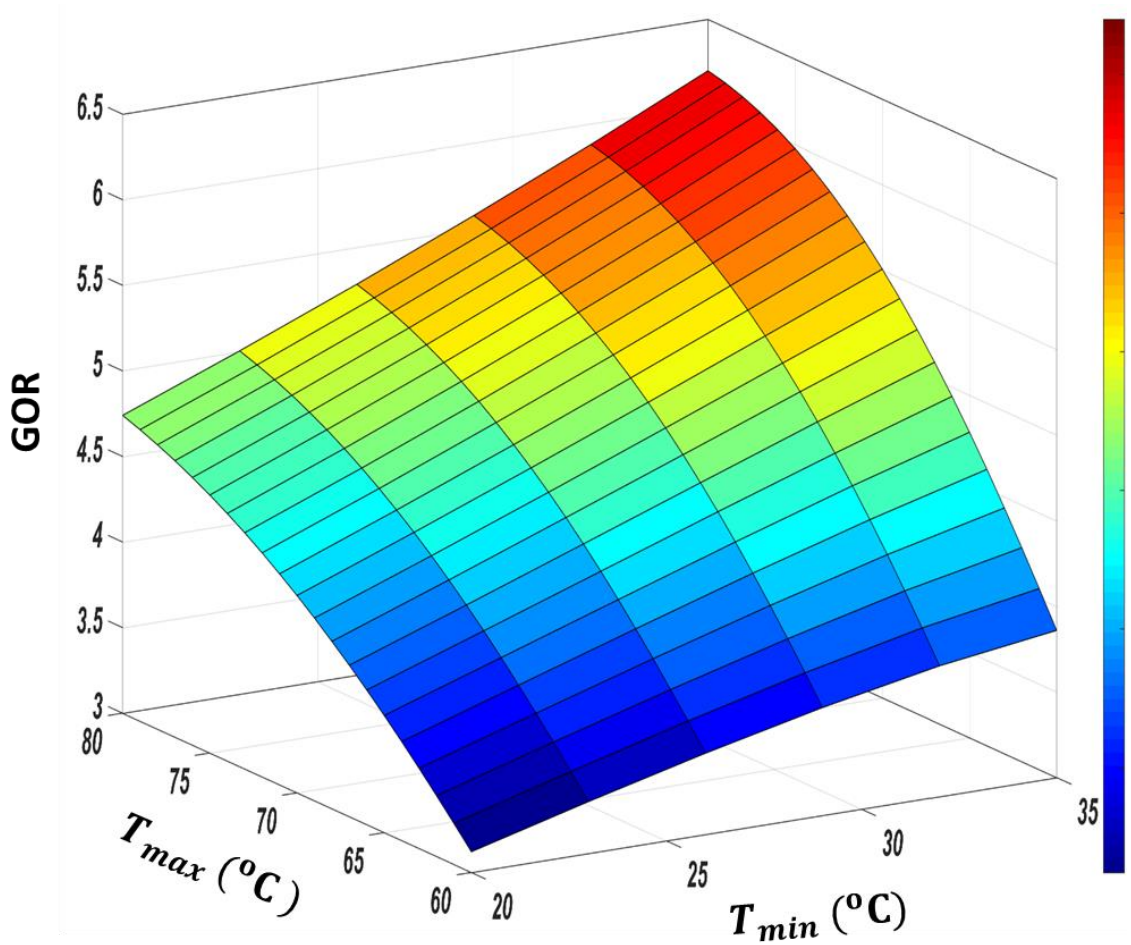

Figure 3-21: The effect of maximum and minimum temperature on GOR of the single extraction cycle at Ψ = 16 kJ/kg.

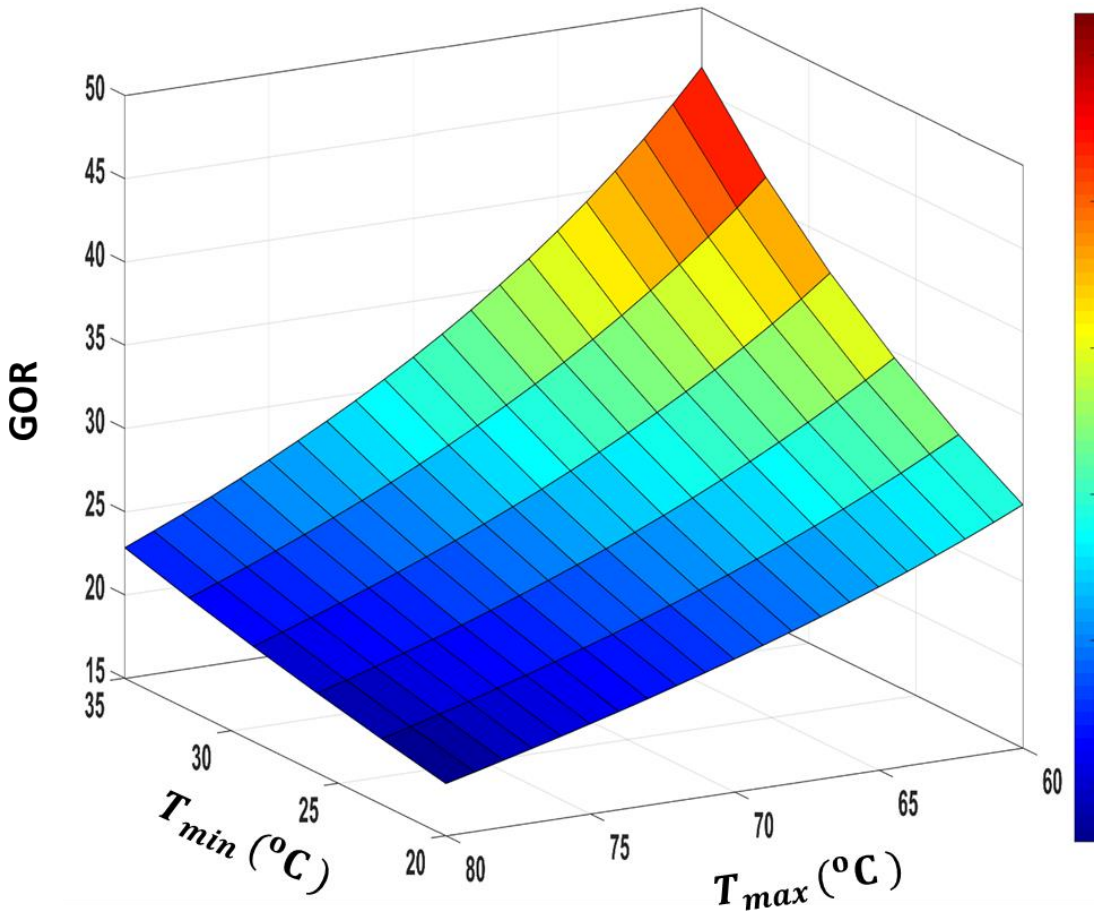

Figure 3-22: The effect of maximum and minimum temperature on GOR of the double extraction cycle at Ψ = 0 kJ/kg.

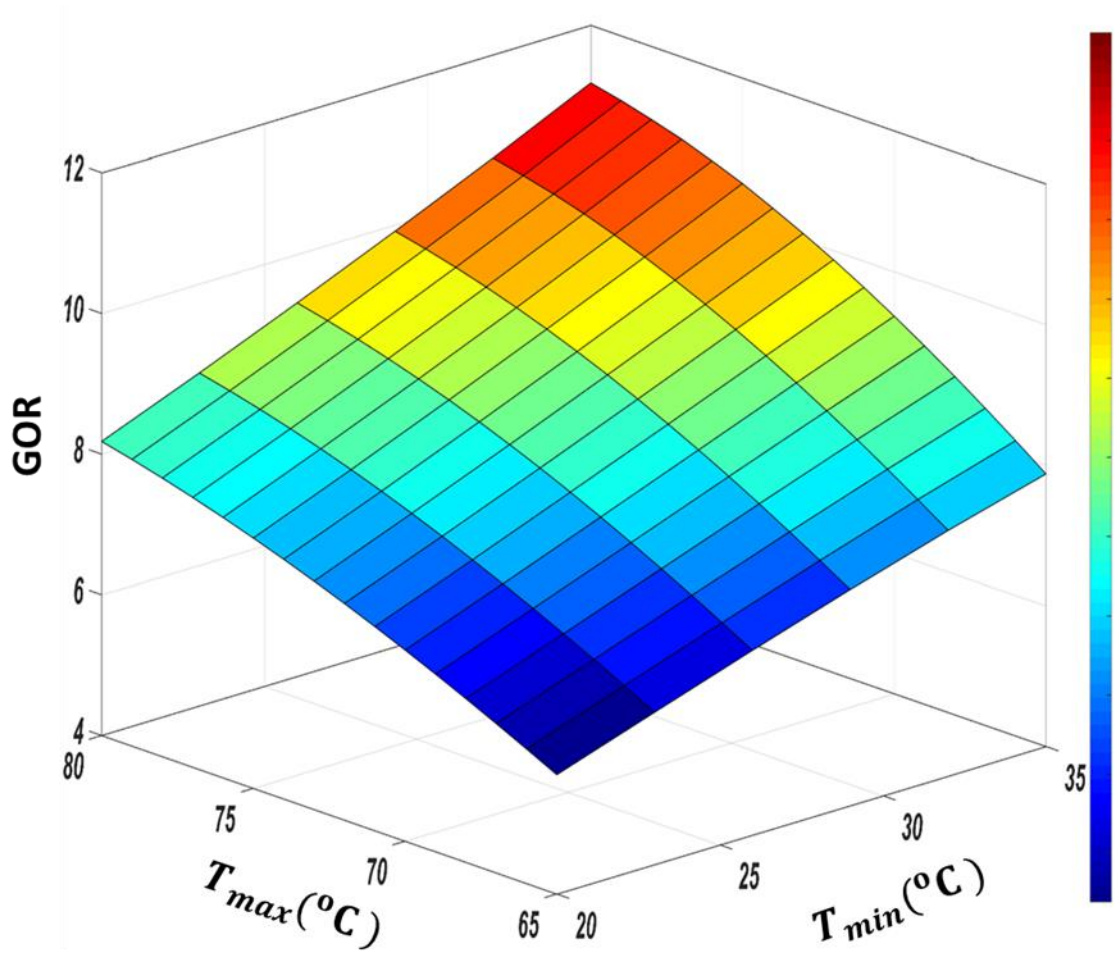

Figure 3-23: The effect of maximum and minimum temperature on GOR of the double extraction cycle at Ψ = 10 kJ/kg.

3.2.5 Limitation of thermodynamic balancing.

Figure 3-24 shows a comparison between GOR of the zero, single, and double extraction cycle versus enthalpy pinch at the same minimum ($T_{min} = 20\ ^{o}C$) and maximum temperature ($T_{max} = 80\ ^{o}C$). Using a single extraction has a positive effect on gain output ratio up to a certain enthalpy pinch (ψ_1) at which the GOR of zero extraction and single extraction cycle are equal. The reason for this observation is that the total exergy destroyed rate of the single extraction cycle and the zero extraction cycle are equal at ψ_1, as shown in Figure 3-14. The enthalpy pinch at which the performance of the single extraction cycle and double extraction cycle are the same is called ψ_2.

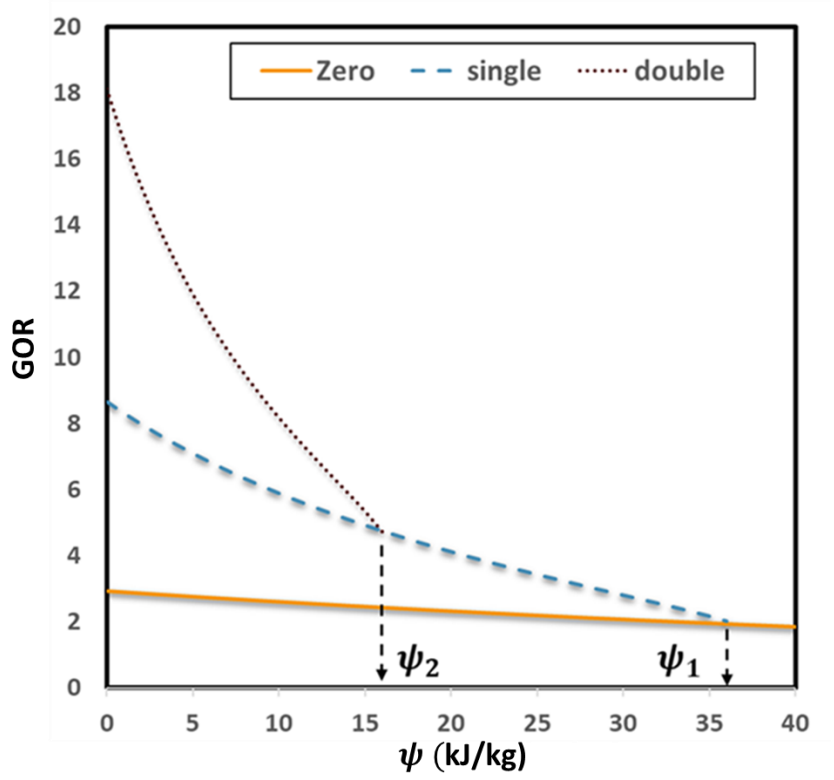

Figure 3-24: The gain output ratio of zero, single and double extraction cycle versus enthalpy pinch at T_{max} = 80 ^{o}C and T_{min} = 20 ^{o}C.

It is recommended that the system enthalpy pinch should be lower than ψ_1 to have a positive impact on the single extraction and lower than ψ_2 for the double extraction. Increasing the maximum temperature and minimum temperature leads to an increase in ψ_1 and ψ_2, as shown in Figure 3-25 and Figure 3-26 respectively. Therefore, Increasing the maximum and minimum temperature facilitates either using the single or double extraction system.

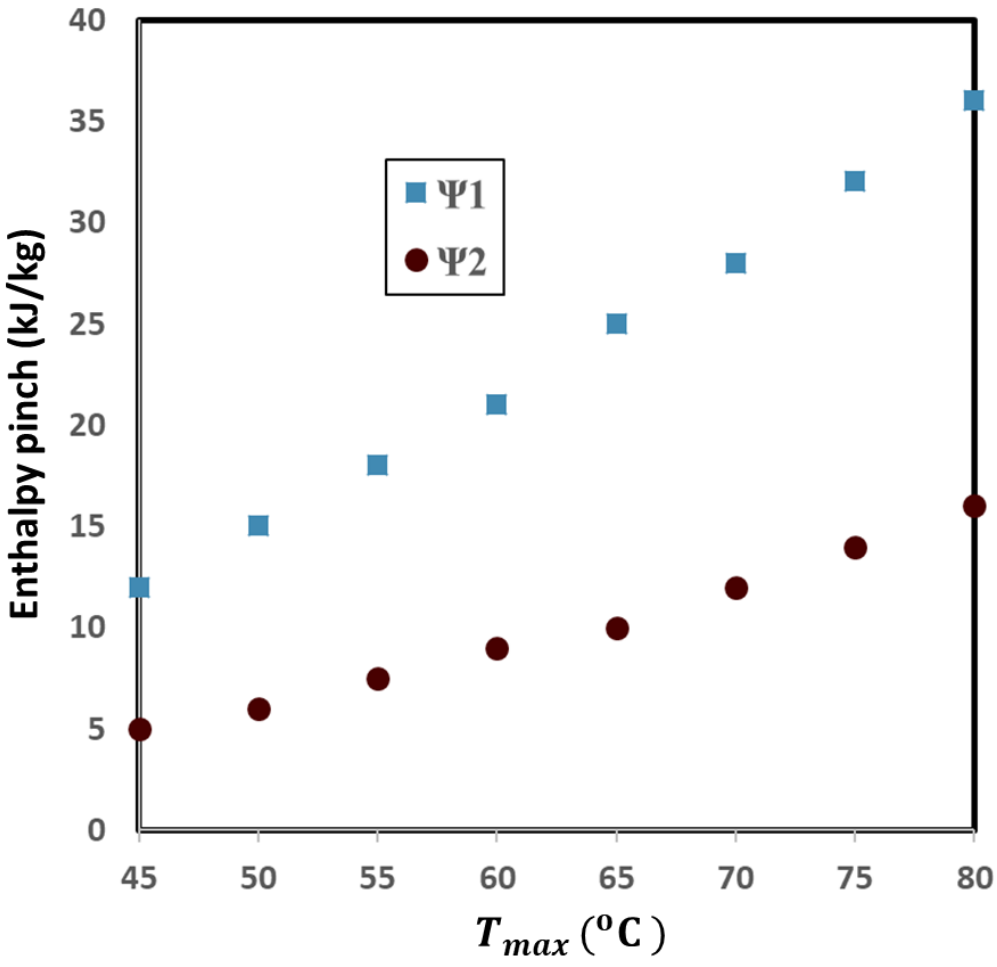

Figure 3-25: The effect of maximum temperature on Ψ_1 and Ψ_2 at T_{min} = 20 °C.

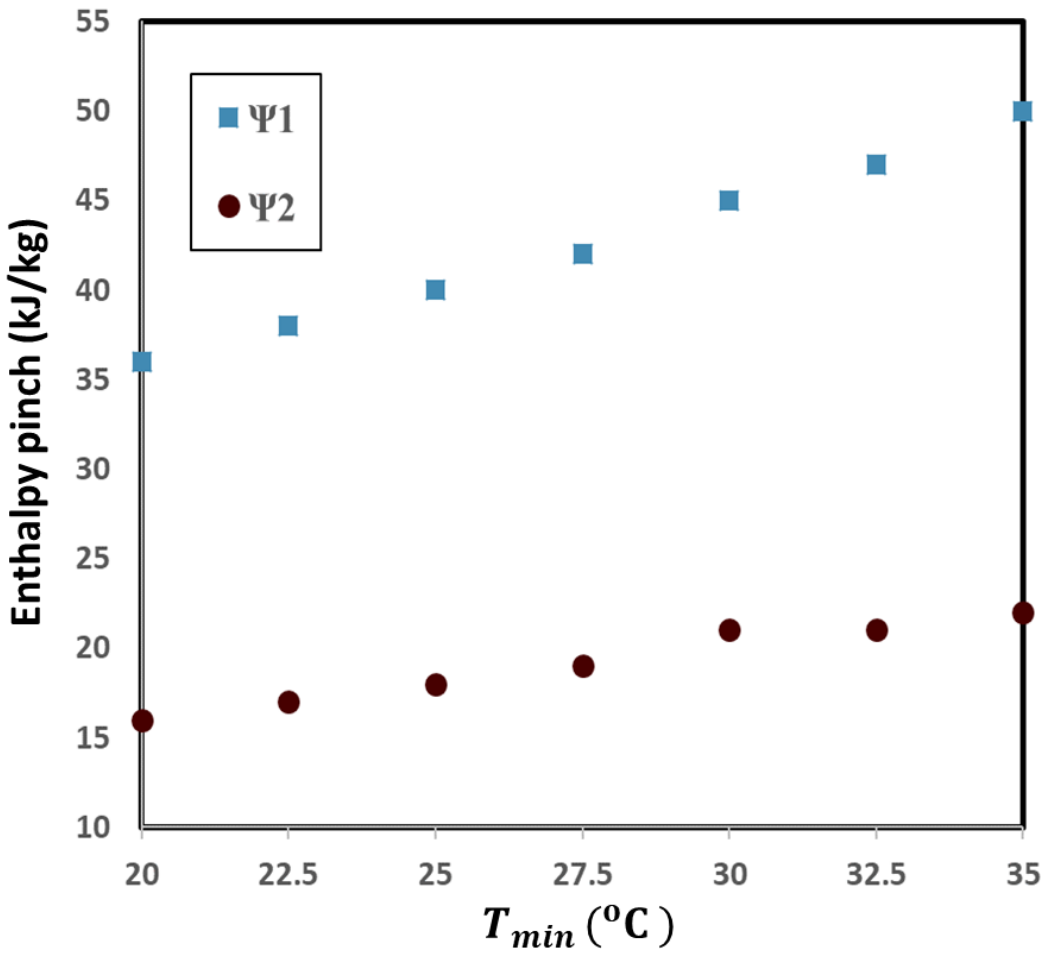

Figure 3-26: The effect of minimum temperature on Ψ_1 and Ψ_2 at T_{max} = 80 °C.

Optimal mass flow rate ratio.

As mentioned in section (3.1.1), thermodynamic balancing means that the dehumidifier modified heat capacity (HCR_{deh}) is equal to unity . For any control volume, the HCR is a function of the inlet temperatures and mass flow rate ratio according to the previous study conducted by Narayan et al. [13]. The numerical model algorithm uses the trial and error approach by guessing the mass flow rate ratio and position of the extraction to satisfy $HCR_{deh} = 1$ at each stage. Therefore, the mass flow rate at each stage satisfying

$HCR_{deh} = 1$ is the optimal mass flow rate ratio. In addition, the position of extraction satisfying $HCR_{deh} = 1$ at each stage is the best position of extraction.

Figure 3-27 shows a schematic diagram of a double extraction cycle. The double extraction divides the cycle into three stages (number of stages = number of extractions +1). Each stage has an optimal mass flow rate ratio (MR1, MR2, and MR3). The best positions of extraction are called x1and x2 (percentage of the total length) that is equivalent to the non-dimensional enthalpy along the fluid flow path as mentioned in the previous investigation by Narayan et al. [13].

The optimal mass flow rate ratio and the best position of extraction are functions of the enthalpy pinch, minimum and maximum temperature, and the number of extractions. In case of not using the optimal mass flow rate ratios and best positions of extraction, the cycle becomes unbalanced, thermodynamically. Therefore, the designer of the HDH system should select the pump and fan that can satisfy the optimal mass flow rate ratio and control the position and amount of air extraction to benefit the thermodynamic balancing of the system.

One of the objectives of this study is to guide the designer to achieve thermodynamic balancing experimentally. The next tables show the optimal conditions (MR and x) and the performance parameters (GOR and RR) of zero, single, and double extraction cycle at different T_{max} , T_{min} and ψ. The minimum allowable enthalpy pinch of single and double extraction cycle (ψ_1 and ψ_2) can be estimated by the data presented.

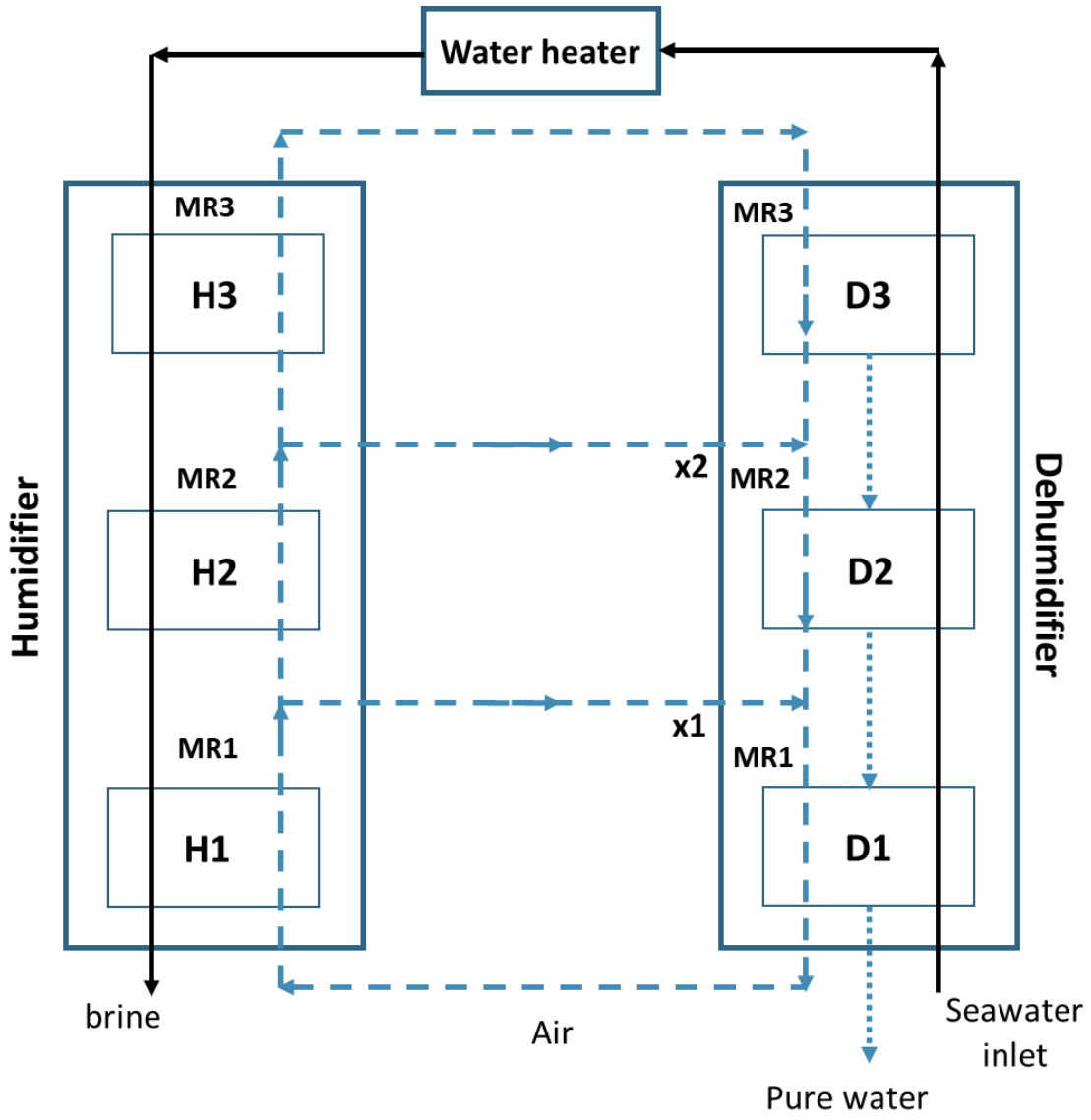

Figure 3-27: A Schematic diagram of a double extraction cycle.

3.2.6 Design example

In this example, the results of three HDH cycles are used to compare optimized water-heated zero-, single-, and double-extraction HDH systems which have a fixed freshwater production rate of 10 kg/h. Given that the feed seawater supply has a temperature of 20 °C, the salinity of 35 g/kg, and a maximum water temperature (at the inlet to the humidifier) of 80 °C. Considering that the enthalpy pinch of both the humidifier and dehumidifier is 10 kJ/kg, it is required to calculate the following:

a) The corresponding effectiveness of both the humidifier and dehumidifier.

b) The rate of thermal heat input ($\dot{Q}$).

c) The amount of feed seawater supply ($\dot{m}_w$)

d) The amount of air that should be circulated ($\dot{m}_{da}$) at each stage and the amount extracted air.

e) The location of extractions (x).

f) The critical enthalpy pinch of using single- and double-extraction (ψ_1 and ψ_2) and the corresponding critical effectiveness values.

The zero-extraction HDH system

For the given temperatures and enthalpy pinch values, we use Table 3-13 to get the ε, GOR, and RR. These values are 0.98, 2.62, and 6.39, respectively. The latent heat of vaporization at the given feed seawater is h_{fg}= 2400 kJ/kg K. Table 3-4 is used to calculate the optimal mass flow rate ratio (MR1 = 3.16).

a) The corresponding effectiveness of both the humidifier and the dehumidifier = 0.98

b) Therefore, the value of GOR is used to estimate the heat input that is 2.54 kW.

c) From the recovery ratio, the feed seawater supply can be calculated as 0.0435 kg/s.

d) From the optimal mass flow rate ratio, the circulated air flow rate is 0.01375 kg/s.

e) This case is without extraction.

f) From Table 3-5 and Table 3-9, the critical enthalpy pinch of using single and double extractions ($\psi_1 \; and \; \psi_2$) are 36 kJ/kg and 15 kJ/kg. From Table 3-17 and Table 3-21, the corresponding critical effectiveness is 0.94 and 0.98, respectively.

The enthalpy pinch of 10 kJ/kg is lower than $\psi_1 = 36 \; kJ/kg$ and $\psi_2 = 15 \; kJ/kg$. Therefore, applying the single and double extractions will improve the HDH system performance.

The single-extraction HDH system

For the given temperatures and enthalpy pinch values, we use Table 3-17 to get the ε, GOR, and RR, their values are 0.989, 5.88, and 7.08, respectively. The latent heat of vaporization at the given feed seawater is h_{fg} = 2400 kJ/kg K. Table 3-5 is used to calculate the optimal mass flow rate ratios (MR1 = 1.65 and MR2 = 7.03) and the best position of extraction (x =17.86 %).

a) The corresponding effectiveness of both the humidifier and dehumidifier = 0.99

b) Therefore, the value of GOR is used to estimate the heat input that is 1.134 kW.

c) From the recovery ratio, the feed seawater supply can be calculated as 0.039 kg/s.

d) From the optimal mass flow rate ratio, the circulated airflow rate in the first stage ($\dot{m}_{da,1}$) is 0.02377 kg/s, in the second stage ($\dot{m}_{da,2}$) is 5.58×10^{-3}kg/s and the extracted air flow rate is 0.0182 kg/s.

e) The location of extraction (x) is at 17.86 % of the total length from the dehumidifier bottom.

f) From Table 3-5 and Table 3-9, the critical enthalpy pinch of using single and double extractions ($\psi_1 \; and \; \psi_2$) are 36 kJ/kg and 15 kJ/kg, respectively. From Table 3-17 and Table 3-21, the corresponding critical effectiveness is 0.937 and 0.984, respectively.

The enthalpy pinch of 10 kJ/kg is lower than $\psi_1 = 36 \; kJ/kg$. Therefore, applying a single extraction leads to increasing the GOR to 5.88 compared with the GOR of the zero extraction cycle of 2.62; that is, a 125 % increase in GOR value.

The double-extraction HDH system

For the given temperatures and enthalpy pinch values, we use Table 3-21 to get the ε, GOR, and RR, These values are 0.99, 8.18, and 7.38, respectively. The latent heat of vaporization at the given feed seawater is h_{fg} = 2400 kJ/kg K. Table 3-9 is used to calculate the optimal mass flow rate ratios (MR1 = 1.17, MR2 = 2.62, and MR3 = 9.19) and the best position of extraction (x1 = 5.26 % and x2 = 25.8%).

a) The corresponding effectiveness of both the humidifier and dehumidifier = 0.99

b) Therefore, the value of GOR is used to estimate the heat input that is 0.815 kW.

c) From the recovery ratio, the feed seawater supply can be calculated as 0.038 kg/s.

d) From the optimal mass flow rate ratios, the circulated airflow rate in the first stage ($\dot{m}_{da,1}$) is 32.2×10^{-3} kg/s, in the second stage ($\dot{m}_{da,2}$) is 14.4×10^{-3} kg/s, in the third stage ($\dot{m}_{da,3}$) is 4.1×10^{-3} kg/s, the first extraction air flow rate is 17.8×10^{-3} kg/s, and the second extraction air flow rate is 10.3×10^{-3} kg/s.

e) The locations of extraction (x1 and x2) are at 5.26 % and 25.8 % of the total length from the dehumidifier bottom.

f) From Table 3-5 and Table 3-9, the critical enthalpy pinch of using single and double extractions (ψ_1 and ψ_2) are 36 kJ/kg and 15 kJ/kg, respectively. From Table 3-17 and Table 3-21, the corresponding critical effectiveness is 0.937 and 0.984, respectively.

The enthalpy pinch of 10 kJ/kg is lower than $\psi_2 = 15\ kJ/kg$. Therefore, applying double extractions leads to increasing the GOR to 8.18 compared with the GOR of the single extraction cycle of 5.88; that is, a 39 % increase in GOR value.

Table 3-4: The optimal mass flow rate ratio of a zero extraction cycle.

Ψ (kJ/kg)	MR1 at T_{min} = 20 (°C)				MR1 at T_{min} = 25 (°C)			
	Maximum Temperature (°C)				Maximum Temperature (°C)			
	50	60	70	80	50	60	70	80
0	1.61	2.01	2.53	3.23	1.82	2.29	2.9	3.72
5	1.58	1.98	2.5	3.19	1.79	2.26	2.87	3.69
10	1.55	1.95	2.47	3.16	1.76	2.23	2.84	3.65
15	1.52	1.92	2.44	3.13	1.73	2.2	2.81	3.62
20	1.49	1.89	2.41	3.1	1.7	2.17	2.77	3.59
25	1.46	1.86	2.38	3.07	1.67	2.14	2.74	3.55
30	1.43	1.83	2.35	3.03	1.64	2.11	2.71	3.52
35	1.4	1.8	2.32	3	1.61	2.07	2.68	3.49
40	1.37	1.77	2.29	2.97	1.58	2.04	2.65	3.45
45	1.34	1.74	2.26	2.94	1.54	2.01	2.61	3.42
50	1.31	1.71	2.22	2.9	1.51	1.98	2.58	3.38
Ψ (kJ/kg)	MR1 at T_{min} = 30 (°C)				MR1 at T_{min} = 35 (°C)			
	Maximum Temperature (°C)				Maximum Temperature (°C)			
	50	60	70	80	50	60	70	80
0	2.06	2.61	3.33	4.3	2.34	2.98	3.83	5
5	2.03	2.58	3.29	4.27	2.31	2.95	3.8	4.96
10	2	2.55	3.26	4.23	2.28	2.91	3.76	4.93
15	1.97	2.51	3.23	4.2	2.25	2.88	3.73	4.89
20	1.94	2.48	3.2	4.17	2.21	2.85	3.7	4.86
25	1.91	2.45	3.17	4.13	2.18	2.82	3.66	4.82
30	1.88	2.42	3.13	4.1	2.15	2.79	3.63	4.79
35	1.85	2.39	3.1	4.06	2.12	2.75	3.6	4.75
40	1.81	2.36	3.07	4.03	2.08	2.72	3.56	4.72
45	1.78	2.32	3.03	3.99	2.05	2.69	3.53	4.68
50	1.75	2.29	3	3.96	2.02	2.65	3.49	4.64

Table 3-5: The optimal conditions of a single extractions cycle at T_{min} = 20 (°C)

Ψ (kJ/kg)	T_{max} = 80 (°C) Ψ1 = 36			T_{max} =70 (°C) Ψ1 = 28		
	MR1	MR2	x (%)	MR1	MR2	x (%)
0	1.79	8	20.67	1.54	5.06	25.28
2	1.76	7.81	20.15	1.51	4.93	24.34
4	1.73	7.62	19.61	1.49	4.79	23.36
6	1.71	7.43	19.05	1.46	4.65	22.34
8	1.68	7.23	18.47	1.43	4.5	21.25
10	1.65	7.03	17.86	1.4	4.35	20.11
12	1.62	6.82	17.22	1.37	4.19	18.88
14	1.59	6.61	16.55	1.33	4.02	17.57
16	1.56	6.39	15.84	1.3	3.85	16.15
18	1.52	6.16	15.09	1.26	3.67	14.59
20	1.49	5.93	14.28	1.22	3.48	12.85
22	1.45	5.68	13.41	1.18	3.27	10.86
24	1.42	5.43	12.47	1.14	3.04	8.526
26	1.37	5.16	11.42	1.08	2.79	5.635
28	1.33	4.87	10.25	1.02	2.48	1.706
30	1.28	4.56	8.894			
32	1.23	4.21	7.266			
34	1.16	3.8	5.165			
36	1.08	3.27	1.986			
Ψ (kJ/kg)	T_{max} = 60 (°C) Ψ1 = 21			T_{max} = 50 (°C) Ψ1 = 14.5		
	MR1	MR2	x (%)	MR1	MR2	x (%)
0	1.35	3.38	30.05	1.19	2.32	35.04
2	1.32	3.27	28.41	1.16	2.24	32.07
4	1.29	3.16	26.66	1.13	2.15	28.83
6	1.26	3.05	24.8	1.1	2.05	25.26
8	1.23	2.93	22.79	1.07	1.95	21.25
10	1.2	2.81	20.61	1.03	1.85	16.69
12	1.16	2.67	18.21	0.994	1.73	11.33
14	1.13	2.54	15.52	0.953	1.61	4.801
16	1.09	2.39	12.46			
18	1.05	2.22	8.84			
20	0.999	2.04	4.373			

Table 3-6: The optimal conditions of a single extractions cycle at T_{min} = 25 (°C)

Ψ (kJ/kg)	T_{max} = 80 (°C) Ψ1 = 40.5			T_{max}= 70 (°C) Ψ1 = 30.5		
	MR1	MR2	x (%)	MR1	MR2	x (%)
0	2.12	8.76	22.02	1.82	5.48	26.91
2	2.09	8.58	21.51	1.79	5.35	25.97
4	2.06	8.39	20.98	1.76	5.21	24.99
6	2.03	8.21	20.43	1.73	5.08	23.97
8	2.01	8.01	19.87	1.7	4.94	22.89
10	1.98	7.82	19.28	1.67	4.79	21.76
12	1.95	7.62	18.67	1.64	4.64	20.57
14	1.91	7.42	18.03	1.61	4.49	19.3
16	1.88	7.21	17.36	1.57	4.33	17.94
18	1.85	6.99	16.66	1.54	4.16	16.47
20	1.81	6.77	15.91	1.5	3.99	14.87
22	1.78	6.55	15.12	1.46	3.8	13.11
24	1.74	6.31	14.28	1.41	3.61	11.12
26	1.7	6.07	13.37	1.37	3.39	8.836
28	1.66	5.81	12.38	1.31	3.16	6.107
30	1.62	5.55	11.3	1.25	2.89	2.65
32	1.57	5.26	10.08			
34	1.52	4.95	8.683			
36	1.46	4.61	7.028			
38	1.4	4.22	4.945			
40	1.31	3.73	1.993			
Ψ (kJ/kg)	T_{max} = 60 (°C) Ψ1 = 22			T_{max}= 50 (°C) Ψ1 = 15		
	MR1	MR2	x (%)	MR1	MR2	x (%)
0	1.59	3.62	31.91	1.4	2.48	37.07
2	1.56	3.52	30.21	1.37	2.4	33.84
4	1.53	3.42	28.41	1.34	2.31	30.32
6	1.5	3.31	26.49	1.3	2.22	26.45
8	1.47	3.2	24.44	1.27	2.13	22.15
10	1.43	3.08	22.24	1.23	2.03	17.28
12	1.4	2.96	19.83	1.2	1.92	11.64
14	1.36	2.83	17.19	1.16	1.81	4.926
16	1.32	2.69	14.23			
18	1.28	2.55	10.85			
20	1.24	2.39	6.892			
22	1.19	2.22	2.042			

Table 3-7: The optimal conditions of a single extractions cycle at T_{min} = 30 (°C).

Ψ (kJ/kg)	T_{max} = 80 (°C) Ψ1 = 45			T_{max} = 70 (°C) Ψ1 = 33		
	MR1	MR2	x (%)	MR1	MR2	x (%)
0	2.53	9.62	23.5	2.16	5.93	28.72
2	2.5	9.44	23	2.13	5.81	27.76
4	2.47	9.26	22.48	2.11	5.68	26.77
6	2.44	9.08	21.94	2.07	5.55	25.74
8	2.41	8.89	21.39	2.04	5.41	24.67
10	2.38	8.7	20.82	2.01	5.28	23.54
12	2.35	8.51	20.23	1.98	5.13	22.36
14	2.32	8.31	19.62	1.94	4.99	21.11
16	2.28	8.11	18.98	1.91	4.84	19.79
18	2.25	7.91	18.31	1.87	4.69	18.39
20	2.22	7.7	17.61	1.84	4.53	16.87
22	2.18	7.49	16.88	1.8	4.36	15.24
24	2.14	7.27	16.11	1.75	4.18	13.45
26	2.1	7.05	15.29	1.71	4	11.47
28	2.06	6.82	14.42	1.66	3.8	9.234
30	2.02	6.58	13.49	1.61	3.59	6.649
32	1.98	6.33	12.48	1.55	3.35	3.551
34	1.93	6.06	11.37			
36	1.88	5.79	10.15			
38	1.83	5.49	8.765			
40	1.77	5.17	7.16			
42	1.71	4.81	5.224			
44	1.63	4.39	2.715			
Ψ (kJ/kg)	T_{max} = 60 (°C) Ψ1 = 23			T_{max} = 50 (°C) Ψ1 = 14.5		
	MR1	MR2	x (%)	MR1	MR2	x (%)
0	1.88	3.89	33.96	1.65	2.65	39.31
2	1.85	3.8	32.17	1.62	2.57	35.66
4	1.82	3.7	30.28	1.59	2.49	31.7
6	1.79	3.59	28.28	1.56	2.4	27.34
8	1.76	3.49	26.15	1.52	2.31	22.49
10	1.72	3.38	23.87	1.48	2.22	17.02
12	1.69	3.26	21.41	1.45	2.12	10.73
14	1.65	3.14	18.73	1.4	2.01	3.336
16	1.61	3.02	15.78			
18	1.57	2.89	12.48			
20	1.53	2.75	8.732			
22	1.48	2.6	4.362			

Table 3-8: The optimal conditions of a single extractions cycle at T_{min} = 35 (°C).

Ψ (kJ/kg)	T_{max} = 80 (°C) Ψ1 = 50			T_{max} = 70 (°C) Ψ1 = 35.5		
	MR1	MR2	x (%)	MR1	MR2	x (%)
0	3.03	10.6	25.12	2.59	6.44	30.68
2	3	10.4	24.62	2.56	6.31	29.71
4	2.97	10.2	24.1	2.53	6.19	28.7
6	2.94	10	23.58	2.49	6.06	27.65
8	2.91	9.87	23.03	2.46	5.93	26.56
10	2.88	9.68	22.48	2.43	5.8	25.42
12	2.85	9.5	21.9	2.39	5.67	24.23
14	2.81	9.31	21.3	2.36	5.53	22.99
16	2.78	9.12	20.69	2.32	5.39	21.68
18	2.75	8.93	20.05	2.29	5.25	20.3
20	2.71	8.73	19.39	2.25	5.1	18.83
22	2.67	8.53	18.7	2.21	4.95	17.26
24	2.64	8.32	17.98	2.17	4.79	15.58
26	2.6	8.11	17.22	2.12	4.62	13.76
28	2.56	7.9	16.43	2.08	4.45	11.76
30	2.52	7.68	15.59	2.03	4.27	9.553
32	2.48	7.45	14.7	1.98	4.07	7.062
34	2.43	7.22	13.75	1.92	3.86	4.192
36	2.39	6.97	12.74	1.86	3.64	0.7759
38	2.34	6.72	11.63			
40	2.29	6.46	10.42			
42	2.23	6.18	9.083			
44	2.18	5.88	7.569			
46	2.11	5.55	5.815			
48	2.04	5.2	3.704			
50	1.95	4.78	0.9897			
Ψ (kJ/kg)	T_{max} = 60 (°C) Ψ1 = 23.5			T_{max} = 50 (°C) Ψ1 = 13		
	MR1	MR2	x (%)	MR1	MR2	x (%)
0	2.24	4.18	36.19	1.97	2.83	41.73
2	2.21	4.09	34.26	1.94	2.75	37.37
4	2.18	4	32.23	1.9	2.67	32.59
6	2.15	3.9	30.09	1.87	2.59	27.3
8	2.11	3.8	27.81	1.83	2.51	21.4
10	2.08	3.69	25.39	1.79	2.42	14.71
12	2.04	3.59	22.78	1.75	2.33	6.988
14	2	3.47	19.97			
16	1.96	3.36	16.9			
18	1.92	3.24	13.52			
20	1.88	3.11	9.752			
22	1.83	2.98	5.479			
24	1.78	2.84	0.5301			

Table 3-9: The optimal conditions of a double extraction cycle at T_{min} = 20 (°C).

Ψ (kJ/kg)	T_{max} = 80 (°C) Ψ2 = 15					T_{max} = 70 (°C) Ψ2 = 12				
	MR1	MR2	MR3	x1 (%)	x2 (%)	MR1	MR2	MR3	x1 (%)	x2 (%)
0	1.41	3.85	11.9	9.8	34.5	1.27	2.82	6.69	13.2	40.7
1	1.39	3.74	11.7	9.42	33.7	1.25	2.72	6.54	12.4	39.4
2	1.36	3.62	11.5	9.04	33	1.22	2.62	6.39	11.7	38.2
3	1.34	3.51	11.2	8.63	32.2	1.2	2.52	6.23	10.9	36.8
4	1.32	3.39	11	8.22	31.4	1.18	2.42	6.06	10	35.4
5	1.3	3.27	10.7	7.78	30.6	1.15	2.31	5.89	9.17	34
6	1.28	3.15	10.4	7.33	29.7	1.13	2.2	5.71	8.24	32.4
7	1.25	3.02	10.1	6.86	28.8	1.1	2.08	5.51	7.25	30.7
8	1.23	2.89	9.84	6.36	27.9	1.07	1.96	5.3	6.17	28.9
9	1.2	2.76	9.52	5.83	26.9	1.04	1.84	5.08	4.99	27
10	1.17	2.62	9.19	5.26	25.8	1	1.7	4.83	3.66	24.8
11	1.14	2.48	8.84	4.64	24.6	0.963	1.55	4.55	2.14	22.3
12	1.11	2.32	8.45	3.96	23.3	0.917	1.39	4.23	0.286	19.3
13	1.07	2.16	8.03	3.2	21.9					
14	1.03	1.98	7.56	2.32	20.2					
15	0.982	1.77	7.01	1.24	18.2					
Ψ (kJ/kg)	T_{max} = 60 (°C) Ψ2 = 8					T_{max} = 50 (°C) Ψ2 = 6				
	MR1	MR2	MR3	x1 (%)	x2 (%)	MR1	MR2	MR3	x1 (%)	x2 (%)
0	1.16	2.14	4.11	16.8	46.4	1.06	1.67	2.66	20.7	52
1	1.13	2.05	4	15.4	44.4	1.04	1.58	2.57	18.1	48.5
2	1.11	1.96	3.89	14	42.3	1.01	1.5	2.49	15.4	44.8
3	1.08	1.87	3.78	12.5	40	0.985	1.41	2.4	12.4	40.9
4	1.06	1.77	3.65	10.9	37.6	0.956	1.32	2.3	9.08	36.6
5	1.03	1.67	3.52	9.12	35	0.925	1.23	2.19	5.42	31.8
6	1	1.57	3.38	7.22	32.2	0.891	1.12	2.07	1.25	26.4
7	0.969	1.46	3.23	5.12	29.2					
8	0.934	1.34	3.06	2.75	25.7					

Table 3-10: The optimal conditions of a double extraction cycle at T_{min} = 25 (°C).

Ψ (kJ/kg)	T_{max} = 80 (°C) Ψ2 = 17					T_{max} = 70 (°C) Ψ2 = 13				
	MR1	MR2	MR3	x1 (%)	x2 (%)	MR1	MR2	MR3	x1 (%)	x2 (%)
0	1.69	4.37	12.7	10.7	36.2	1.52	3.18	7.05	14.4	42.7
1	1.67	4.26	12.5	10.3	35.5	1.5	3.08	6.91	13.6	41.5
2	1.65	4.14	12.3	9.94	34.8	1.47	2.98	6.77	12.8	40.2
3	1.62	4.03	12	9.54	34.1	1.45	2.88	6.62	12	38.9
4	1.6	3.91	11.8	9.13	33.3	1.42	2.78	6.47	11.2	37.6
5	1.58	3.79	11.6	8.7	32.6	1.4	2.67	6.31	10.3	36.2
6	1.55	3.67	11.3	8.26	31.7	1.37	2.56	6.14	9.35	34.7
7	1.53	3.55	11	7.79	30.9	1.34	2.45	5.97	8.37	33.1
8	1.5	3.42	10.8	7.31	30	1.31	2.34	5.78	7.33	31.4
9	1.47	3.29	10.5	6.8	29.1	1.28	2.21	5.59	6.21	29.6
10	1.45	3.16	10.2	6.27	28.1	1.25	2.09	5.38	4.98	27.7
11	1.42	3.02	9.88	5.7	27.1	1.21	1.95	5.15	3.63	25.5
12	1.38	2.88	9.56	5.1	26	1.17	1.81	4.89	2.1	23.1
13	1.35	2.73	9.21	4.44	24.8	1.12	1.65	4.6	0.294	20.3
14	1.31	2.57	8.83	3.72	23.5					
15	1.28	2.4	8.42	2.91	22					
16	1.23	2.21	7.96	1.97	20.3					
17	1.18	2	7.42	0.84	18.3					
Ψ (kJ/kg)	T_{max} = 60 (°C) Ψ2 = 9					T_{max} = 50 (°C) Ψ2 = 6				
	MR1	MR2	MR3	x1 (%)	x2 (%)	MR1	MR2	MR3	x1 (%)	x2 (%)
0	1.38	2.41	4.3	18.2	48.6	1.27	1.86	2.77	22.3	54.2
1	1.36	2.32	4.21	16.8	46.5	1.24	1.78	2.7	19.5	50.5
2	1.33	2.23	4.1	15.3	44.4	1.22	1.7	2.62	16.4	46.6
3	1.31	2.14	4	13.7	42.1	1.19	1.61	2.53	13.1	42.4
4	1.28	2.04	3.88	12	39.7	1.16	1.52	2.44	9.55	37.9
5	1.25	1.94	3.76	10.2	37.2	1.13	1.43	2.34	5.61	33
6	1.22	1.84	3.64	8.27	34.5	1.09	1.33	2.24	1.2	27.4
7	1.19	1.73	3.5	6.17	31.5					
8	1.15	1.62	3.35	3.86	28.3					
9	1.12	1.5	3.19	1.24	24.6					

Table 3-11: The optimal conditions of a double extraction cycle at T_{min} = 30 (° C).

Ψ (kJ/kg)	T_{max} = 80 (°C) Ψ2 = 19					T_{max} = 70 (°C]) Ψ2 = 14				
	MR1	MR2	MR3	x1 (%)	x2 (%)	MR1	MR2	MR3	x1 (%)	x2 (%)
0	2.04	4.98	13.6	11.7	38.1	1.83	3.6	7.44	15.7	44.8
1	2.02	4.87	13.4	11.4	37.5	1.81	3.5	7.31	14.9	43.6
2	2	4.76	13.2	11	36.8	1.78	3.4	7.18	14.1	42.4
3	1.97	4.64	12.9	10.6	36.1	1.76	3.3	7.04	13.3	41.1
4	1.95	4.52	12.7	10.2	35.4	1.73	3.2	6.9	12.4	39.8
5	1.93	4.4	12.5	9.73	34.6	1.71	3.1	6.75	11.5	38.4
6	1.9	4.28	12.3	9.29	33.8	1.68	2.99	6.6	10.6	37
7	1.87	4.16	12	8.84	33.1	1.65	2.88	6.44	9.6	35.5
8	1.85	4.04	11.8	8.36	32.2	1.62	2.76	6.28	8.56	33.9
9	1.82	3.91	11.5	7.88	31.4	1.59	2.65	6.1	7.47	32.3
10	1.79	3.78	11.2	7.36	30.5	1.55	2.53	5.92	6.3	30.5
11	1.76	3.65	11	6.83	29.5	1.52	2.4	5.72	5.04	28.6
12	1.73	3.51	10.7	6.27	28.6	1.48	2.27	5.51	3.66	26.5
13	1.7	3.37	10.4	5.67	27.5	1.44	2.13	5.28	2.13	24.2
14	1.66	3.22	10.1	5.03	26.4	1.39	1.97	5.03	0.383	21.6
15	1.63	3.07	9.72	4.34	25.2					
16	1.59	2.91	9.36	3.6	23.9					
17	1.55	2.74	8.97	2.76	22.5					
18	1.5	2.55	8.54	1.82	20.9					
19	1.45	2.35	8.05	0.705	19					
Ψ (kJ/kg)	T_{max} = 60 (°C) Ψ2 = 9					T_{max} = 50 (°C) Ψ2 = 4				
	MR1	MR2	MR3	x1 (%)	x2 (%)	MR1	MR2	MR3	x1 (%)	x2 (%)
0	1.67	2.71	4.51	19.8	50.8	1.53	2.1	2.89	24.2	56.5
1	1.64	2.63	4.42	18.3	48.7	1.5	2.01	2.82	20.9	52.5
2	1.62	2.53	4.33	16.6	46.5	1.47	1.93	2.75	17.4	48.2
3	1.59	2.44	4.23	14.9	44.3	1.44	1.84	2.67	13.6	43.7
4	1.56	2.35	4.12	13.2	41.8	1.41	1.75	2.59	9.55	38.7
5	1.53	2.25	4.01	11.3	39.3					
6	1.5	2.15	3.9	9.29	36.6					
7	1.46	2.04	3.78	7.14	33.7					
8	1.43	1.94	3.65	4.8	30.5					
9	1.39	1.82	3.51	2.23	27.1					

Table 3-12: The optimal conditions of a double extraction cycle at T_{min} = 35 (^{o}C).

Ψ (kJ/kg)	T_{max} = 80 (^{o}C) Ψ2 = 21					T_{max} = 70 (^{o}C) Ψ2 = 13				
	MR1	MR2	MR3	x1 (%)	x2 (%)	MR1	MR2	MR3	x1 (%)	x2 (%)
0	2.49	5.71	14.5	12.9	40.2	2.23	4.09	7.86	17.2	47.1
1	2.46	5.59	14.3	12.5	39.5	2.2	4	7.74	16.4	45.9
2	2.44	5.48	14.1	12.1	38.8	2.18	3.9	7.61	15.5	44.7
3	2.41	5.36	13.9	11.7	38.2	2.15	3.79	7.48	14.7	43.4
4	2.39	5.24	13.7	11.3	37.5	2.12	3.69	7.35	13.8	42.1
5	2.36	5.12	13.5	10.9	36.8	2.09	3.59	7.22	12.8	40.8
6	2.34	5	13.3	10.4	36	2.07	3.48	7.08	11.9	39.4
7	2.31	4.88	13	9.99	35.3	2.04	3.37	6.93	10.9	37.9
8	2.28	4.76	12.8	9.52	34.5	2	3.26	6.78	9.84	36.4
9	2.26	4.63	12.6	9.04	33.7	1.97	3.15	6.63	8.75	34.8
10	2.23	4.5	12.3	8.54	32.9	1.94	3.03	6.47	7.6	33.1
11	2.2	4.37	12.1	8.03	32	1.9	2.91	6.29	6.37	31.4
12	2.17	4.24	11.8	7.49	31.1	1.87	2.78	6.12	5.07	29.5
13	2.13	4.11	11.6	6.93	30.2	1.83	2.65	5.93	3.66	27.4
14	2.1	3.97	11.3	6.34	29.2					
15	2.06	3.82	11	5.72	28.2					
16	2.03	3.67	10.7	5.06	27.1					
17	1.99	3.52	10.4	4.35	25.9					
18	1.95	3.36	10.1	3.59	24.7					
19	1.9	3.19	9.69	2.76	23.3					
20	1.86	3.01	9.3	1.84	21.8					
21	1.8	2.82	8.87	0.781	20.1					
Ψ (kJ/kg)	T_{max} = 60 (^{o}C) Ψ2 = 9					T_{max} = 50 (^{o}C) Ψ2 = 5				
	MR1	MR2	MR3	x1 (%)	x2 (%)	MR1	MR2	MR3	x1 (%)	x2 (%)
0	2.02	3.07	4.73	21.6	53.3	1.85	2.36	3.02	26.2	58.9
1	2	2.98	4.65	19.9	51	1.82	2.28	2.96	22.2	54.2
2	1.97	2.89	4.56	18.1	48.8	1.79	2.19	2.89	17.9	49.3
3	1.94	2.8	4.47	16.3	46.4	1.76	2.11	2.81	13.3	44
4	1.91	2.7	4.37	14.3	43.9	1.73	2.02	2.74	8.35	38.3
5	1.88	2.61	4.27	12.3	41.2	1.69	1.92	2.66	2.96	32.1
6	1.84	2.51	4.17	10.2	38.5					
7	1.81	2.4	4.06	7.86	35.5					
8	1.77	2.3	3.94	5.41	32.4					
9	1.74	2.19	3.82	2.76	29					

Table 3-13: Performance parameters of a zero extraction cycle at T_{min} = 20 (°C).

Ψ (kJ/kg)	T_{max} = 80 (°C)			T_{max} = 70 (°C)		
	ε	GOR	RR (%)	ε	GOR	RR (%)
0	1	2.94	6.55	1	3.42	5.55
5	0.99	2.78	6.47	0.99	3.09	5.44
10	0.98	2.62	6.39	0.97	2.8	5.33
15	0.97	2.47	6.3	0.96	2.55	5.22
20	0.96	2.33	6.21	0.95	2.32	5.1
25	0.96	2.2	6.12	0.93	2.12	4.97
30	0.95	2.08	6.03	0.92	1.93	4.85
35	0.94	1.96	5.93	0.9	1.76	4.72
40	0.92	1.86	5.83	0.88	1.61	4.58
45	0.91	1.75	5.72	0.87	1.47	4.44
50	0.9	1.65	5.62	0.85	1.34	4.29
Ψ (kJ/kg)	T_{max} = 60 (°C)			T_{max} = 50 (°C)		
	ε	GOR	RR (%)	ε	GOR	RR (%)
0	1	4.11	4.49	1	5.22	3.39
5	0.98	3.42	4.35	0.97	3.64	3.21
10	0.96	2.89	4.21	0.94	2.69	3.03
15	0.94	2.46	4.06	0.9	2.06	2.84
20	0.92	2.11	3.9	0.86	1.61	2.63
25	0.89	1.82	3.74	0.81	1.27	2.42
30	0.87	1.58	3.57	0.76	1	2.2
35	0.84	1.36	3.4	0.71	0.78	1.96
40	0.81	1.18	3.21	0.64	0.61	1.71
45	0.78	1.02	3.02	0.57	0.46	1.45
50	0.74	0.88	2.82	0.48	0.33	1.17

Table 3-14: Performance parameters of a zero extraction cycle at T_{min} = 25 (°C).

Ψ (kJ/kg)	T_{max} = 80 (°C)			T_{max} = 70 (°C)		
	ε	GOR	RR (%)	ε	GOR	RR (%)
0	1	3.1	6.12	1	3.69	5.11
5	0.99	2.93	6.05	0.99	3.33	5.02
10	0.98	2.77	5.98	0.98	3.01	4.92
15	0.98	2.61	5.9	0.96	2.74	4.82
20	0.97	2.47	5.82	0.95	2.49	4.71
25	0.96	2.34	5.74	0.94	2.27	4.6
30	0.95	2.21	5.66	0.92	2.07	4.49
35	0.94	2.1	5.57	0.91	1.9	4.37
40	0.93	1.98	5.48	0.89	1.74	4.25
45	0.92	1.88	5.39	0.87	1.59	4.13
50	0.91	1.78	5.3	0.86	1.45	4
Ψ (kJ/kg)	T_{max} = 60 (°C)			T_{max} = 50 (°C)		
	ε	GOR	RR (%)	ε	GOR	RR (%)
0	1	4.58	4.05	1	6.12	2.93
5	0.98	3.75	3.92	0.97	4.03	2.77
10	0.96	3.14	3.79	0.93	2.88	2.6
15	0.94	2.65	3.66	0.89	2.15	2.42
20	0.92	2.26	3.52	0.85	1.65	2.24
25	0.89	1.94	3.37	0.8	1.28	2.05
30	0.87	1.68	3.22	0.75	1	1.85
35	0.84	1.45	3.07	0.69	0.77	1.64
40	0.81	1.26	2.9	0.63	0.59	1.42
45	0.78	1.09	2.74	0.55	0.44	1.19
50	0.75	0.94	2.56	0.46	0.32	0.94

Table 3-15: Performance parameters of a zero extraction cycle at T_{min} = 30 (°C).

Ψ (kJ/kg)	T_{max} = 80 (°C)			T_{max} = 70 (°C)		
	ε	GOR	RR (%)	ε	GOR	RR (%)
0	1	3.28	5.67	1	4.01	4.66
5	0.99	3.1	5.61	0.99	3.6	4.57
10	0.99	2.93	5.54	0.98	3.25	4.48
15	0.98	2.77	5.47	0.96	2.95	4.39
20	0.97	2.63	5.4	0.95	2.68	4.29
25	0.96	2.49	5.33	0.94	2.44	4.2
30	0.95	2.36	5.26	0.92	2.23	4.1
35	0.94	2.24	5.18	0.91	2.04	4
40	0.94	2.12	5.11	0.89	1.87	3.89
45	0.93	2.01	5.03	0.88	1.71	3.79
50	0.92	1.91	4.95	0.86	1.57	3.68
Ψ (kJ/kg)	T_{max} = 60 (°C)			T_{max} = 50 (°C)		
	ε	GOR	RR (%)	ε	GOR	RR (%)
0	1	5.18	3.57	1	7.45	2.43
5	0.98	4.16	3.46	0.96	4.44	2.28
10	0.96	3.42	3.34	0.93	3.01	2.13
15	0.94	2.86	3.22	0.88	2.17	1.97
20	0.92	2.42	3.09	0.84	1.62	1.8
25	0.89	2.06	2.96	0.79	1.23	1.63
30	0.87	1.77	2.83	0.73	0.94	1.45
35	0.84	1.52	2.69	0.66	0.71	1.26
40	0.81	1.31	2.55	0.59	0.53	1.07
45	0.78	1.14	2.4	0.5	0.38	0.87
50	0.75	0.98	2.25	0.4	0.26	0.66

Table 3-16: Performance parameters of a zero extraction cycle at T_{min} = 35 (°C).

Ψ (kJ/kg)	T_{max} = 80 (°C)			T_{max} = 70 (°C)		
	ε	GOR	RR (%)	ε	GOR	RR (%)
0	1	3.49	5.2	1	4.41	4.17
5	0.99	3.29	5.14	0.99	3.93	4.09
10	0.99	3.12	5.08	0.98	3.53	4.01
15	0.98	2.95	5.02	0.96	3.19	3.93
20	0.97	2.8	4.96	0.95	2.89	3.85
25	0.96	2.65	4.9	0.94	2.62	3.76
30	0.96	2.51	4.84	0.93	2.39	3.68
35	0.95	2.39	4.77	0.91	2.18	3.59
40	0.94	2.27	4.71	0.9	2	3.5
45	0.93	2.15	4.64	0.88	1.83	3.4
50	0.92	2.05	4.57	0.87	1.68	3.31
Ψ (kJ/kg)	T_{max} = 60 (°C)			T_{max} = 50 (°C)		
	ε	GOR	RR (%)	ε	GOR	RR (%)
0	1	6	3.07	1	9.63	1.89
5	0.98	4.65	2.96	0.96	4.82	1.75
10	0.96	3.73	2.86	0.91	3.01	1.61
15	0.94	3.06	2.75	0.87	2.05	1.47
20	0.91	2.55	2.64	0.81	1.47	1.32
25	0.89	2.15	2.52	0.75	1.07	1.16
30	0.86	1.83	2.4	0.68	0.78	1
35	0.84	1.56	2.28	0.6	0.56	0.84
40	0.81	1.34	2.16	0.5	0.39	0.67
45	0.78	1.15	2.03	0.39	0.25	0.49
50	0.74	0.99	1.9	0.26	0.14	0.3

Table 3-17: Performance parameters of a single extraction cycle at T_{min} = 20 (°C).

Ψ (kJ/kg)	T_{max} = 80 (°C)			T_{max} = 70 (°C)		
	ε	GOR	RR (%)	ε	GOR	RR (%)
0	1	8.65	7.33	1	10.72	6.14
2	0.998	7.97	7.29	0.997	9.3	6.09
4	0.996	7.36	7.24	0.993	8.15	6.02
6	0.994	6.82	7.19	0.989	7.2	5.96
8	0.992	6.33	7.13	0.986	6.41	5.89
10	0.989	5.88	7.08	0.982	5.72	5.82
12	0.987	5.47	7.02	0.978	5.13	5.75
14	0.985	5.09	6.96	0.973	4.61	5.67
16	0.982	4.74	6.89	0.969	4.15	5.58
18	0.979	4.41	6.83	0.963	3.74	5.49
20	0.977	4.11	6.76	0.958	3.36	5.39
22	0.974	3.82	6.68	0.952	3.01	5.28
24	0.97	3.55	6.6	0.945	2.68	5.16
26	0.967	3.29	6.51	0.936	2.36	5.02
28	0.963	3.04	6.41	0.925	2.04	4.84
30	0.959	2.79	6.31			
32	0.953	2.55	6.18			
34	0.947	2.3	6.03			
36	0.937	2.01	5.83			
Ψ (kJ/kg)	T_{max} = 60 (°C)			T_{max} = 50 (°C)		
	ε	GOR	RR (%)	ε	GOR	RR (%)
0	1	13.6	4.91	1	18.16	3.65
2	0.994	10.54	4.84	0.99	11.17	3.56
4	0.988	8.47	4.76	0.979	7.81	3.47
6	0.982	6.98	4.69	0.968	5.83	3.38
8	0.975	5.85	4.6	0.955	4.52	3.27
10	0.968	4.96	4.51	0.942	3.58	3.16
12	0.961	4.24	4.42	0.927	2.87	3.03
14	0.952	3.63	4.31	0.909	2.3	2.89
16	0.943	3.12	4.19			
18	0.933	2.67	4.07			
20	0.921	2.27	3.92			

Table 3-18: Performance parameters of a single extraction cycle at T_{min} = 25 (ºC).

Ψ (kJ/kg)	T_{max} = 80 (ºC)			T_{max} = 70 (ºC)		
	ε	GOR	RR (%)	ε	GOR	RR (%)
0	1	9.25	6.86	1	11.75	5.66
2	0.998	8.54	6.82	0.997	10.17	5.61
4	0.996	7.91	6.77	0.993	8.91	5.55
6	0.994	7.35	6.73	0.99	7.87	5.5
8	0.992	6.83	6.68	0.986	7	5.44
10	0.99	6.37	6.63	0.982	6.27	5.38
12	0.988	5.94	6.58	0.978	5.63	5.31
14	0.985	5.55	6.53	0.974	5.08	5.24
16	0.983	5.19	6.48	0.969	4.59	5.17
18	0.98	4.85	6.42	0.965	4.15	5.1
20	0.978	4.54	6.36	0.96	3.76	5.02
22	0.975	4.25	6.3	0.954	3.4	4.93
24	0.972	3.97	6.24	0.948	3.06	4.83
26	0.969	3.71	6.17	0.941	2.75	4.73
28	0.966	3.46	6.09	0.934	2.46	4.61
30	0.962	3.22	6.01	0.924	2.16	4.46
32	0.958	2.99	5.92			
34	0.954	2.76	5.83			
36	0.949	2.54	5.72			
38	0.943	2.3	5.59			
40	0.934	2.05	5.42			
Ψ (kJ/kg)	T_{max} = 60 (ºC)			T_{max} = 50 (ºC)		
	ε	GOR	RR (%)	ε	GOR	RR (%)
0	1	15.42	4.41	1	21.71	3.13
2	0.994	11.72	4.35	0.989	12.38	3.06
4	0.988	9.32	4.28	0.977	8.38	2.98
6	0.982	7.62	4.21	0.965	6.14	2.89
8	0.975	6.36	4.14	0.952	4.71	2.8
10	0.968	5.39	4.06	0.938	3.72	2.7
12	0.96	4.6	3.98	0.922	2.97	2.59
14	0.952	3.96	3.89	0.904	2.4	2.47
16	0.943	3.42	3.79			
18	0.934	2.95	3.69			
20	0.923	2.54	3.57			
22	0.91	2.17	3.43			

Table 3-19: Performance parameters of a single extraction cycle at T_{min} = 30 (°C).

Ψ (kJ/kg)	T_{max} = 80 (°C)			T_{max} = 70 (°C)		
	ε	GOR	RR (%)	ε	GOR	RR (%)
0	1	9.94	6.35	1	13	5.14
2	0.998	9.19	6.31	0.997	11.2	5.09
4	0.996	8.53	6.27	0.993	9.77	5.04
6	0.994	7.93	6.24	0.99	8.62	4.99
8	0.992	7.4	6.2	0.986	7.66	4.94
10	0.99	6.91	6.16	0.982	6.86	4.89
12	0.988	6.46	6.11	0.978	6.17	4.84
14	0.986	6.05	6.07	0.974	5.57	4.78
16	0.984	5.67	6.02	0.97	5.04	4.72
18	0.981	5.33	5.98	0.965	4.58	4.65
20	0.979	5	5.93	0.96	4.16	4.59
22	0.976	4.7	5.88	0.955	3.78	4.52
24	0.974	4.41	5.82	0.95	3.44	4.44
26	0.971	4.15	5.77	0.944	3.12	4.36
28	0.968	3.89	5.71	0.938	2.83	4.27
30	0.965	3.65	5.65	0.931	2.55	4.17
32	0.962	3.42	5.58	0.922	2.28	4.06
34	0.958	3.2	5.51			
36	0.954	2.99	5.44			
38	0.95	2.78	5.35			
40	0.945	2.57	5.26			
42	0.939	2.36	5.15			
44	0.932	2.14	5.03			
Ψ (kJ/kg)	T_{max} = 60 (°C)			T_{max} = 50 (°C)		
	ε	GOR	RR (%)	ε	GOR	RR (%)
0	1	17.79	3.87	1	26.98	2.58
2	0.994	13.14	3.82	0.988	13.61	2.51
4	0.987	10.26	3.76	0.975	8.78	2.44
6	0.981	8.3	3.7	0.961	6.28	2.36
8	0.974	6.88	3.63	0.947	4.74	2.28
10	0.967	5.8	3.56	0.931	3.7	2.19
12	0.959	4.94	3.49	0.914	2.95	2.1
14	0.951	4.25	3.42	0.895	2.37	2
16	0.942	3.68	3.34			
18	0.933	3.19	3.25			
20	0.923	2.77	3.16			
22	0.911	2.4	3.05			

Table 3-20: Performance parameters of a single extraction cycle at T_{min}= 35 (ºC).

Ψ (kJ/kg)	T_{max} = 80 (ºC)			T_{max} = 70 (ºC)		
	ε	GOR	RR (%)	ε	GOR	RR (%)
0	1	10.74	5.81	1	14.56	4.58
2	0.998	9.94	5.78	0.997	12.44	4.54
4	0.996	9.23	5.75	0.993	10.79	4.5
6	0.994	8.59	5.71	0.989	9.47	4.46
8	0.992	8.02	5.68	0.986	8.39	4.42
10	0.99	7.5	5.65	0.982	7.49	4.37
12	0.988	7.03	5.61	0.978	6.73	4.32
14	0.986	6.6	5.57	0.974	6.08	4.27
16	0.984	6.2	5.53	0.97	5.5	4.22
18	0.982	5.83	5.5	0.965	5	4.17
20	0.98	5.49	5.46	0.961	4.56	4.12
22	0.977	5.17	5.41	0.956	4.16	4.06
24	0.975	4.88	5.37	0.951	3.8	4
26	0.972	4.6	5.32	0.945	3.47	3.93
28	0.97	4.34	5.28	0.94	3.17	3.86
30	0.967	4.09	5.23	0.933	2.89	3.79
32	0.964	3.85	5.18	0.927	2.63	3.71
34	0.961	3.63	5.12	0.919	2.38	3.62
36	0.958	3.42	5.07	0.91	2.14	3.52
38	0.954	3.21	5.01			
40	0.95	3.01	4.94			
42	0.946	2.82	4.87			
44	0.942	2.63	4.8			
46	0.937	2.44	4.71			
48	0.931	2.25	4.62			
50	0.923	2.05	4.5			
Ψ (kJ/kg)	T_{max} = 60 (ºC)			T_{max} = 50 (ºC)		
	ε	GOR	RR (%)	ε	GOR	RR (%)
0	1	21.06	3.3	1	35.67	1.98
2	0.993	14.83	3.25	0.985	14.52	1.92
4	0.987	11.27	3.2	0.97	8.74	1.86
6	0.98	8.96	3.15	0.954	6.03	1.79
8	0.972	7.34	3.09	0.937	4.46	1.72
10	0.965	6.14	3.03	0.918	3.43	1.65
12	0.957	5.21	2.97	0.898	2.7	1.57
14	0.948	4.47	2.91			
16	0.939	3.86	2.84			
18	0.93	3.35	2.77			
20	0.92	2.92	2.69			
22	0.908	2.54	2.61			
24	0.896	2.21	2.52			

Table 3-21: Performance parameters of a double extraction cycle at T_{min} = 20 (°C).

Ψ (kJ/kg)	T_{max} = 80 (°C)			T_{max} = 70 (°C)		
	ε	GOR	RR (%)	ε	GOR	RR (%)
0	1	18.13	7.72	1	22.97	6.42
1	0.9992	16.56	7.7	0.9985	19.63	6.38
2	0.9983	15.19	7.67	0.9969	17.02	6.35
3	0.9975	13.97	7.64	0.9954	14.91	6.31
4	0.9966	12.89	7.61	0.9938	13.17	6.27
5	0.9957	11.92	7.57	0.9921	11.71	6.23
6	0.9948	11.04	7.54	0.9904	10.45	6.19
7	0.9938	10.24	7.5	0.9886	9.36	6.14
8	0.9929	9.5	7.46	0.9867	8.39	6.09
9	0.9918	8.82	7.42	0.9848	7.52	6.03
10	0.9908	8.18	7.38	0.9826	6.72	5.97
11	0.9897	7.58	7.33	0.9803	5.97	5.9
12	0.9885	7.01	7.28	0.9777	5.24	5.81
13	0.9872	6.45	7.22			
14	0.9858	5.91	7.15			
15	0.9841	5.35	7.07			
Ψ (kJ/kg)	T_{max} = 60 (°C)			T_{max} = 50 (°C)		
	ε	GOR	RR (%)	ε	GOR	RR (%)
0	1	29.61	5.08	1	39.98	3.75
1	0.9973	22.38	5.05	0.9952	23.64	3.7
2	0.9946	17.73	5	0.9902	16.3	3.65
3	0.9918	14.48	4.96	0.985	12.12	3.6
4	0.9889	12.06	4.91	0.9796	9.39	3.54
5	0.9858	10.19	4.86	0.9739	7.46	3.48
6	0.9827	8.68	4.81	0.9677	6	3.4
7	0.9793	7.43	4.74			
8	0.9757	6.36	4.67			

Table 3-22: Performance parameters of a double extraction cycle at T_{min} = 25 (°C).

Ψ (kJ/kg)	T_{max} = 80 (°C)			T_{max} = 70 (°C)		
	ε	GOR	RR (%)	ε	GOR	RR (%)
0	1	19.47	7.21	1	25.29	5.9
1	0.9992	17.84	7.19	0.9985	21.57	5.87
2	0.9984	16.4	7.16	0.9969	18.68	5.84
3	0.9975	15.14	7.14	0.9953	16.37	5.8
4	0.9966	14.01	7.11	0.9937	14.47	5.77
5	0.9958	13	7.08	0.9921	12.89	5.74
6	0.9949	12.08	7.05	0.9904	11.53	5.7
7	0.994	11.24	7.02	0.9886	10.36	5.66
8	0.993	10.48	6.99	0.9868	9.33	5.62
9	0.992	9.77	6.95	0.9849	8.42	5.57
10	0.991	9.12	6.92	0.9829	7.59	5.52
11	0.99	8.5	6.88	0.9808	6.83	5.47
12	0.9889	7.93	6.84	0.9785	6.13	5.4
13	0.9878	7.38	6.79	0.976	5.45	5.33
14	0.9866	6.85	6.75			
15	0.9852	6.34	6.69			
16	0.9838	5.83	6.63			
17	0.9821	5.31	6.56			
Ψ (kJ/kg)	T_{max} = 60 (°C)			T_{max} = 50 (°C)		
	ε	GOR	RR (%)	ε	GOR	RR (%)
0	1	33.69	4.55	1	47.97	3.21
1	0.9972	24.97	4.52	0.9947	26.19	3.17
2	0.9944	19.56	4.48	0.9893	17.5	3.12
3	0.9915	15.87	4.45	0.9837	12.8	3.08
4	0.9885	13.18	4.4	0.9779	9.84	3.03
5	0.9854	11.12	4.36	0.9718	7.8	2.97
6	0.9822	9.49	4.31	0.9653	6.28	2.91
7	0.9789	8.15	4.26			
8	0.9753	7.03	4.2			
9	0.9715	6.06	4.14			

Table 3-23: Performance parameters of a double extraction cycle at T_{min} = 30 (°C).

Ψ (kJ/kg)	T_{max} = 80 (°C)			T_{max} = 70 (°C)		
	ε	GOR	RR (%)	ε	GOR	RR (%)
0	1	21.02	6.66	1	28.11	5.34
1	0.9992	19.29	6.64	0.9984	23.86	5.31
2	0.9984	17.78	6.62	0.9969	20.6	5.29
3	0.9975	16.44	6.6	0.9953	18.02	5.26
4	0.9967	15.25	6.57	0.9936	15.92	5.23
5	0.9958	14.18	6.55	0.992	14.17	5.2
6	0.9949	13.22	6.53	0.9903	12.7	5.17
7	0.994	12.34	6.5	0.9885	11.43	5.14
8	0.9931	11.54	6.47	0.9867	10.32	5.1
9	0.9922	10.8	6.45	0.9849	9.35	5.06
10	0.9912	10.12	6.42	0.9829	8.48	5.02
11	0.9902	9.48	6.39	0.9809	7.7	4.98
12	0.9892	8.89	6.35	0.9788	6.98	4.93
13	0.9882	8.33	6.32	0.9766	6.31	4.88
14	0.9871	7.8	6.28	0.9741	5.68	4.82
15	0.9859	7.29	6.24			
16	0.9847	6.81	6.2			
17	0.9834	6.33	6.15			
18	0.982	5.86	6.1			
19	0.9803	5.39	6.04			
Ψ (kJ/kg)	T_{max} = 60 (°C)			T_{max} = 50 (°C)		
	ε	GOR	RR (%)	ε	GOR	RR (%)
0	1	39.05	3.99	1	59.84	2.63
1	0.9971	28.05	3.96	0.9941	28.72	2.59
2	0.9941	21.58	3.92	0.988	18.33	2.55
3	0.991	17.32	3.89	0.9817	13.11	2.51
4	0.9879	14.29	3.86	0.9752	9.96	2.47
5	0.9847	12.02	3.82			
6	0.9814	10.24	3.78			
7	0.978	8.82	3.74			
8	0.9744	7.63	3.69			
9	0.9706	6.63	3.64			

Table 3-24: Performance parameters of a double extraction cycle at T_{min} = 35 (°C).

Ψ (kJ/kg)	T_{max} = 80 (°C)			T_{max} = 70 (°C)		
	ε	GOR	RR (%)	ε	GOR	RR (%)
0	1	22.83	6.08	1	4.35	4.11
1	0.9992	20.97	6.07	0.9978	4.25	4.1
2	0.9984	19.35	6.05	0.9955	4.15	4.08
3	0.9975	17.92	6.03	0.9933	4.05	4.07
4	0.9967	16.64	6.01	0.991	3.96	4.05
5	0.9958	15.5	5.99	0.9887	3.87	4.04
6	0.995	14.47	5.97	0.9863	3.79	4.02
7	0.9941	13.54	5.95	0.984	3.71	4.01
8	0.9932	12.69	5.92	0.9816	3.63	3.99
9	0.9923	11.9	5.9	0.9792	3.55	3.97
10	0.9913	11.18	5.88	0.9768	3.47	3.96
11	0.9904	10.52	5.85	0.9743	3.4	3.94
12	0.9894	9.9	5.83	0.9719	3.33	3.93
13	0.9884	9.31	5.8	0.9694	3.26	3.91
14	0.9874	8.77	5.77			
15	0.9863	8.25	5.74			
16	0.9852	7.76	5.71			
17	0.984	7.3	5.68			
18	0.9828	6.85	5.64			
19	0.9815	6.41	5.6			
20	0.9802	5.98	5.56			
21	0.9787	5.56	5.51			
Ψ (kJ/kg)	T_{max} = 60 (°C)			T_{max} = 50 (°C)		
	ε	GOR	RR (%)	ε	GOR	RR (%)
0	1	46.42	3.38	1	79.4	2.01
1	0.9968	31.69	3.36	0.9929	30.49	1.98
2	0.9936	23.72	3.33	0.9857	18.25	1.95
3	0.9904	18.72	3.3	0.9782	12.67	1.91
4	0.987	15.28	3.27	0.9704	9.47	1.88
5	0.9836	12.77	3.24	0.9623	7.38	1.84
6	0.9801	10.84	3.21			
7	0.9764	9.32	3.17			
8	0.9727	8.08	3.13			
9	0.9687	7.04	3.09			

3.3 Chapter conclusions.

In this chapter, the theoretical performance of the thermodynamically balanced HDH cycle has been investigated using the temperature - enthalpy diagram model. To sum up, the next following points summarize this study:

a) For the heat and mass exchangers, the system is called thermodynamically balanced when HCR = 1.
b) As the enthalpy pinch decreases, GOR increases due to minimizing the total exergy destroyed rate.
c) The dehumidifier enthalpy pinch is more dominating on the performance than the humidifier enthalpy pinch.
d) Using a single extraction has a positive effect on the performance of the cycle up to a certain enthalpy at which GOR of the zero and single extraction cycle are equal. This critical enthalpy pinch is called ψ_1.
e) Using double extraction has a positive effect on the performance of the cycle up to a certain enthalpy at which the GOR of the double and single extraction cycle is equal. This critical enthalpy pinch is called ψ_2.
f) The enthalpy pinch of the system must be smaller than ψ_1 and ψ_2 to be able to make use of the single and double extraction.
g) Decreasing the maximum temperature in the cycle leads to an increase in GOR at only low enthalpy pinch values.
h) Increasing the maximum or minimum temperature leads to an increase in the value of ψ_2 and ψ_1.

CHAPTER 4

EXPERIMENTAL WORK

This experimental study has been conducted on water heated CAOW HDH cycle at the steady-state condition to investigate:

a) The effect of mass flow rate ratio for different values of input heat rates on the performance parameters like the gain output ratio (GOR), recovery ratio (RR), and productivity.

b) Specifying the optimum operating mass flow ratio by balancing the dehumidifier thermodynamically (at HCR_{deh} = 1 or $\psi_{deh,cold} = \psi_{deh,hot}$).

c) The effect of single and double extraction on the performance of the HDH cycle.

4.1 Experimental setup description.

Figure 4-1 and Figure 4-2 illustrate a schematic diagram and a photograph of the test rig used in the present work, respectively. The test rig mainly consist of packed bed humidifier on the left of the schematic, a finned tube dehumidifier on the right of the schematic, an electric air heater on the top (11), an electric water heater (10), a circulated air fan (8), a circulated water pump (3), float valve (1), seawater tank (2), distilled water tank (4), level indicator (5), valve (6), flow meter (7), water coil (heat exchanger) (9), sprinklers (12), and a packing material (13). The next sections present a full description of the humidifier, dehumidifier, and other components of the system.

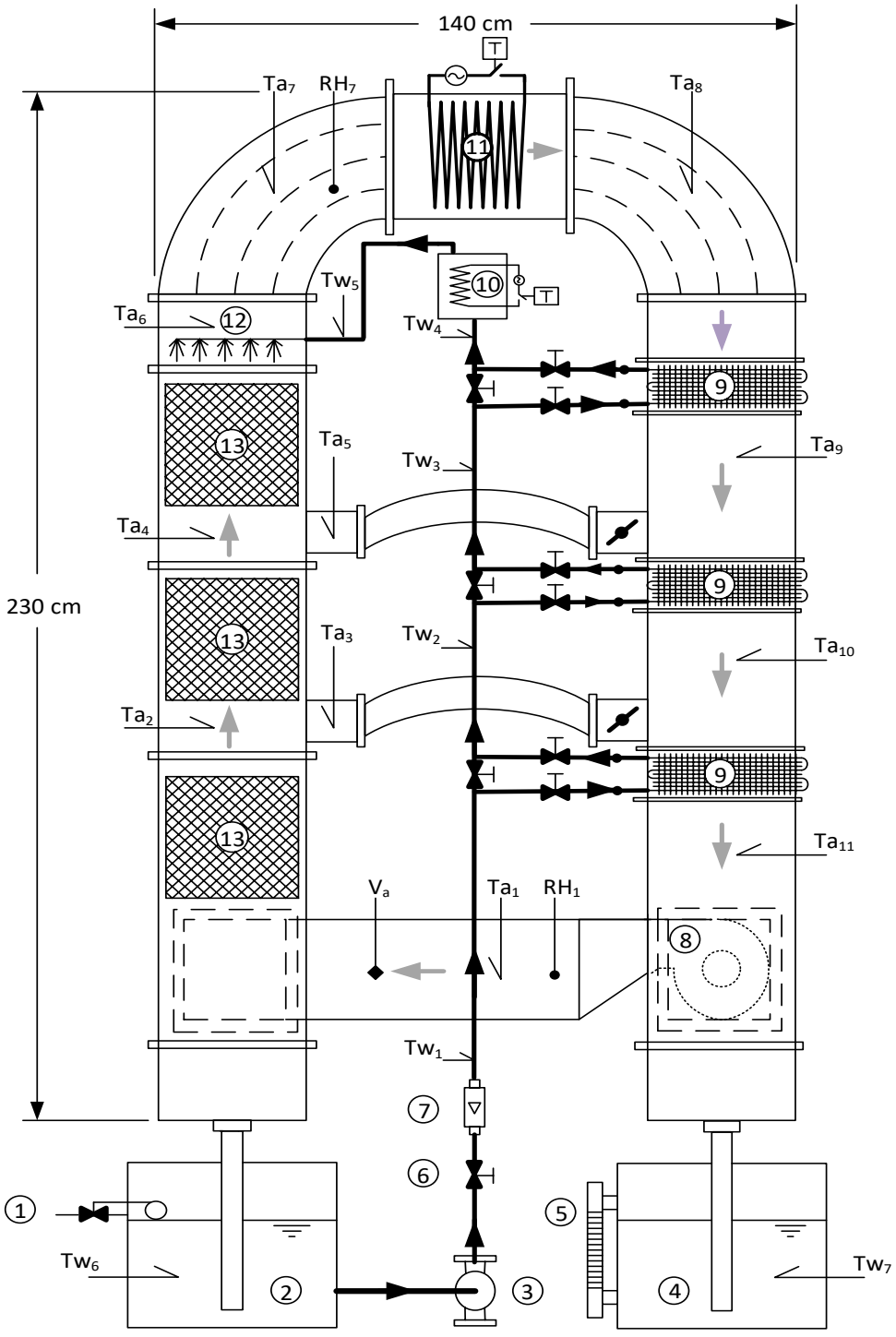

Figure 4-1: Schematic diagram of the HDH experimental setup for studying water-heated, air-heated, and balanced HDH cycles [50]: (1) float valve, (2) seawater tank, (3) pump, (4) distilled water tank, (5) level indicator,(6) valve, (7) flow meter, (8) air fan, (9) water coil (heat exchanger), (10) water heater, (11) air heater, (12) sprinklers, (13) packing material.

Figure 4-2: Photograph of the HDH experimental setup for studying water-heated and air-heated HDH cycles.

4.1.1 Humidifier.

The test-rig is of 1.7 m height structured packing humidifier with a square cross-sectional area of 30 × 30 cm^2 made of galvanized mild steel sheets of 1 mm thickness. The humidifier column was built with three separated partitions inside the column: (1) the top part involved spray nozzles that distribute the hot seawater over the fill material. (2) The middle section consists of the packing material to enhance mass and heat transfer in which the air and water are contacted in direct contact. (3) The bottom part for accumulating the brine water. The three partitions were assembled by flanges that can be removed and disassembled. Three pieces of fill material in the second part are made of black PVC square cooling tower fill material (model number CF1200 MA) has the same humidifier column cross-sectional area and each piece of 30 cm height (specific area of 226 m^2/m^3).

4.1.2 Dehumidifier

A 1.7 m height dehumidifier was built and involved two main sections: (1) the top and middle parts include the square copper coils through which water is partially gained the heat indirectly from moist air, and the copper coil has a square dimension of 30 cm × 30 cm and the coil diameter of ¼ inches. In addition, the height is 6 in. (152.4 mm), while the bottom section is designed to accumulate the condensed water.

4.1.3 Other components

Air is circulated by using a fan (model of HREOB-250-B-2-0.5 HP) and the flow rate is measured by measuring the velocity of air by a hot wire anemometer (model of HHF-SD1) with an accuracy of $\pm$ 3 %. The water mass flow rate is pumped to the system through PVC pipes and controlled by the main valve is shown in the schematic which is attached

to a 0.5 HP pump while a rotameter and turbine flow meter are both used to measure the flow rate with an accuracy of $\pm$ 5 %.

The test rig was designed for heating either water or air. In the case of heating water, an electric water heater (model of FTH-5000-240) with a maximum capacity of 8.8 kW was used to heat the water and adjust the water temperature before entering the humidifier. Standard K-type thermocouple probes with an accuracy of $\pm$ 2 % are used to measure the water temperature at the inlet to the dehumidifier column, before and after water heaters, the rejected water at the bottom of the humidifier and freshwater that come out from the dehumidifier. For air also, standard K-type thermocouple probes were used to measure the top and bottom moist air temperatures. All thermocouples and flow meters are connected to a data acquisition system that uses 6 slots with ATA flash memory drive which has a 128 Mb memory card made by Fluke (model number: FL46305).

4.1.4 Instrumentation

Air Temperatures: dry bulb temperatures measured by standard K-type thermocouples which is a quick connect thermocouple probes with miniature connectors made by Omega (model number: KMQSS-125G-6) used in the experimental setup for the air path at different points as shown in Figure 4-1 (Ta_1, Ta_2, Ta_3, Ta_4, Ta_5, Ta_6, Ta_7, Ta_8, Ta_9, Ta_{10}, and Ta_{11}). Ta_7 is the outlet temperature of air for the humidifier, Ta_1 is the outlet temperature of air for the dehumidifier.

Relative humidity: RH_1 and RH_7 are the relative humidity at the inlet and outlet of the humidifier, respectively, measured by relative humidity/temperature transmitter (RH and T Probe), duct style made by Omega (model number: HX94V) with an accuracy of $\pm$ 2 %.

Water temperatures: The water temperatures measured by standard K-type thermocouples a rugged pipe plug thermocouple probe with 1/4 or 1/8 NPT fitting made by Omega (model number: TC-K-NPT-G-72-SMP) at different points, as shown in Figure 4-2 (Tw_1, Tw_2, Tw_3, Tw_4, Tw_5, Tw_6, and Tw_7). Tw_1 is water temperature after the main valve, Tw_2, Tw_3, and Tw4 are the water temperatures after the cooling coils, Tw_5 is the water temperature after the water heater, Tw_6 and Tw_7 are the water temperatures in the seawater container and the distilled water container, respectively.

4.2 Test Procedure.

Figure 4-3 shows the experimental test procedure for collecting different levels of data sets. The input parameters that may be controlled in this experimental setup are the inlet feed water temperature to the dehumidifier, the water mass flow rate, the air mass flow rate and the input heat rate.

Inlet water temperature.

The inlet feedwater temperature to the dehumidifier may be controlled to be nearly fixed during a certain level of data sets by filling a big supply tank (3m ×1m ×1m) of water before operating the experimental setup.

Water mass flow rate.

The water mass flow rate may be adjusted by a valve located after the pump to be fixed during each level of data sets.

Air mass flow rate.

The air mass flow rate can be adjusted to different values by changing the speed shaft of the blower. Changing the electric current from the electrical control panel can adjust the shaft speed and consequently the airflow rate. As the feedwater mass flow rate is fixed during a certain level of data sets, the mass flow ratio can be adjusted by changing the air mass flow rate.

Input heat rate.

The electric heater consists of four coils and every two coils are connected to a single on/off switch. The first two coils have a capacity of about 3.3 kW and the other two coils have a capacity of about 5.5 kW. Therefore, the available input heat rates are 3.3 kW, 5.5 kW, and 8.8 kW. The experimental data sets of different mass flow rate ratios can be collected for different values of input heat rates.

Data collection.

The experimental setup needs about 30 minutes to reach the steady-state condition for each point of the measured data sets. After reaching the steady-state condition, another 30 minutes were needed to collect the pure water. After collecting the pure water, all the experimental measured parameters could be collected as shown in Table 4-1. An experimental data set of 4 different mass flow ratios were recorded for a fixed input heat rate. The same procedure was repeated for 3 different values of heat input heat rate. Moreover, the same procedure was also repeated for the single and double extraction cycle.

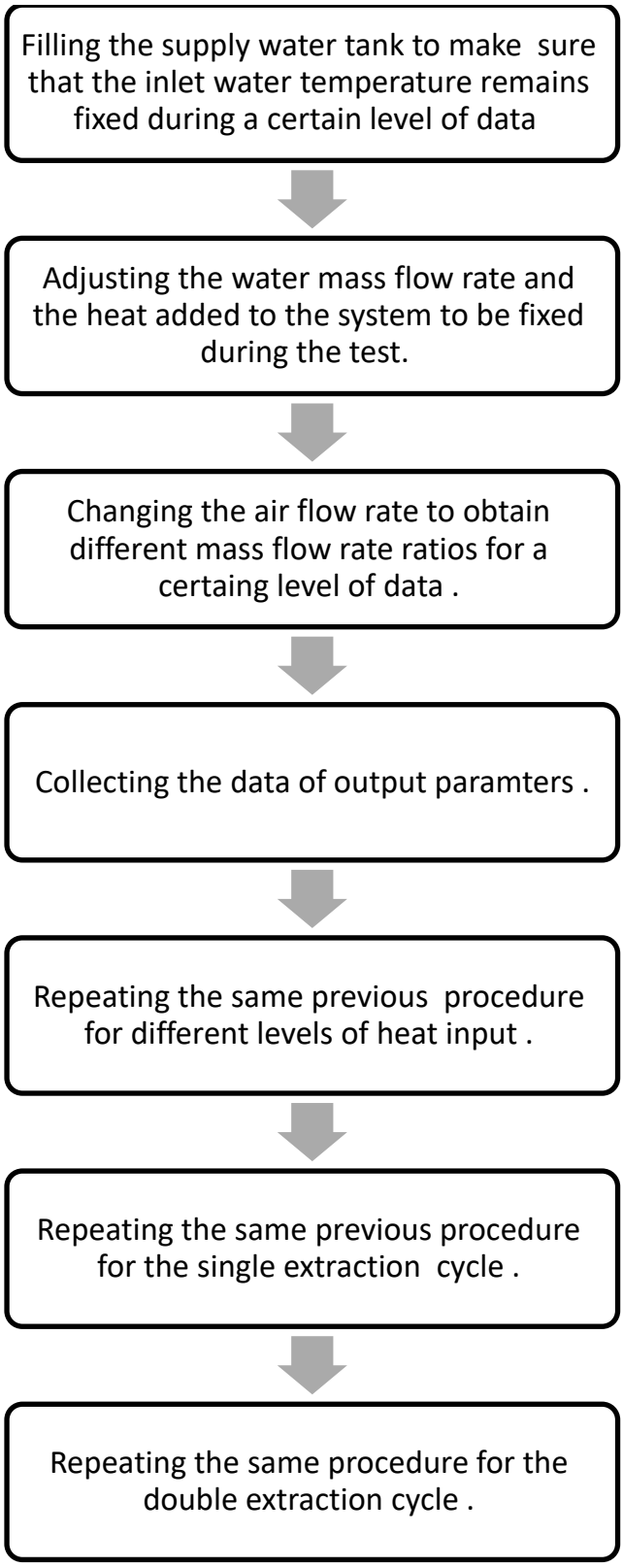

Figure 4-3: The experimental test procedure.

Table 4-1: A summary of test parameters.

Parameter Name		Parameter Symbol	Units
Mass Flow rate	Water	$\dot{m}_w$	kg/s
	Air	$\dot{m}_{da}$	
	Product water	$\dot{m}_{pw}$	
Water Temperature	Dehumidifier inlet	$T_{w,D,in}$	°C
	Different positions along the dehumidifier length	$T_{w,D,inside}$	
	Dehumidifier outlet	$T_{w,D,out}$	
	Humidifier inlet	$T_{w,H,in}$	
	Humidifier outlet	$T_{w,H,out}$	
Air Temperature	Humidifier inlet	$T_{a,H,in}$	°C
	Different positions along the humidifier length	$T_{a,H,inside}$	
	Different positions of extraction	$T_{a,H,ext}$	
	Humidifier outlet	$T_{a,H,out}$	
	Dehumidifier inlet	$T_{a,D,in}$	
	Different positions along the dehumidifier length	$T_{a,D,inside}$	
	Dehumidifier outlet	$T_{a,D,out}$	
Relative Humidity	Humidifier inlet	$\phi_{H,in}$	-
	Humidifier outlet	$\phi_{H,out}$	
Heat added rate		$\dot{Q}$	kW

4.3 Results and Discussion.

According to the experimental test procedure described earlier in Section 4.2, three levels of experimental data sets have been conducted and each level consists of 4 readings. Table 4-2, Table 4-3, and Table 4-4 present the measured air and water temperatures, relative humidity, and mass flow rates for the three levels of data sets for different heat input rates (3.3 kW, 5.5 kW, and 8.2 kW).

The performance parameters described in Chapter 2 were calculated by using the EES program that has built-in seawater and humid air properties (see Appendix B).

Table 4-2: Table of test parameters for Q = 3.3 kW

Water Temperatures (°C)	$T_{w,D,in}$	29.85	29.71	29.52	29.31
	$T_{w,D,out}$	37.04	37.95	38.82	35.89
	$T_{w,H,in}$	45.07	46.03	46.90	44.25
	$T_{w,H,out}$	35.50	35.85	35.90	36.60
Air Temperatures (°C)	$T_{a,H,in}$	36.24	36.06	34.76	31.24
	$T_{a,H,out}$	40.13	41.70	43.89	44.27
	$T_{a,D,in}$	39.28	40.63	42.69	43.72
	$T_{a,D,out}$	36.56	36.51	34.95	30.49
Relative Humidity	$\phi_{H,in}$	99.20	99.20	99.20	99.19
	$\phi_{H,out}$	99.10	99.09	99.11	99.10
Mass Flow Rate (kg/s)	$\dot{m}_{pw}$	0.00079	0.001096	0.0012	0.000894
	$\dot{m}_{da}$	0.121	0.086	0.055	0.027
	$\dot{m}_{w}$	0.098	0.098	0.098	0.098
Mass Flow Rate Ratio	MR	0..8105	1.14	1.79	3.63

Table 4-3: Table of test parameters for Q = 5.5 kW.

Water Temperatures (^oC)	$T_{w,D,in}$	27.38	27.13	26.93	26.78
	$T_{w,D,out}$	39.76	41.12	42.84	39.86
	$T_{w,H,in}$	52.89	54.38	56.15	53.55
	$T_{w,H,out}$	37.41	37.83	38.03	38.96
Air Temperatures (^oC)	$T_{a,H,in}$	37.63	37.42	35.79	29.96
	$T_{a,H,out}$	43.91	46.11	49.4	51.47
	$T_{a,D,in}$	42.37	44.28	47.3	50.36
	$T_{a,D,out}$	37.84	37.76	35.96	29.06
Relative Humidity	$\phi_{H,in}$	99.19	99.19	99.19	99.18
	$\phi_{H,out}$	99.05	99.06	99.07	99.08
Mass Flow Rate (kg/s)	$\dot{m}_{pw}$	0.0016	0.0019	0.0021	0.0017
	$\dot{m}_{da}$	0.120	0.086	0.055	0.027
	$\dot{m}_{w}$	0.098	0.098	0.098	0.098
Mass Flow Rate Ratio	MR	0.82	1.14	1.79	3.63

Table 4-4: Table of test parameters for Q = 8.2 kW.

Water Temperatures (^oC)	$T_{w,D,in}$	23.06	23.02	23.42	24.26
	$T_{w,D,out}$	41.78	43.72	45.99	40.60
	$T_{w,H,in}$	60.55	62.75	64.59	59.99
	$T_{w,H,out}$	38.22	38.82	38.82	41.04
Air Temperatures (^oC)	$T_{a,H,in}$	37.81	37.48	35.20	26.52
	$T_{a,H,out}$	46.60	49.62	53.72	56.80
	$T_{a,D,in}$	44.76	47.48	51.51	55.39
	$T_{a,D,out}$	38.24	38.01	35.57	26.180
Relative Humidity	$\phi_{H,in}$	99.20	99.20	99.19	99.18
	$\phi_{H,out}$	99.20	99.20	99.197	99.18
Mass Flow Rate (kg/s)	$\dot{m}_{pw}$	0.0023	0.003	0.0032	0.0024
	$\dot{m}_{da}$	0.121	0.086	0.053	0.027
	$\dot{m}_{w}$	0.102	0.102	0.102	0.102
Mass Flow Rate Ratio	MR	0.85	1.19	1.91	3.76

4.3.1 Optimum performance at the thermodynamic balancing condition.

Figure 4-4, Figure 4-5, and Figure 4-6 show the effect of both the mass flow rate (MR) and the input heat rate (Q) on the productivity, recovery ratio, and GOR of the water heat HDH system. It is evident that the productivity, the recovery ratio, and the GOR have optimum values at MR = 1.78 for Q = 3.3 kW, at MR = 1.78 for Q = 5.5 kW, and at MR = 1.92 for Q = 8.2 kW. The reason for this observation is that the dehumidifier modified heat capacity is equal to unity at the optimum mass flow rate ratio, as shown in Table 4-5. It is evident that the enthalpy pinch of the cold stream ($\psi_{deh,c}$) and hot stream ($\psi_{deh,c}$) at the terminal positions of the dehumidifier are almost the same at the optimum condition . This result is consistent with the previous theoretical studies [27, 29–31, 33, 34, 36] on the thermodynamic balancing of the HDH system.

4.3.2 Minimum dehumidifier energy effectiveness at the on-design condition.

The case at which the modified heat capacity ratio of the dehumidifier is equal to unity is called the on-design condition. On the other hand, the case at which the modified heat capacity ratio of the dehumidifier is not equal to unity is called the off-design condition. As shown in Table 4-5, although the energy effectiveness of the dehumidifier (ε_{deh}) has a minimum value at the on-design condition, the GOR has an optimum value at the on-design condition. The reason for this observation is that the energy effectiveness of the dehumidifier at the off-design condition is high for one stream only. For instance, as shown in Table 4-5, the water stream has higher energy effectiveness compared with the airstream at $HCR_{deh} < 1$ and the air stream has a higher energy effectiveness compared with the water stream at $HCR_{deh} > 1$. On the other hand, the air stream effectiveness ($\varepsilon_{deh,air}$)

and the water stream effectiveness ($\varepsilon_{deh,water}$) are almost the same at the on-design condition.

4.3.3 Input heat rate effect on the performance parameters.

Figure 4-4 shows that increasing the input heat rate leads to increasing the productivity for different mass flow rate ratios. The reason for this observation is that increasing the heat input rate leads to increasing the difference between the minimum air temperature (inlet to humidifier) and the maximum air temperature (exit from the humidifier). Therefore, the difference between the humidity ratio at the humidifier exit and the humidity ratio at the humidifier inlet increases and consequently, the dehumidifier becomes more effective, thus able to condensate more water vapor. As the inlet feed water flow rate is nearly fixed, the recovery ratio increases as shown in Figure 4-5. It is evident in Figure 4-6 that increasing the heat input rate leads to increasing the GOR at on-design conditions. The reason for this observation is that the on-design energy effectiveness of the dehumidifier increases as the heat input rate increases, as shown in Table 4-5.

The increase in input heat rate has a higher effect on productivity than the GOR value. The reason for this observation is that the GOR is not a function only of the productivity but also in the input heat rate according to Eq. (2-1). For instance, increasing the heat input rate leads to increasing the denominator in Eq. (2-1) but it also leads to an increase in productivity in the numerator. Therefore, the total effect of the input heat rate on the GOR is small compared with its effect on productivity.

The maximum productivity, recovery ratio and GOR of this system are about 11.5 L/h, 3.2% and 0.99, respectively at the on-design condition when the input heat rate is equal to 8.2 kW.

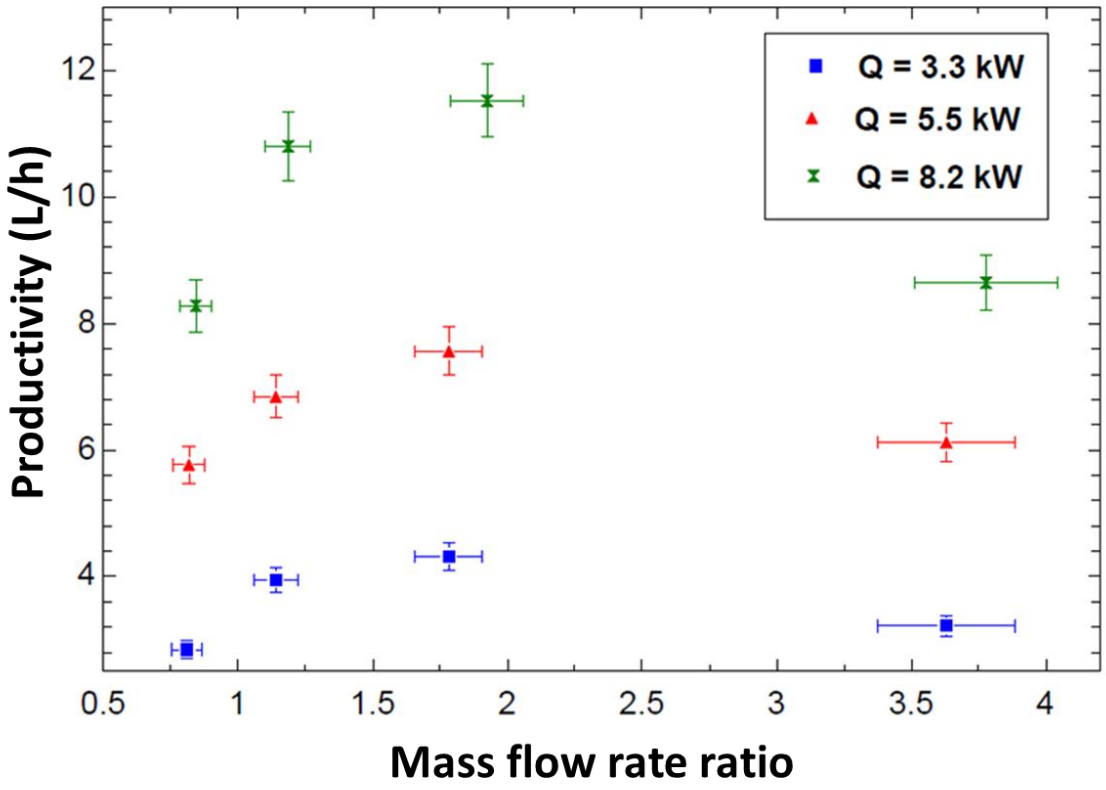

Figure 4-4: The effect of MR and input heat rate on productivity.

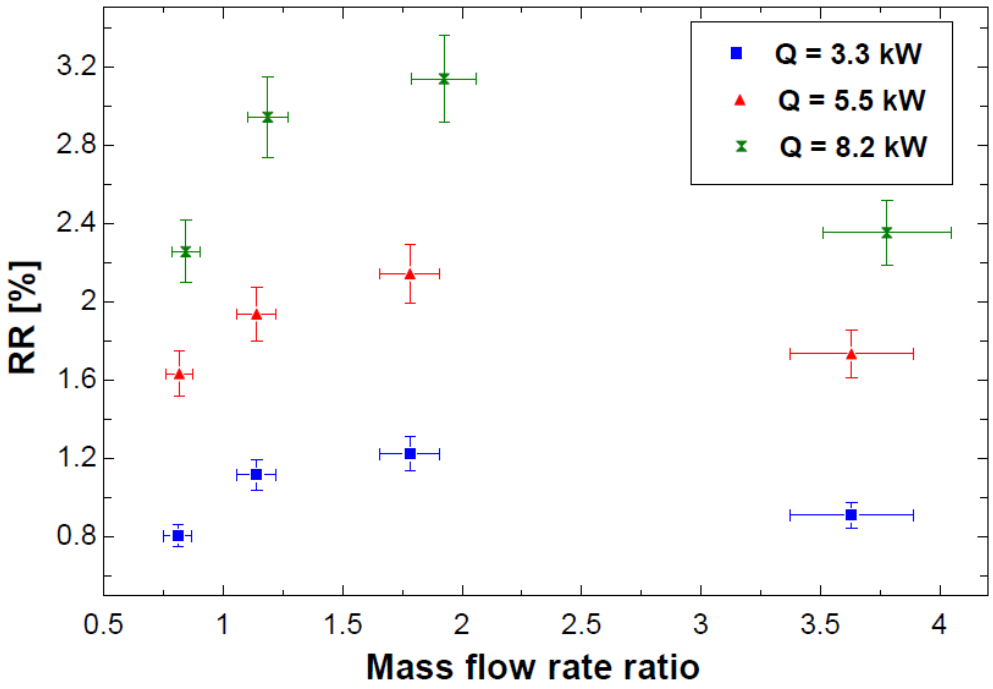

Figure 4-5: The effect of MR and input heat rate on the recovery ratio.

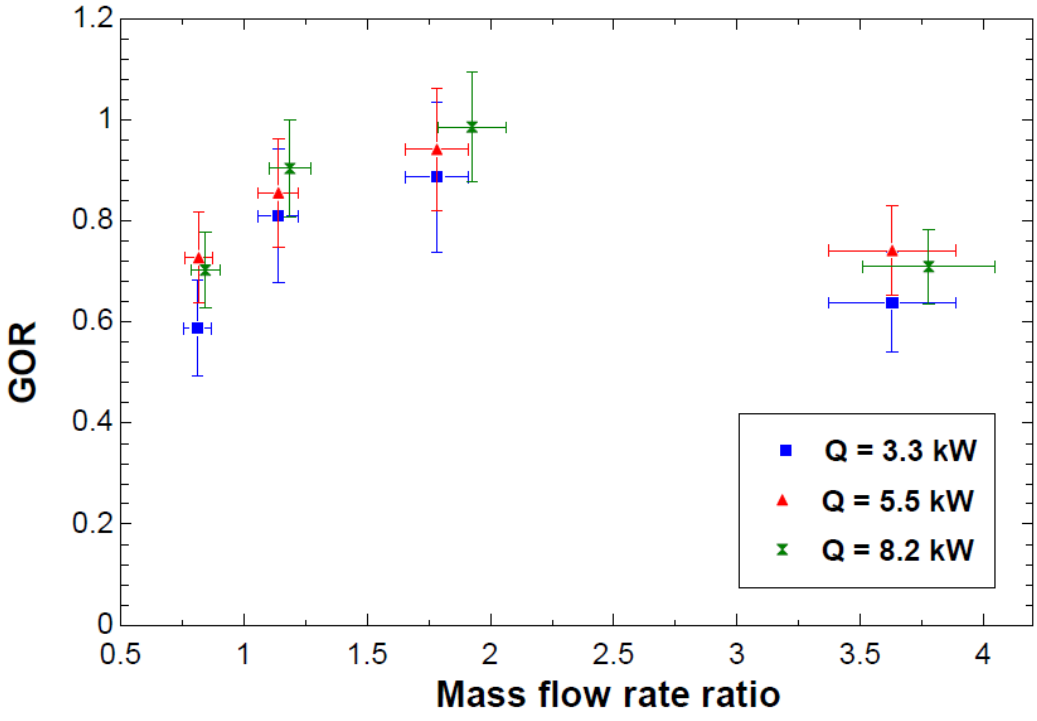

Figure 4-6: The effect of MR and input heat rate on the gain output ratio.

Table 4-5: The effect of MR and input heat rate on the performance parameters.

Q (kW)	MR	HCR_{deh}	$\psi_{deh,c}$ (kJ/kg)	$\psi_{deh,h}$ (kJ/kg)	$\varepsilon_{deh,air}$	$\varepsilon_{deh,water}$	ε_{deh}
3.3	0.81±0.06	0.53±0.05	11.6±7	39.7±6.4	0.34±0.11	0.76±0.1	0.76±0.1
	1.14±0.08	0.72±0.06	20.2±7.6	40±6.3	0.44±0.09	0.75±0.09	0.75±0.09
	1.78±0.13	1.08±0.09	37.3±9.6	30.5±5.8	0.67±0.06	0.71±0.08	0.71±0.08
	3.63±0.26	2.14±0.18	121.7±18.8	5.4±4.6	0.95±0.04	0.46±0.06	0.95±0.04
5.5	0.82±0.06	0.52±0.04	13.5±8.6	61±6.6	0.38±0.08	0.83±0.07	0.83±0.07
	1.14±0.08	0.69±0.06	24.9±9.8	61.6±6.6	0.48±0.06	0.82±0.06	0.82±0.06
	1.78±0.13	0.99±0.08	48.9±13.3	49.7±5.9	0.67±0.04	0.78±0.06	0.78±0.06
	3.63±0.26	1.86±0.15	175.3±27	10.2±4	0.95±0.02	0.55±0.04	0.95±0.02
8.2	0.84±0.06	0.54±0.04	18.3±10.3	82.4±6.5	0.41±0.06	0.86±0.05	0.86±0.05
	1.19±0.08	0.71±0.06	30.9±12.6	80.8±6.4	0.53±0.05	0.85±0.05	0.85±0.05
	1.92±0.14	1.01±0.08	64.6±18.8	61.9±5.5	0.72±0.03	0.8±0.04	0.8±0.04
	3.78±0.27	1.73±0.15	215.3±36.3	7.6±3.2	0.97±0.01	0.52±0.03	0.97±0.01

4.3.4 Experimental validation against the theoretical model.

According to the previous experimental results, there is a thermodynamically balanced dehumidifier case at each value of input heat rate. Table 4-6 shows the minimum and maximum temperature inside the HDH cycle in addition to the enthalpy pinch of both the humidifier and dehumidifier corresponding to the thermodynamically balanced

dehumidifier case at each value of input heat rate. The enthalpy pinch of the humidifier and the dehumidifier is estimated from the experimental results according to its definition in section 3.1.

Using the T_{min} , the T_{max} , the ψ_{hum} and the ψ_{deh} in Table 4-6 as input parameters to the zero extraction model described in Chapter 3, the corresponding GOR may be estimated theoretically. Table 4-7 shows the comparison between the theoretical and experimental performance at the thermodynamic balanced condition in addition to the corresponding percentage error. The maximum percentage error is about 6.2 %. The difference between the theoretical results and experimental results is due to the uncertainty in the instruments, heat losses from the different components of the cycle.

Table 4-6: Balanced cases for different added heat rates.

Balanced cases	$\boldsymbol{T_{min}}$ (^{o}C)	$\boldsymbol{T_{max}}$ (^{o}C)	ψ_{hum} (kJ/kg)	ψ_{deh} (kJ/kg)
Case (1): Q = 3.3 kW	29.52	46.94	14	37.3
Case (2): Q = 5.5 kW	26.93	56.29	36	49.7
Case (3): Q = 8.2 kw	23..42	64.59	45.8	61.9

Table 4-7: Validation between experimental balanced cases and zero extraction model.

Balanced cases	GOR (Experimental)	GOR (by model)	Percentage error (%)
Case (1)	0.8861	0.90	1.54
Case (2)	0.941	0.96	1.98
Case (3)	0.9854	1.05	6.2

4.3.5 The single and double extraction effect on the performance

Figure 4-7, Figure 4-8, and Figure 4-9 show the single and double extraction effect on the performance parameters (GOR, RR, and Productivity) at the same input heat rate (Q = 5.5 kW). It is evident that using extraction in the previously described experimental setup does not improve the performance. The reason for this observation is that the dehumidifier size is not large enough to make use of the positive effect of using extractions. The size of both the dehumidifier and humidifier governs the value of ψ_{deh} and ψ_{hum}. Therefore, the values of ψ_{hum} and ψ_{deh} depend on the design of humidifier and dehumidifier. As mentioned in Section 3.2, to be able to make use of single extraction, the enthalpy pinch of the system (ψ_{hum} and ψ_{deh}) must be smaller than ψ_1. In addition, to be able to make use of the double extraction, the enthalpy pinch of the system (ψ_{hum} and ψ_{deh}) must be smaller than ψ_2.

Figure 4-10 shows the GOR versus the enthalpy pinch of zero, single and double extraction cycle at the thermodynamic balancing condition having the same minimum and maximum temperature of the case (2) in Table 4-6. It is evident that ψ_1 is equal to $20\ kJ/kg$ and ψ_2

is equal to 9 kJ/kg (see Figure 4-10) which are smaller than the system enthalpy pinch ($\psi_{hum} = 36\ kJ/kg$ and $\psi_{deh} = 49.7\ kJ/kg$) of case (2). Therefore, using single and double extractions does not improve the cycle performance.

Table 4-8 shows a comparison between the system enthalpy pinch and the critical enthalpy pinch ($\psi_1\ and\ \psi_2$) for the balanced cases of the three values of input heat rates. It is evident that the ψ_{deh} and ψ_{hum} is higher than ψ_1 and ψ_2 for the three cases. Therefore, to be able to make use of the single and double extraction, the size of the humidifier and dehumidifier must increase.

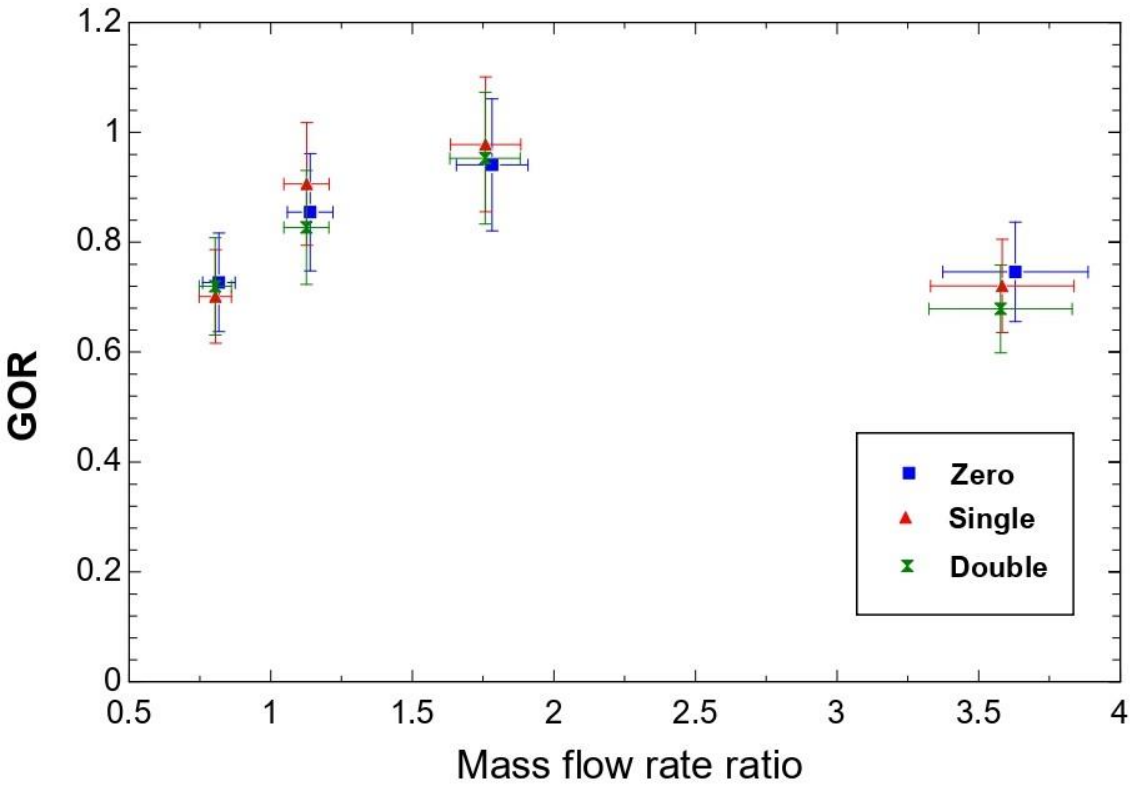

Figure 4-7: The Single and double extraction effect on the GOR at Q = 5.5 kW.

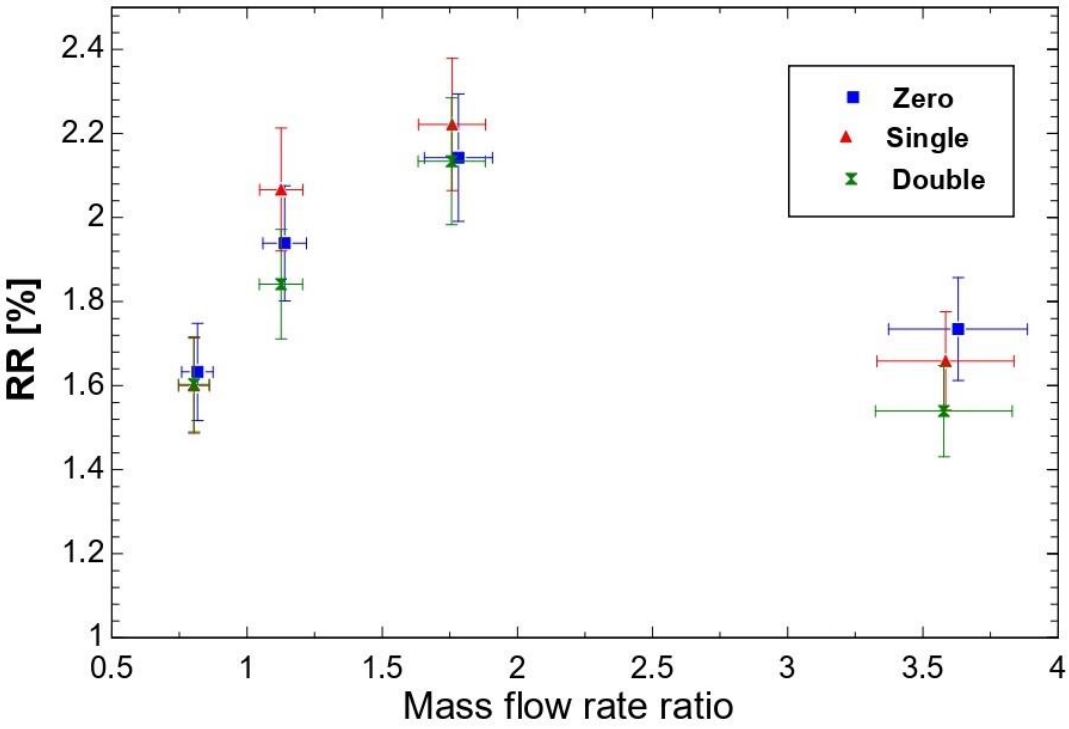

Figure 4-8: The Single and double extraction effect on the RR at Q = 5.5 kW.

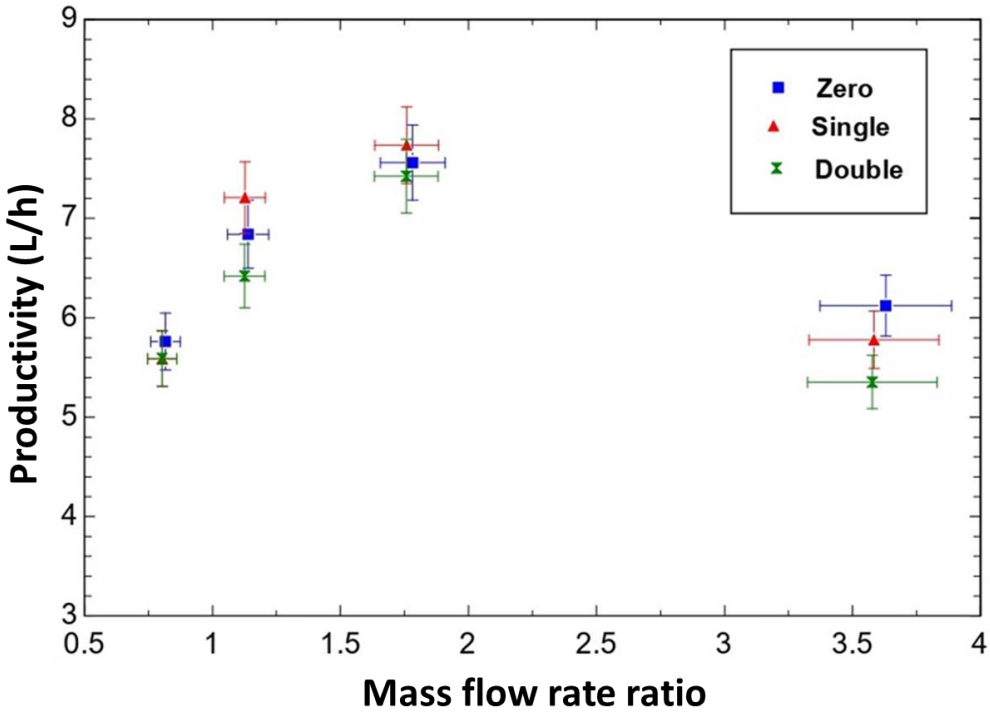

Figure 4-9: The single and double extraction effect on productivity at Q = 5.5 kW.

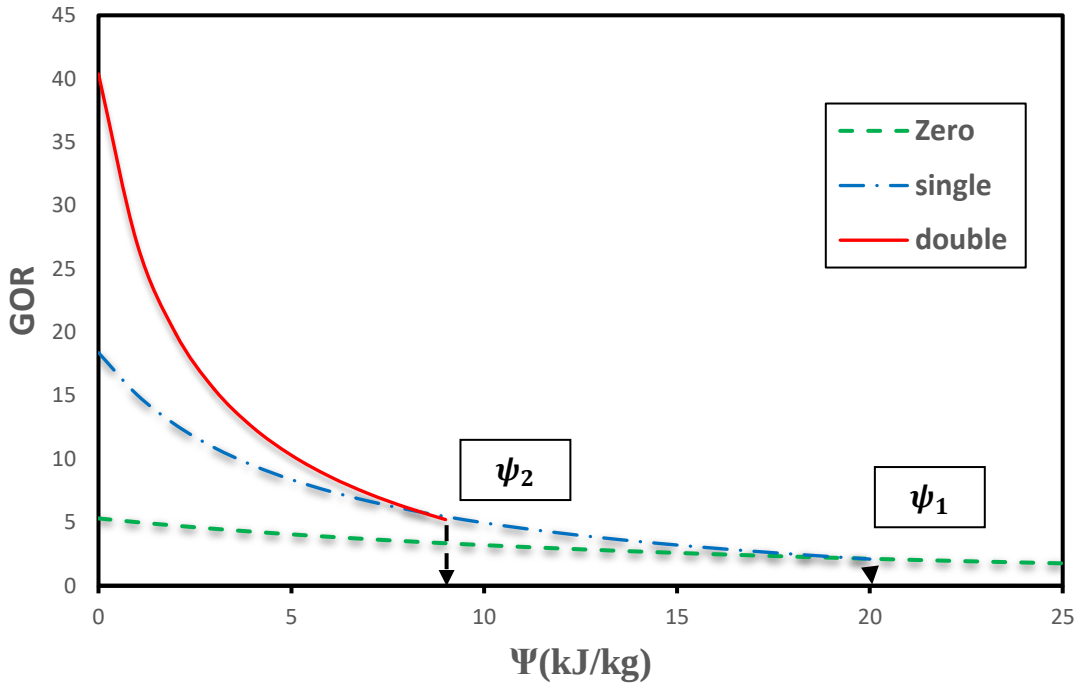

Figure 4-10: Enthalpy pinch effect on GOR for zero, single and double extraction cycle at T_{max} = 56.3 °C and T_{min} = 26.9 °C using the theoretical model.

Table 4-8: Comparison between the system enthalpy pinch and the critical enthalpy pinch (Ψ_1 and Ψ_2).

Balanced case	ψ_1 (kJ/kg)	ψ_2 (kJ/kg)	System (kJ/kg)	
			ψ_{hum}	ψ_{deh}
Case (1)	12	5	14	37.3
Case (2)	20	9	36	49.7
Case (3)	25	10	45.8	61.9

4.4 Chapter conclusions.

In this chapter, some experimental results have been presented at which the thermodynamically balanced dehumidifier cases are consistent with the theoretical model presented in Chapter 3. The next following points summarize the experimental study in this chapter:

a) At $HCR_{deh} = 1$, the dehumidifier is thermodynamically balanced, and this is the on-design condition.
b) At $HCR_{deh} = 1$, The HDH cycle has an optimum performance (maximum GOR, RR, and productivity).
c) The maximum productivity, RR, and GOR of this system are about 11.5 L/h, 3.2 %, and 0.99, respectively at the on-design condition of Q = 8.2 kW.
d) At $HCR_{deh} = 1$, the enthalpy pinch of the cold- and hot-stream at the inlet and outlet of the dehumidifier are nearly the same.
e) At $HCR_{deh} = 1$, the air stream effectiveness, and the water stream effectiveness are nearly the same in the dehumidifier.
f) At $HCR_{deh} = 1$, The dehumidifier energy effectiveness has a minimum value.
g) At $HCR_{deh} = 1$, As the dehumidifier energy effectiveness increases, the GOR increases.
h) Increasing the input heat rate has a positive effect on productivity and the RR more than the GOR.
i) For this experimental setup, using single and double extraction does not have a positive effect on the performance as the system size is not large enough to make use of extractions.

CHAPTER 5

Conclusions and Recommendations

The theoretical performance of the thermodynamically balanced HDH cycle has been investigated using the temperature - enthalpy diagram model. The next following points summarize this study:

a) The dehumidifier enthalpy pinch is more dominating on the performance than the humidifier enthalpy pinch.
b) Using a single extraction has a positive effect on the performance of the cycle up to a certain enthalpy at which GOR of zero and a single extraction cycle are equal. This critical enthalpy pinch is called ψ_1.
c) Using double extraction has a positive effect on the performance of the cycle up to a certain enthalpy at which the GOR of the double and single extraction cycle is equal. This critical enthalpy pinch is called ψ_2.
d) The enthalpy pinch of the system must be smaller than ψ_1 and ψ_2 to be able to make use of the single and double extraction.
e) Decreasing the maximum temperature in the cycle leads to an increase in GOR at only low enthalpy pinch values.
f) Increasing the maximum temperature leads to an increase in the value of ψ_2 and ψ_1.
g) Increasing the minimum temperature in the cycle leads to an increase in GOR.

h) Increasing the minimum temperature leads to an increase in the value of ψ_2 and ψ_1.

Some experimental results have been presented at which the thermodynamically balanced dehumidifier cases are consistent with the theoretical model presented in Chapter 3. The next following points summarize the experimental study:

a) The maximum productivity, RR, and GOR of this system are about 11.5 L/h, 3.2 %, and 0.99, respectively at the on-design condition of Q = 8.2 kW.
b) For this experimental setup, using single and double extraction does not have a positive effect on the performance as the system size is not large enough to make use of extractions.

Recommendations

As our experimental study failed to achieve the thermodynamic balancing for the single and double extraction cycle. The following points may guide the designer to make use of the single and double extractions:

a) Using extractions is useful only at high effectiveness only, especially for the dehumidifier. Therefore, the system size must be large enough to make use of extractions.

b) As the size is a critical issue for applying extractions, a transport model, heat and mass transfer model, may be developed to estimate the size accurately.

c) Using a bubble column dehumidifier may lead to obtaining high effectiveness with a small size.

d) The designed system must be flexible to change the position of extraction. As the position of extractions is very critical for satisfying the thermodynamic balancing at each stage.

e) The designed system must have a flow control valve to adjust the amount of extracted air. Therefore, the optimum mass flow rate ratio at each stage can be achieved.

REFERENCES

[1] G. P. Narayan, M. H. Sharqawy, E. K. Summers, J. H. Lienhard V, S. M. Zubair, and M. A. Antar, "The potential of solar-driven humidification–dehumidification desalination for small-scale decentralized water production," Renewable and Sustainable Energy Reviews, vol. 14, no. 4, pp. 1187–1201 (2010).

[2] S. O. Liburd, "Solar-driven humidification dehumidification desalination for potable use in haiti," M.S. thesis, Massachusetts Institute of Technology, Cambridge MA, USA (2010).

[3] I. Mohan, S. Yadav, H. Panchal, and S. Brahmbhatt, "A review on solar still: a simple desalination technology to obtain potable water," Int. J. Ambient Energy, vol. 40, no. 3, pp. 335–342 (2019).

[4] A. Kaushal and Varun, "Solar stills: A review," Renew. Sustain. Energy Rev., vol. 14, no. 1, pp. 446–453 (2010).

[5] A. E. Kabeel, Y. A. F. El-Samadony, and W. M. El-Maghlany, "Comparative study on the solar still performance utilizing different PCM," Desalination, vol. 432, pp. 89–96 (2018).

[6] H. E. S. Fath, "Solar distillation: a promising alternative for water provision with free energy, simple technology and a clean environment," Desalination, vol. 116, no. 1, pp. 45–56 (1998).

[7] G. N. Tiwari, H. N. Singh, and R. Tripathi, "Present status of solar distillation," Solar Energy, vol. 75, no. 5, pp. 367–373 (2003).

[8] G. P. Narayan, M. H. Sharqawy, J. H. Lienhard V, and S. M. Zubair, "Thermodynamic analysis of humidification dehumidification desalination cycles," Desalin. Water Treat., vol. 16, no. 1–3, pp. 339–353 (2010).

[9] M. H. Sharqawy, M. A. Antar, S. M. Zubair, and A. M. Elbashir, "Optimum thermal design of humidification dehumidification desalination systems," Desalination, vol. 349, pp. 10–21 (2014).

[10] O. K. Siddiqui, M. H. Sharqawy, M. A. Antar, and S. M. Zubair, "Performance evaluation of variable pressure humidification-dehumidification systems," Desalination, vol. 409, pp. 171–182 (2017).

[11] J.F. Klausner, R. Mei, Y. Li, "Innovative Fresh Water Production Process for Fossil Fuel Plants," DOE–Energy Information Administration annual report, US (2003).

[12] G. P. Narayan, K. H. Mistry, M. H. Sharqawy, S. M. Zubair, and J. H. Lienhard V, "Energy effectiveness of simultaneous heat and mass exchange devices," Frontiers in Heat and Mass Transfer, vol. 1, no. 2, pp. 1-13 (2010).

[13] P. N. Govindan, "Thermal design of humidification dehumidification systems for

affordable and small-scale desalination," Ph.D. thesis, Massachusetts Institute of Technology, Cambridge MA, USA (2012).

[14] A. S. Nafey, H. E. S. Fath, S. O. El-Helaby, and A. Soliman, "Solar desalination using humidification–dehumidification processes. Part II. An experimental investigation," Energy Convers. Manag., vol. 45, no. 7–8, pp. 1263–1277 (2004).

[15] S. Al-Hallaj, M. M. Farid, and A. R. Tamimi, "Solar desalination with a humidification-dehumidification cycle: performance of the unit," Desalination, vol. 120, no. 3, pp. 273–280 (1998).

[16] H. B. Bacha, T. Damak, M. Bouzguenda, and A. Y. Maalej, "Experimental validation of the distillation module of a desalination station using the SMCEC principle," Renew. Energy, vol. 28, no. 15, pp. 2335–2354 (2003).

[17] M. Farid and A. W. Al-Hajaj, "Solar desalination with a humidification-dehumidification cycle," Desalination, vol. 106, no. 1–3, pp. 427–429 (1996).

[18] H. P. Garg, R. S. Adhikari, and R. Kumar, "Experimental design and computer simulation of multi-effect humidification (MEH) - dehumidification solar distillation," Desalination, vol. 153, no. 1–3, pp. 81–86 (2003).

[19] H. Müller-Holst, "Solar thermal desalination using the multiple effect humidification (MEH) - method," in Solar Desalination for the 21st Century, Dordrecht: Springer Netherlands, pp. 215–225 (2007).

[20] N. K. Nawayseh, M. M. Farid, S. Al-Hallaj, and A. R. Al-Timimi, "Solar desalination based on humidification process - I. Evaluating the heat and mass transfer coefficients," Energy Convers. Manag., vol. 40, no. 13, pp. 1423–1439, (1999).

[21] M. A. Younis, M. A. Darwish, and F. Juwayhel, "Experimental and theoretical study of a humidification-dehumidification desalting system," Desalination, vol. 94, no. 1, pp. 11–24 (1993).

[22] H. Müller-Holst, "Mehrfacheffekt-feuchtluftdestillation bei umgebungsdruck," Technische Universität München, Germany (2002).

[23] N. A. A. Qasem, M. A. Ahmed, and S. M. Zubair, "The impact of thermodynamic balancing on performance of a desiccant-based humidification-dehumidification system to harvest freshwater from atmospheric air," Energy Convers. Manag., vol. 199, p. 112011 (2019).

[24] M. A. Ahmed, N. A. A. Qasem, and S. M. Zubair, "Analytical and numerical schemes for thermodynamically balanced humidification-dehumidification desalination systems," Energy Convers. Manag., vol. 200, p. 112052 (2019).

[25] S. M. Elmutasim, M. A. Ahmed, M. A. Antar, P. Gandhidasan, and S. M. Zubair, "Design strategies of conventional and modified closed-air open-water humidification dehumidification systems," Desalination, vol. 435, pp. 114–127

(2018).

[26] M. Zamen, S. M. Soufari, and M. Amidpour, “Improvement of solar humidification-dehumidification desalination using multi-stage process,” vol. 25, pp. 1091–1096 (2011).

[27] G. P. Narayan, K. M. Chehayeb, R. K. McGovern, G. P. Thiel, S. M. Zubair, and J. H. Lienhard V, “Thermodynamic balancing of the humidification dehumidification desalination system by mass extraction and injection,” Int. J. Heat Mass Transf., vol. 57, no. 2, pp. 756–770 (2013).

[28] J.A. Miller, “Numerical balancing in a humidification dehumidificationdesalination system,” M.S. thesis, Massachusetts Institute of Technology, Cambridge MA, USA (2011).

[29] K. M. Chehayeb, G. P. Narayan, S. M. Zubair, and J. H. Lienhard V, “Thermodynamic balancing of a fixed-size two-stage humidification dehumidification desalination system,” Desalination, vol. 369, pp. 125–139 (2015).

[30] K. M. Chehayeb, “Numerical fixed-effectiveness and fixed-area models of the humidification dehumidification desalination system with air extractions and injections,” M.S. thesis, Massachusetts Institute of Technology, Cambridge MA, USA (2014).

[31] R. K. McGovern, G. P. Thiel, G. Prakash Narayan, S. M. Zubair, and J. H. Lienhard V, “Performance limits of zero and single extraction humidification-dehumidification desalination systems,” Applied Energy, vol. 102, pp. 1081–1090 (2013).

[32] S. Hou, “Two-stage solar multi-effect humidification dehumidification desalination process plotted from pinch analysis,” Desalination, vol. 222, no. 1–3, pp. 572–578 (2008).

[33] G. P. Thiel, J. A. Miller, S. M. Zubair, and J. H. Lienhard V, “Effect of mass extractions and injections on the performance of a fixed-size humidification–dehumidification desalination system,” Desalination, vol. 314, pp. 50–58 (2013).

[34] K. M. Chehayeb, G. Prakash Narayan, S. M. Zubair, and J. H. Lienhard V, “Use of multiple extractions and injections to thermodynamically balance the humidification dehumidification desalination system,” Int. J. Heat Mass Transf., vol. 68, pp. 422–434 (2014).

[35] G. P. Narayan, R. K. McGovern, G. P. Thiel, J. A. Miller, J. H. Lienhard V, M. H. Sharqawy, S. M. Zubair, M. A. Antar, “Status of humidification dehumidification desalination technology,” International Desalination Association World Water Congress, Perth, Australia (2011).

[36] G. Prakash Narayan, J. H. Lienhard V, and S. M. Zubair, “Entropy generation minimization of combined heat and mass transfer devices,” Int. J. Therm. Sci., vol.

49, no. 10, pp. 2057–2066 (2010).

[37] I. Dincer and M. A. Rosen, "Exergy: energy, environment and sustainable development," Elsevier (2007).

[38] M. J. Moran, H. N. Shapiro, Fundamentals of Engineering Thermodynamics, 6th Edition, John Wiley & Sons, Inc., New Jersey (2007).

[39] K. H. Mistry, J. H. Lienhard V, and S. M. Zubair, "Effect of entropy generation on the performance of humidification-dehumidification desalination cycles," Int. J. Therm. Sci., vol. 49, no. 9, pp. 1837–1847 (2010).

[40] A. Bejan, Advanced Engineering Thermodynamics, 3rd Edition, John Wiley & Sons, Inc., Hoboken, New Jersey (2006).

[41] D. U. Lawal, S. M. Zubair, and M. A. Antar, "Exergo-economic analysis of humidification-dehumidification (HDH) desalination systems driven by heat pump (HP)," Desalination, vol. 443, pp. 11–25 (2018).

[42] K. H. Mistry, "Second Law Analysis and Optimization of Humidification-Dehumidification Desalination Cycles," M.S. thesis, Massachusetts Institute of Technology, Cambridge MA, USA (2010).

[43] J. A. Miller and J. H. Lienhard V, "Impact of extraction on a humidification dehumidific ation desalination system," Desalination, vol. 313, pp. 87–96 (2013).

[44] S. A. Klein, Engineering Equation Solver (EES) Version 10, Madison, USA (2019).

[45] E. W. Lemmon, R. T. Jacobsen, S. G. Penoncello, and D. G. Friend, "Thermodynamic properties of air and mixtures of nitrogen, argon, and oxygen from 60 to 2000 K at pressures to 2000 MPa," J. Phys. Chem. Ref. data, vol. 29, no. 3, pp. 331–385 (2000).

[46] R. W. Hyland, A. Wexler, Formulations for the thermodynamic properties of the saturated phases of H_2O from 173.15 K to 473.15 K, ASHRAE Transactions Part 2A, pp. 500-519 (1983).

[47] D. J. Wessel, ed., ASHRAE fundamentals handbook (SI Edition), American Society of Heating, Refrigerating, and Air-Conditioning Engineers, Atlanta, USA (2001).

[48] W. Wagner and A. Pruss, "The IAPWS formulation 1995 for the thermodynamic properties of ordinary water substance for general and scientific use," J. Phys. Chem. Ref. data, vol. 31, no. 2, pp. 387–535 (2002).

[49] M. H. Sharqawy, J. H. Lienhard V, and S. M. Zubair, "Thermophysical properties of seawater: a review of existing correlations and data," Desalin. Water Treat., vol. 16, no. 1–3, pp. 354–380 (2010).

[50] M. H. Sharqawy, M. A. Antar, S. M. Zubair, P. Gandhidasan, "Innovative Solar Desalination Systems for Decentralized Small-Scale Water Production," final

report, Project 11-WAT1625-04, Maarifah, KACST, KSA (2014).

Appendix A: Solution algorithm for the fixed-effectiveness modeling

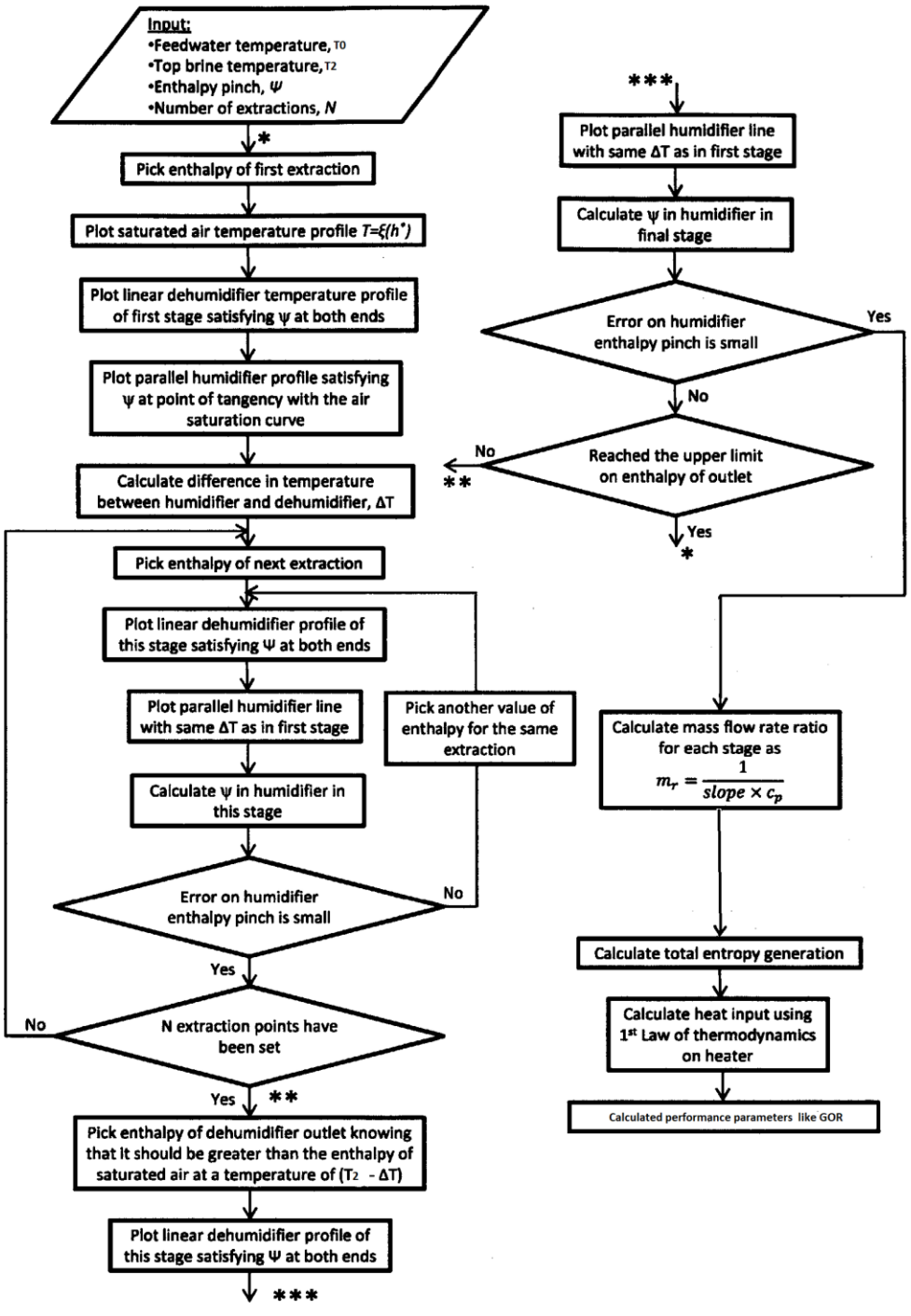

Appendix B: Experimental data analysis

$P1 = 101.3$

----------water side ----------

$m_{water} = 0.098$ *water mass flow rate kg/s*

$m_{pw} = 0.0021$ *pure water mass flow rate kg/s*

$T_{w1} = 29.53$ *inlet water temperature to the humidifier*

$T_{w4} = 38.82$ *outlet water temperature from the humidifier*

$T_{w5} = 44$ *outlet water temperature from water heater*

----------air side ----------

$m_{da} = 0.055$ *air water mass flow rate kg/s*

$T_{a7} = 42.69$ *inlet air dry bulb temperature to the dehumidifier*

$T_{a10} = 34.96$ *outlet air dry bulb temperature from the dehumidifier*

$rh_d = 0.99$ *humidity ratio at humdifier inlet*

$rh_h = 0.99$ *humidity ratio at humdifier outlet*

----------Dehumidifier analysis ----------

$hw_1 = \mathbf{h}(water, T = T_{w1}, P = P1)$

$hw_4 = \mathbf{h}(water, T = T_{w4}, P = P1)$

$hw_{ideal} = \mathbf{h}(water, T = T_{a7}, P = P1)$ *ideal outlet water temperature exiting from the dehumidifer = the inlet air dry bulb temperature to dehumidifier (T_{a7})*

$ha_7 = \mathbf{h}(AIRH2O, T = T_{a7}, R = rh_d, P = P1)$

$ha_{10} = \mathbf{h}(AIRH2O, T = T_{a10}, R = rh_d, P = P1)$

$ha_{ideal} = \mathbf{h}(AIRH2O, T = T_{w1}, R = 1, P = P1)$ *ideal outlet air temperature exiting from the dehumidifer =the inlet water temperature to the dehumidifer(T_{w1})*

----------Dehumidifer effectiveness----------

$$\varepsilon_{d,w} = \frac{hw_4 - hw_1}{hw_{ideal} - hw_1}$$ *Dehumidifer effectiveness based on water side*

$$\varepsilon_{d,a} = \frac{ha_7 - ha_{10}}{ha_7 - ha_{ideal}}$$ *Dehumidifer effectiveness based on air side*

$\varepsilon_d = \mathbf{Max}(\varepsilon_{d,a}, \varepsilon_{d,w})$

----------Dehumidifer modified heat capacity ratio ----------

$\dot{\delta h}_{max,w,1} = m_{water} \cdot (hw_{ideal} - hw_1)$ *maximum allowable heat capacity for water stream (cold side)*

$\dot{\delta h}_{max,a,1} = m_{da} \cdot (ha_7 - ha_{ideal})$ *maximum allowable heat capacity for air stream (hot side)*

$$HCR_d = \frac{\dot{\delta h}_{max,w,1}}{\dot{\delta h}_{max,a,1}}$$

Dehumidifer modified heat capacity ratio

----------*Dehumidifer enthalpy pinch*----------

$$\dot{\delta h}_{max,w2,1} = \frac{\dot{\delta h}_{max,w,1}}{m_{da}}$$

$$\psi_c = \dot{\delta h}_{max,w2,1} - (ha_7 - ha_{10})$$ *enthalpy pinch for cold side (water)*

$$\dot{\delta h}_{max,a2,1} = \frac{\dot{\delta h}_{max,a,1}}{m_{da}}$$

$$\psi_h = \dot{\delta h}_{max,a2,1} - (ha_7 - ha_{10})$$ *enthalpy pinch for hot side (air)*

----------*performance parameters* ----------

$$MR = \frac{m_{water}}{m_{da}}$$ *mass flow rate ratio*

$$\Delta h_{vap} = 2444$$ *latent heat of evaporation*

$$hw_5 = \mathbf{h}(water, T = T_{w5}, P = P1)$$

$$Q_{heater} = m_{water} \cdot (hw_5 - hw_4)$$

$$GOR = m_{pw} \cdot \frac{\Delta h_{vap}}{Q_{heater}}$$ *Gain output ratio*

$$RR = m_{pw} \cdot \frac{100}{m_{water}}$$ *recovery ratio (%)*

$$productivity = m_{pw} \cdot 3600$$ *(Lit/hour)*

Vitae

Name	Mohamed Sobhy Aly Elzayed
Nationality	Egyptian
Date of Birth	1/10/1991
Email	msaz123.ms@gmail.com
Address	11 Gamal Abdel Nasser St., Sintris (32817), Ashmoun, Menofia, Egypt. Phone: +20483406969
Academic Background	**M.Sc. in Mechanical Engineering (April 2019)** King Fahd University of Petroleum & Minerals Dhahran, Saudi Arabia. **B.Sc. in Mechanical Engineering (May 2013)** Menofia University Shebien El kom, Menofia, Egypt.
Research Interests	Desalination; Heat and mass transfer exchangers. Thermodynamic balancing; Enthalpy pinch; Remnant irreversibility; Entropy generation minimization; Mass extraction.
Publications	Mohamed S. Elzayed, M.A. Ahmed, Naef A.A. Qasem, Mohamed A. Antar, Syed M. Zubair, Enthalpy pinch: A Design

Procedure for Thermodynamically-Balanced Closed-Air Open-Water HDH Desalination System, Desalination, in progress.

Mohamed S. Elzayed, M.A. Ahmed, Mohamed A. Antar, Mostafa H. Sharqawy, Syed M. Zubair, Experimental and Theoretical Investigation of HDH Desalination Systems by Thermodynamic Balancing, Energy Convers. Manag., in progress.